# On the microtubule-based transport of Marek's Disease Virus

**Gokhan Tut**

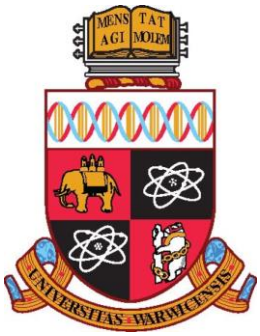


Supervisors:
Dr. Anne Straube
Prof. Venugopal Nair

**Thesis**

Submitted to The University of Warwick, Warwick Medical School
for the degree of
Doctor of Philosophy in Interdisciplinary Biomedical Research
October 2018

# Table of Contents

# List of tables



# List of figures

# Acknowledgments

I would like to thank Anne Straube, my primary supervisor for all the support and advice she has provided me with over the last years. I would like to additionally thank everyone in the Straube lab, especially the current members Manas Chakraborty, Nida Siddiqui, Jonathan Brandt, Daniel Roth for their discussion, advice and for creating a fun environment to work in. I would particularly like to express thanks to Clare Garcin for the advice and aid she provided during my write up. I would like to also acknowledge my secondary supervisor Venugopal Nair and his post-doc Ashley Roberts for helping me with the virology aspect of my thesis. I would also like to express my gratitude to Nicholas Clarke for his help with electron microscopy. I would also like to thank Dan Peet for helping me with microfluidics chip design and implementation. I would like to acknowledge the Medical Research Council for the funding of my project (MR/J003964/1) and the Interdisciplinary Biomedical Research Doctorial Training Partnership for providing and excellent environment to carry out my research

I would always be grateful for my family: my parents and two brothers for their unconditional support and love throughout this whole process. They were always there to reach out with a helping hand, and I am thankful for that. Finally, I would like to give my special thanks to my wife Elif for her support and always believing in me, even when I certainly didn't believe in myself.

# Declaration

This thesis is submitted to the University of Warwick in support of my application for the degree of Doctor of Philosophy in Interdisciplinary Biomedical Research. It has been composed by myself and has not been submitted in any previous application for any degree.

The work presented (including data generated and data analysis) was carried out by the author except in the case outlined below:

- The high pressure freezing, resin emending, sectioning and EM initial imaging of RB1B UL35-GFP infected CEFs was carried out in collaboration with Nicholas Clarke, Royle Lab, CMCB University of Warwick.

## Abstract

Viruses hijack the host machinery for their proliferation and spread. This includes the host cytoskeleton. *Alphaherpesvirus* viral capsids are assembled in the nucleus of an infected cell and then require to be trafficked to various host compartments for tegumentation, secondary envelopment and egress. Microtubules are important for long-distance transport of viral particles inside host cells. Marek's Disease Virus (MDV) is an *Alphaherpesvirus* and is the causative agent of a lymphoproliferative disease called Marek's Disease (MD) in poultry. Here, we demonstrate that both microtubules and actin are required for cell-to-cell spread of MDV in culture. We show that MDV infection induces cell shape changes and these changes depend on dynamic microtubules. Using live cell super-resolution microscopy, we show that the majority of MDV viral particles are associated with microtubules and that MDV particles are transported along microtubules. Cytoplasmic dynein and KIF13B molecular motors have been identified to contribute to the directional transport of MDV viral particles along microtubules. Thus, the findings from this study identify new components of the host machinery required for MDV biology and open new avenues of research for the MDV field.

# List of abbreviations

| | |
|---|---|
| Adenosine diphosphate | ADP |
| Adenosine triphosphate | ATP |
| Alpha/beta tubulin | α/β tubulin |
| Amine terminus | N-terminal |
| Amino acid | AA/aa |
| bacterial artificial chromosome | BAC |
| Bovine Herpesvirus 1 | BoV-1 |
| Carboxyl terminus | C-terminal |
| Chicken embryo fibroblasts | CEF |
| Cluster differentiation | CD – e.g CD4 |
| cytoplasmic linker-associated proteins | (CLASP/s) |
| Days post infection | DPI |
| Double stranded DNA | dsDNA |
| Dynein intermediate chain 1a | IC-1a |
| End binding | EB |
| Endosomal sorting complexes required for transport | ESCRT |
| Enhanced GFP | eGFP |
| Feather follicle epithelium | FFE |
| Fetal calf serum | FCS |
| Forkhead-associated | FHA |
| Gallid Herpesvirus 2 | GaHV-2 |
| Green fluorescent protein | GFP |
| Guanosine-5'-diphosphate | GDP |
| Guanosine-5'-triphosphate | GTP |
| Guanylate kinase-associated kinesin (Kif13B) | GAKIN |
| Heat inactivated FCS | HI-FCS |
| Herpes Simplex Virus 1 | HSV-1 |
| Herpesvirus of Turkeys | HVT |
| Hours post infection | HPI |
| Human immunodeficiency virus -1 | HIV-1 |
| Immunofluresence | IF |
| Inner nuclear membrane | INM |
| Internal repeats long | IRL |
| Internal repeats short | IRS |
| JNK-interacting protein-1 | JIP1 |
| Kinase complex–associated protein | IKAP |
| Kinesin associated protein | KAP |
| Kinesin Heavy chain | KHC |
| Kinesin light chain | KLC |
| Lissencephaly 1 | LISI |
| Marek’s Disease | MD |
| Marek’s Disease Virus | MDV |
| Microtubule affinity-regulating kinase 2 | MARK2 |
| Microtubule associated protein/s | MAP/s |
| Microtubule organizing centre | MTOC |
| Microtubules | MT |
| Myosin light chain kinase | MLCK |
| Nuclear distribution E | NUDE |
| Open reading frame | OPF |

| | |
|---|---|
| Outer nuclear membrane (INM) | ONM |
| p21-activated kinases | PAK/s |
| PBS-Tween | PBST |
| Peripheral Blood Lymphocytes | PBL |
| Phosphate buffered saline | PBS |
| phosphatidylinositol 4,5-bisphosphate | (PtdIns(4,5)-P2) |
| Pleckstrin homology | PH |
| Post-transcriptional modification | PTM |
| Pseudorabis virus | PRV |
| Respiratory syncytial virus | RSV |
| Retinal pigment epithelium | RPE |
| Room temperature | RT |
| Simian Virus 40 | SV40 |
| Stochastic Optical Reconstruction Microscopy | STORM |
| Terminal repeats long | TRL |
| Terminal repeats shot | TRS |
| Tetratricopeptide repeat | TPR |
| Total internal reflection fluorescence | TIRF |
| Trans-Golgi-Network | TGN |
| Unique Long region | UL |
| Unique Short region | US |
| Vanilloid 1 | TPRV01 |
| Varicella Zoster virus | VZV |
| Vascular endothelial growth factor receptor 2 | VEGFR 2 |

# Chapter 1: Introduction

## 1.1: Cytoskeleton: Microtubules and Filamentous Actin

The eukaryotic cytoskeleton, comprised of actin filaments, intermediate filaments, microtubules and other structural molecules, performs a broad range of complex functions. These include: cell motility, determination of cell shape, internal structure, vesicle trafficking and chromosome transport during mitosis (Ayscough and Drubin, 1996, Barkalow and Hartwig, 1995, Goodson et al., 1997, Kuriyama and Nislow, 1992, McLean and Lane, 1995). The individual components of the cytoskeleton are interlinked to form a dynamic network to access all parts of the cytoplasm and the plasma membrane (Cowin and Burke, 1996, Svitkina et al., 1996). This makes the host cytoskeleton an essential target for exploitation during a viral infection.

### 1.1.1: Microtubules

Microtubules (MT) are cytoplasmic hollow tubular structures 25 nm in diameter (Mandelkow and Mandelkow, 1989). They are comprised of polymers of heterodimeric alpha (α) and beta (β) tubulin. Tubulin is arranged in a manner where the α-tubulin and β-tubulin are exposed at the plus and minus ends respectively (Fig 1.1A-B). Nucleation of microtubules is dependent on γ-tubulin ring complexes which have a 13-fold symmetry that acts as a template for α/ β-tubulin dimers to bind and extend (Kollman et al., 2010). Usually a microtubule originating centre (MTOC) is located in the perinuclear region of the cell (de Forges et al., 2012). It contains a gamma tubulin ring complex (γ-TuRC) and anchors the minus end of microtubules and thereby stabilizes them. The plus end of a microtubule is much more dynamic compared to the minus end and extends towards the cell periphery.

The plus end of a microtubule structurally switches between polymerisation and depolymerisation, undergoing catastrophes. A catastrophe is a rapid switch from growth to microtubule shrinkage. This dynamic instability of microtubules is driven by GTP/GDP hydrolysis (Howard and Hyman, 2009).

GTP is associated with β-tubulin subunits at the plus end of the microtubule this forms a GTP cap, and if new GTP subunits are quickly incorporated, then hydrolysis of GTP to GDP does not occur fast enough to lose the stabilizing cap. However, if new subunits are not incorporated faster than GTP hydrolysis, possibly due to low local tubulin subunit concentrations, then the cap is lost. Exposed GDP-tubulin will trigger microtubule depolymerisation (Mitchison and Kirschner, 1984, Weisenberg, 1972, Weisenberg et al., 1976) (Fig 1.1B). This inherent instability of the microtubule cytoskeleton makes it highly dynamic, enabling rapid structural changes to the microtubule network in response to extracellular stimuli.

Microtubule-associated proteins (MAPs) are responsible for the maintenance and regulation of the microtubule network. Microtubule dynamics change drastically during the life time of the cell. This is due to MAPs that promote growth and disassembly. XMAP215 is a microtubule polymerase that binds to the plus end and recruits tubulin dimers to increase the rate of growing microtubules (Al-Bassam et al., 2012, Brouhard et al., 2008). End binding (EB) proteins are another family of proteins that and promote microtubule polymerisation (Komarova et al., 2009, Zanic et al., 2013). Kinesin-13 family members like mitotic centromere-associated kinesin (MCAK) promote microtubule disassembly by removing tubulin subunits from the microtubule plus end (Asenjo et al., 2013, Burns et al., 2014, Desai et al., 1999, Hunter et al., 2003, Moores et al., 2002). Kinesin-8 family members have also been suggested to remove tubulin subunits from the growing plus end of a microtubule (Gardner et al., 2011). Kinesin-4 family members have been suggested to inhibit microtubule growth and supress catastrophes (Bieling et al., 2010, van der Vaart et al., 2013). This leads to the formation of microtubules of particular length which are important for microtubules in the spindle and cell cortex. Cytoplasmic linker protein (CLIP) –associated proteins (CLASPs) have also shown catastrophe inhibiting and rescue promoting activity. They have been shown to bind to the microtubule lattice and recruit tubulin dimers (Al-Bassam et al., 2010). Tau, a microtubule lattice binding protein has also been shown to induce microtubule stability (Kadavath et al.,

2015). These proteins and many others can tightly control and regulate microtubule dynamics and ensure its proper function.

Post-translational modifications (PTMs) of tubulin have been shown to control and regulate the microtubule network. These include; polyglutamylation, polyglycylation, acetylation and detyrosination (Arce et al., 1975, Edde et al., 1990, Hallak et al., 1977, L'Hernault and Rosenbaum, 1985, Redeker et al., 1994). The majority of PTMs occur on tubulin subunits after polymerization, apart from phosphorylation of serine residue S172 of β-tubulin by the Cdk1 kinase. This phosphorylation inhibits subunits incorporating into growing microtubules, thereby controlling rate of microtubule growth (Fourest-Lieuvin et al., 2006). Acetylation of the ε-amino group of residue K40 of α-tubulin is highly conserved and occurs in the microtubule lumen. Acetylation is a marker of stable microtubules (L'Hernault and Rosenbaum, 1985, LeDizet and Piperno, 1987, Nogales et al., 1998). Tubulin detyrosination is the removal of the C-terminal tyrosine residue on α-tubulin and occurs after tubulin subunits are incorporated into the microtubule lattice. This PTM is thought to limit the amount of α-tubulin that undergoes recycling and has been shown to be involved in: microtubule and intermediate filament interactions, cell differentiation and polarization of cells (Hallak et al., 1977, Kreitzer et al., 1999, Kumar and Flavin, 1981, Quinones et al., 2011, Zink et al., 2012). In migrating cells, a subset of microtubules that are oriented towards the leading edge are much more stable and enriched with acetylation and detyrosination (Palazzo et al., 2004). Glutamylation and glycylation are PTMs that form peptide chains on the C-terminal tail of α-tubulin. The chains branch with multiple glutamic acids from the C-terminal tail. This PTM is abundant on microtubules of centrioles, axons and basal bodies, and on some cytoplasmic and spindle microtubules (Bobinnec et al., 1998, Bre et al., 1994, Edde et al., 1990, Redeker et al., 1994, Wolff et al., 1992). The distribution of different PTMs at different cellular sites and during different stages of the cell cycle indicates their importance in facilitating the multiple roles of the microtubule network.

Detyrosination has been suggested to play a role in motor protein function. The kinesin-13 family of motors has been shown to preferentially bind to the

tyrosinated plus end of microtubules suggesting detyrosination may protect against kinesin-13 mediated depolymerisation (Ghosh-Roy et al., 2012, Peris et al., 2009). Detyrosination has also been suggested to increase affinity of kinesin-1 binding to microtubules (Liao and Gundersen, 1998). Kinesin-1 has also been shown to preferentially bind to detyrosinated microtubules and have a slower rate of movement in neurons (Dunn et al., 2008). Acetylation of microtubules have also been suggested to increase kinesin-based transport, especially kinesin-1 (Reed et al., 2006). From these studies it is clear that PTMs have a distinct role to play when determining where and when kinesins can be active on microtubules.

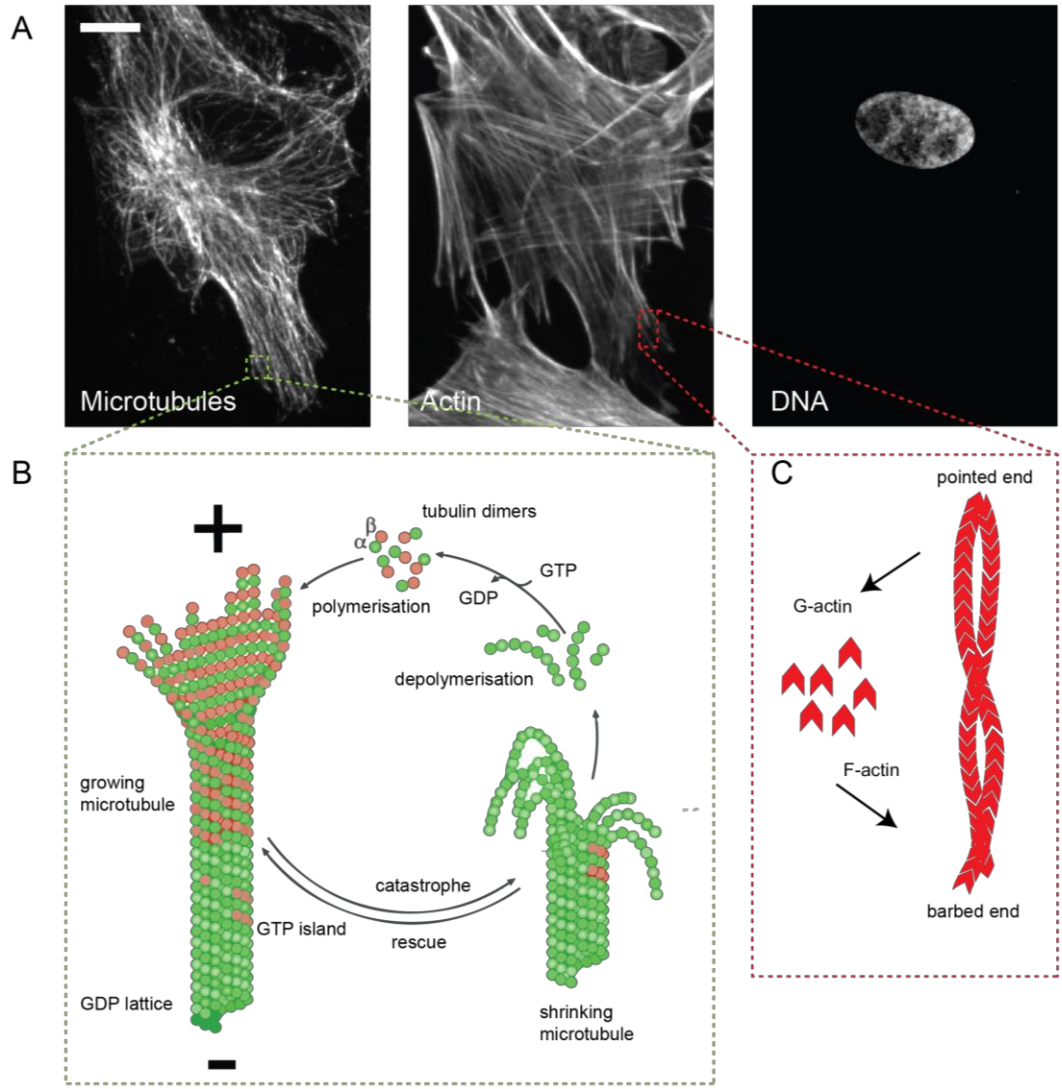


**Figure 1.1: The cellular cytoskeleton**

(A) Visualization of the cytoskeleton in cells. Images show microtubules, actin and the nucleus from the same fibroblast cell. Scale bar is 10 μm. (B) Schematic representation of microtubules and dynamic instability. The cycle of tubulin polymerization and disassembly is powered by hydrolysis of the GTP bound to β-tubulin, which enables microtubules to switch between catastrophes and rescues. GTP-bound tubulin dimers are incorporated into polymerizing microtubules. GTP hydrolysis occurs, with a delay, after a GTP-tubulin dimer incorporates into the growing microtubule plus end. Growing microtubule ends maintain a GTP cap, the loss of which leads to a catastrophe and depolymerization. (C) Schematic representation of F-actin polymerization. G-actin monomers are lost at the pointed end. New G-actin monomers are in-cooperated to the barbed end of actin.

The polarity of microtubules is essential to the function of microtubules for transport and cargo positioning. Cargo includes but is not limited to organelles, vesicles and chromosomes (Tanenbaum and Medema, 2010). Transport of cargo is dependent on the microtubule-associated molecular motors dynein and kinesin. These molecular motors hydrolyse ATP to ‘walk' on microtubules to transport cargo. Cytoplasmic dynein is a minus end directed transporter and most kinesins are plus end-directed motors (Hepperla et al., 2014). These molecular motors allow the movement of cargo to and from the nucleus (Allan, 2011, Hirokawa et al., 2009) as well as vesicles from the endoplasmic reticulum (ER) to the Trans-Golgi-Network (TGN) and then to the plasma membrane for protein secretion (Aplin et al., 1992).

The dense environment in the cytoplasm is a major barrier to the free movement of large structures like viral particles. Microtubule dependent transport of viral particles has been shown to be essential to many different viruses like pox, herpes and retro viruses (Martinez et al., 2008, Mettenleiter et al., 2009)

### 1.1.2: Filamentous Actin

Filamentous actin is crucial to the maintenance of the cell shape, muscle contraction, formation of cell protrusions and constrictive fibres (Pollard and Cooper, 2009). Actin is found in two distinct states in the cell: the globular monomeric G-actin and the filamentous F-actin. F-actin filaments are polarised like microtubules. ATP-bound actin monomers are incorporated into the barbed end, and ADP bound actin is lost at the pointed end of the filament (Fig 1.1C) (Khaitlina, 2014, Woodrum et al., 1975). G-actin is abundant in cells, and F-actin is self-assembling, however, the initial nucleation step (formation of F-actin from G-actin) is rate limiting.

Several proteins control nucleation and dynamics of actin. Formins are dimeric membrane-bound proteins that interact with F-actin. These proteins increase the rate of barbed end elongation and inhibit the role of capping protein, which in turn inhibits elongation. Barbed end elongation allows the generation of

forces required to push the plasma membrane for filopodia (actin rich membrane protrusions) formation (Yang and Svitkina, 2011). The Arp2/3 complex is a heptameric protein complex made from Arp2, Arp3 and five other additional subunits. This complex initiates the formation of a branched actin network for endocytosis and cell motility (Machesky et al., 1994, Mullins et al., 1998, Pollard and Borisy, 2003). The Arp2/3 complex typically requires activation from nucleation-promoting factors. Wiskott-Aldrich Syndrome protein (WASP) or WASP-family verprolin-homologous protein (WAVE) families of proteins are examples of these (Pollard and Beltzner, 2002).

Myosin is a superfamily of actin-dependent molecular motors similar to kinesins and dynein motors that are microtubule dependent. The motors have a semi-conserved catalytic N-terminal head domain that contains both actin and ATP binding sites (Masters et al., 2017). Myosins are involved in multiple cellular processes such as muscle contraction, actin stress fibre contraction, contraction of the actin/myosin ring during cytokinesis and transport of cellular cargo along F-actin. The majority of myosin motors move towards the barbed end of F-actin, with myosin VI as an exception that moves towards the pointed end (Hartman and Spudich, 2012, Masters et al., 2017, Thompson and Langford, 2002).

Viral infection has been shown to exploit the normal functions of the cell, this also includes the actin cytoskeleton. Actin reorganisation has been shown during many viral infections, including Respiratory syncytial virus (RSV), SV40, adenoviruses and herpesviruses (Bachvaroff et al., 1980, Bellett et al., 1989, Graessmann et al., 1980, Marchisio et al., 1984).

## 1.2: *Alphaherpesviruses*

The family *Herpesviridae* that is in the order of *Herpesvirales* contains over one hundred different viruses of which 8 have tropism for humans. This family is divided into a further 3 sub families called; *Alpha-*, *Beta-* and *Gammaherpesvirinae* based on genetic sequences, biological characteristics and the cell types in which viral latency is established (Davison et al., 2009).

The *Alphaherpesvirinae* or *Alphaherpesviruses* family contains many clinically and economically important viruses like Herpes Simplex Virus -1/2 (HSV 1/2), Pseudorabies virus (PRV), Varicella-Zoster Virus (VZV) and Marek's Disease Virus (MDV) (Fig 1.2). The members of this sub family are generally associated with establishing latency in neurons. Clinically, HSV manifests in individuals as ocular, orolabial or genital lesions. It is also implicated in neonatal encephalitis in immunocompromised or immunonaive patients (Al-Dujaili et al., 2011). VZV is the causative agent of human chicken pox and reactivation later in life results in singles (Pergam et al., 2009). PRV infection is associated with high mortality rates in young swine (Muller et al., 2011). MDV is associated with strong immunosuppression, tumours, and neurological disorders in poultry and is a great economic burden to the poultry industry costing £1 billion worldwide (Nair, 2005). MDV was originally classified as a *Gammaherpesvirus* due to its lymphotropism, however it was changed to a member of the *Alphaherpesvirinae* due to it more closely being related these neurotropic viruses at the nucleotide level as the MDV genome structure more closely resembles those of the *Alphaherpesvirinae* family members (Buckmaster et al., 1988). The life cycle and disease progression of MDV is very similar to VZV, even though sites of latency differ.

While there are many differences between the viruses of the *Alphaherpesvirinae* subfamily, there is sufficient homology to study homologous proteins in order to further develop understanding of viral trafficking and replication during the *Alphaherpesvirus* life cycle. For all *Alphaherpesviruses* viral replication occurs in the nucleus (Hay and Ruyechan, 2007). Therefore, transport mechanisms are required for viral

nucleocapsids (viral capsid containing dsDNA) to and from the nucleus. It has been calculated that it could take up to 200 years of passive diffusion for viral capsids to travel 1cm in the cytoplasm due to the crowdedness of proteins in the cytoplasm and the size of the nucleocapsids (Sodeik, 2000). Therefore, active transport of viral capsids is necessary for efficient *Alphaherpesvirus* infection. Investigating viral transport will also highlight crucial virus-host interactions. The discovery of these mechanisms will benefit the understanding of the *Alphaherpesvirus* life cycle and potentially lead to novel therapeutic options as previously unknown aspects of the viral life cycle can be therapeutically targeted.

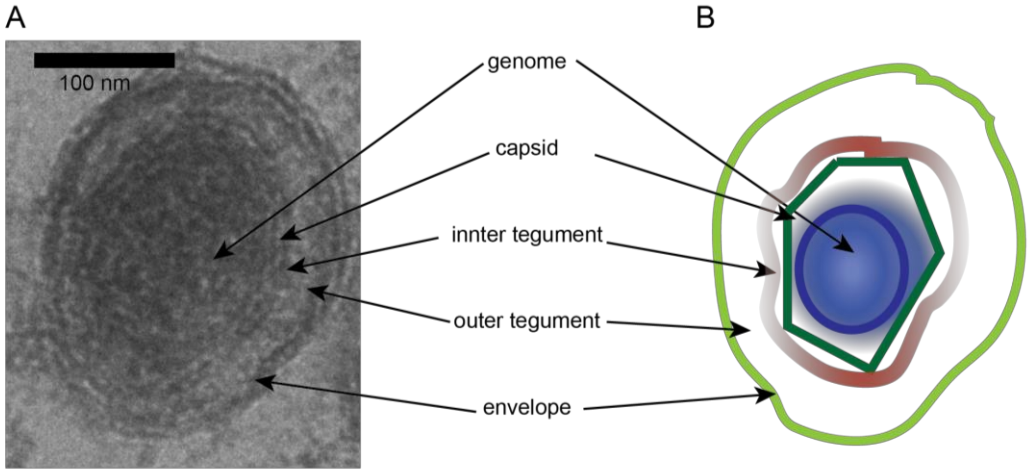


**Figure 1.2: A direct view of an MDV viral particle**

(A) High-pressure frozen electron micrograph (EM) image of an MDV viral particle. Image taken at 40,000 x magnification. Scale bar is 100 nm. (B) Schematic representation of MDV viral particle from A. Arrows indicate to various aspects of the MDV viral particle.

### 1.2.1: *Alphaherpesviruses*: life-cycle

*Alphaherpesviruses* HSV-1 and PRV have been extensively studied to attempt to understand the molecular events underlying *Alphaherpesvirus* entry, replication, maturation, assembly and egress. Infection of host cells is usually initiated by a nucleocapsid surrounded by a protein tegument layer and is encapsulated in a host-derived viral envelope (mature viral particle) (Fig 1.2). *Alphaherpesvirus* nucleocapsids follow a *T*=16 icosahedral symmetry with 162 capsomers. Of the 12 vertices one is occupied by a ring-like dodecameric complex termed the portal. This is the channel where dsDNA is packaged and released from the viral capsid (Chang et al., 2007, Deng et al., 2007, Johnson

and Chiu, 2007, Nellissery et al., 2007). The mature viral particle enters the host cell via membrane fusion or by endocytosis (Fig 1.3). Cell entry is mediated by viral glycoproteins present on the viral envelope called gB, gC, gD, gH and gL (Campadelli-Fiume et al., 2007, Spear, 2004). The nucleocapsid, still containing the inner tegument layer with viral proteins such as US3, UL36 and UL37, is then transported along microtubules via tegument protein interactions with dynein. The viral particle has lost both the envelope and most outer tegument layer during entry into the cytoplasm (Antinone and Smith, 2010, Granzow et al., 2005). Once in the perinuclear region, the dsDNA genome is passed from the viral capsid portal through a nuclear pore complex. Upon entry, replication and transcription of viral genes occurs (Kornfeind and Visalli, 2018).

The viral mRNA is synthesized by the host cell RNA-polymerase II with the aid of viral factors. Transcription of viral proteins occurs in distinct stages: immediate early, early and late. Initial expression of immediate early proteins occurs via tegument protein VP16 recruiting Oct-1 and HCFC1 to form a complex that activates the transcription of immediate early proteins (Herrera and Triezenberg, 2004, Mackem and Roizman, 1982). Immediate early proteins then facilitate the expression of early genes that includes UL30, a virally encoded DNA polymerase that starts the replication of the viral genome (Digard et al., 1993, Skaliter and Lehman, 1994, Stow, 1993, Zuccola et al., 2000). Late phase protein production is facilitated by the early phase proteins and these include the expression of viral structural proteins that form the capsid (Newcomb et al., 1996)

For viral capsid assembly viral capsid proteins UL19, the major capsid protein forming the capsomer pentons and hexons, UL18 and UL38, the triplex proteins residing between and connecting the capsomers, as well as UL26 the maturational protease are required (Desai et al., 1998, Gibson, 2008). The small capsid protein UL35, which decorates hexon tips has been shown to be nonessential to *Alphaherpesviruses* (Krautwald et al., 2008).

Packaged nucleocapsids undergo nuclear egress to leave to nucleus. Several models have been suggested as to how nucleocapsids leave the host nucleus. The most widely accepted and best evidenced model is the primary envelopment-de-envelopment-secondary envelopment process. For this to occur nucleocapsids need to approach and contact the inner nuclear membrane (INM). This is achieved by intranuclear movement of nucleocapsids via actin filaments present in the nucleus during HSV-1 and PRV infection (Feierbach et al., 2006, Forest et al., 2005). The nuclear egress complex (NEC) is responsible for this (Fuchs et al., 2002). The NEC is made up of conserved viral proteins UL31 and UL34 and US3 (Reynolds et al., 2002). UL34 is anchored to the INM by the C-terminal transmembrane helix (Shiba et al., 2000). UL31 is a phosphoprotein that localises to the INM via UL34 interactions and localises to nucleocapsids (Chang and Roizman, 1993, Funk et al., 2015, Roller et al., 2000). The NEC is required for efficient nuclear egress. In the absence of either NEC element viral replication is impaired and a vast majority of viral nucleocapsids accumulate in the nucleus (Fuchs et al., 2002, Roller et al., 2000). The multifunctional viral protein US3 has also been shown to be associated with the NEC by phosphorylating UL31 and UL34. Phosphorylation of UL31 by US3 has been shown to be important for regulating the localisation of both UL31 and UL34 to the INM (Mou et al., 2009, Reynolds et al., 2002). Once at the INM, the nucleocapsid then fuses with the INM and enters the space between the two nuclear membranes and gains a primary, inner nuclear membrane derived envelope. This primary envelope is then lost by fusion of the primary envelope with the outer nuclear membrane (ONM). This results in the nucleocapsid being translocated into the cytoplasm (Mettenleiter, 2002, Mettenleiter, 2004, Mettenleiter et al., 2006, Stackpole, 1969).

The naked viral capsid is then tegumented, whereby the viral capsid acquires viral proteins that form the tegument matrix. The nucleocapsid acquires a multitude of tegument proteins at different stages through a protein-protein network of interactions. The most abundant tegument proteins are UL47, UL48 and UL49 which are present at 600-1300 copies per viral particle (Newcomb et al., 2012). The viral proteins US3, US9 and UL36 are of particular note here

as they have been shown to interact with host molecular motors and viral capsids (Antinone and Smith, 2010, Granzow et al., 2005). UL36 has been shown to drive the transport of HSV-1 nucleocapsids to sites were further tegument proteins can be incorporated in to the existing tegument layer before acquiring a secondary envelope (Ivanova et al., 2016, Sandbaumhuter et al., 2013).

The secondary viral envelope is thought to be derived from the Trans-Golgi Network (TGN) or an endosome and there is evidence for both (Granzow et al., 2001, Hambleton et al., 2004, Henaff et al., 2012, Hollinshead et al., 2012). The evidence for the TGN being the site of final envelopment is from co-localisation studies that show several envelope proteins co-localising with TGN markers (McMillan and Johnson, 2001, Foster et al., 2004c, Crump et al., 2004, Beitia Ortiz de Zarate et al., 2004). Additionally, it was shown that in-cooperating TGN localisation signals to HSV-1 glycoproteins results in correct in-corporation into viral particles (Whiteley et al., 1999) and finally, inhibiting the TGN function using brefeldin A, results in a block in HSV-1 assembly, suggesting HSV-1 envelopment occurs by the TGN membrane (Koyama and Uchida, 1994, Cheung et al., 1991). More recently there has been emerging evidence to support secondary envelopment originating from endosomes rather than the TGN. Electron microscopy studies have shown the presence of endocytic tracers in plasma membrane endosome compartments that wrap around nucleocapsids, this is the most direct evidence to suggest that secondary envelopment occurs from plasma membrane derived endocytic tubules (Hollinshead et al., 2012). Additionally, blocking the function of specific Rab GTPases like Rab6, Rab43 and Rab1a/b that are associated with endosomal transport inhibits HSV-1 assembly (Johns et al., 2014, Zenner et al., 2011) and prevents the in-cooperation of viral glycoproteins into virions (Albecka et al., 2016). Taken together these data suggest that the membrane used for secondary envelopment is derived from endosomal compartments. However, due to the dynamic and fluid nature of the secretory and endocytic pathways and their markers it is hard to accurately come to distinct conclusions as to the identity of the secondary membrane. Especially when the cytopathic effects of *Alphaherpesvirus* infection during its life cycle are

taken in to account, as they are known to perturb membrane trafficking and cellular organelle structure (Henaff et al., 2012). What is certain is that secondary envelopment membranes are derived from the late secretory pathway and or the endosomal pathway components and not from early secretory pathway membranes such as the ER, as artificially targeting viral envelope proteins to the ER prevents in-cooperation in virions and blocking ER-Golgi transport inhibits viral assembly and leads to accumulation of viral proteins in the ER (Whiteley et al., 1999, Browne et al., 1996, Zenner et al., 2011). During secondary envelopment the viral nucleocapsid buds into vesicles that contain viral glycoproteins that are presented on the surface of a mature viral particle. This process results in the simultaneous packaging of the viral particle into the vesicle. There is still much debate on where secondary envelopment occurs as *Alphaherpesviruses* are known to reorganise the host cytoskeleton, secretory and endocytic pathways. Therefore, determining the origin of the secondary envelopment site becomes anything but straightforward (Avitabile et al., 1995, Campadelli et al., 1993).

Tegument proteins are thought to contribute to secondary envelopment by forming interactions that bridge the viral capsid and vesicle membrane by interacting directly with capsid proteins and with the cytoplasmic tails of viral glycoproteins or membrane-associated tegument proteins on the vesicle (Crump, 2018). The interactions between the tegument and envelope proteins are thought to be co-operative and partially redundant. The redundant nature of these interactions was described by single deletion analysis of gB, gD or gE that has no effect on attenuation of secondary envelopment. The combined deletion of gB and gD or gD and gE results in large amounts of cytoplasmic non-enveloped viral capsids (Johnson et al., 2011, Farnsworth et al., 2003). Direct interaction between gM and lipid-anchored viral protein UL11, where deletion of each protein individually results in minor defects but dual deletion results in a profound inhibition of secondary envelopment (Leege et al., 2009).

Besides these interactions, the envelope proteins gK and UL20 form a complex that depend upon each other for correct subcellular localisation (Foster et al., 2004a). The gK-UL20 complex is essential for efficient

secondary envelopment and requires both elements as deletion of either element results in significant defects in secondary envelopment (Jayachandra et al., 1997, Melancon et al., 2004, Foster et al., 2004b). This complex interacts with UL37 viral protein and is important for the subcellular localization of gD and gH-gL envelope proteins. These interactions suggest that the gK-UL20 complex is important for organising the viral envelope proteins and mediating their interactions with tegument proteins (Lau and Crump, 2015, Jambunathan et al., 2014). Several other tegument proteins have been suggested to directly interact with the cytoplasmic domains of envelope proteins, these are; UL48 with gH, UL49 with gD, gE and gM, UL11 with gD and gE and UL37 with gK (Jambunathan et al., 2014, Han et al., 2011, Farnsworth et al., 2007, Maringer et al., 2012, Gross et al., 2003). The interaction between these tegument and envelope proteins are sufficient to drive secondary envelopment as light particles are formed in the absence of capsids. These contain most, but not all of the tegument and envelope proteins (Szilágyi and Cunningham, 1991, Rixon et al., 1992). These observations support the hypothesis that interactions between envelope proteins and the tegument layer occur to ensure correct secondary envelopment of viral capsids.

Secondary envelopment membrane scission is thought to be mediated by the ESCRT pathway (Calistri et al., 2007, Crump et al., 2007, Kharkwal et al., 2014, Pawliczek and Crump, 2009a) and a fully mature viral particle is created and packaged simultaneously as the virion is contained in the lumen of the vesicle. It is not fully understood how *Alphaherpesviruses* recruit and regulate the ESCRT machinery at sites of secondary envelopment. There is evidence that UL36 interacts with the ESCRT-I subunit TSG101, however this interaction is not essential (Pawliczek and Crump, 2009b, Calistri et al., 2015)

Finally, the fully mature viral particle must be transported to the plasma membrane to undergo exocytosis. Very little is known regarding how mature viral particles are transported after secondary envelopment in non-neuronal cells. Several Rab proteins have been suggested to traffic with viral tegument and glycoproteins during egress (Hogue *et al* 2014, Miranda-Saksena *et al*

2009). The gE-gL complex has been established to be important for cell-to-cell spread of HSV in epithelial cells. Deletion or loss of function of the gE-gL complex results in a significant reduction in the spread of infection between cells in a monolayer. This is thought to be due to the reduced targeting of viral particles to cell junctions (Johnson et al., 2001, Dingwell and Johnson, 1998, Dingwell et al., 1994). The cytoplasmic domains of both gE and gL are thought to be the source of how HSV-1 targets the cell-to-cell junctions in epithelial cells for viral spread (Farnsworth and Johnson, 2006a, McMillan and Johnson, 2001). Microtubule based molecular motors have also been shown to transport HSV-1 and PRV viral capsids particularly in neurons (Daniel et al., 2015, Diefenbach et al., 2002, Kramer et al., 2012), this is introduced in greater detail later on. To date there are no reports in the literature reporting MDV association or transport along microtubules.

Upon the mature viral particle reaching the cell periphery it encounters the cortical actin, which is a dense mesh of filamentous actin underlying the plasma membrane. This is thought to pose as a barrier to the vesicle carrying the mature viral particle. This is a similar problem faced by large cellular secretory vesicles, such as melanosomes. Actin based motors such as Myosin Va has been shown to reorganise the dense network to allow large secretory vesicles through and Myosin Va has been shown to be essential for efficient HSV-1 release (Roberts and Baines, 2010), other than this very little is known regarding how virus containing vesicles pass though the actin cortex. The final stage of egress is the fusion of the vesicle containing the viral particle with the plasma membrane. Several Rab proteins like Rab3A, Rab6A, Rab8A and Rab11A as well as SNARE protein SNAP-25 have been shown to localise to vesicles containing viral particles, but their functional role has not been investigated (Hogue et al., 2014b, Miranda-Saksena et al., 2009) . Exactly how an *Alphaherpesvirus* viral particle containing vesicles release their cargo is still not fully understood.

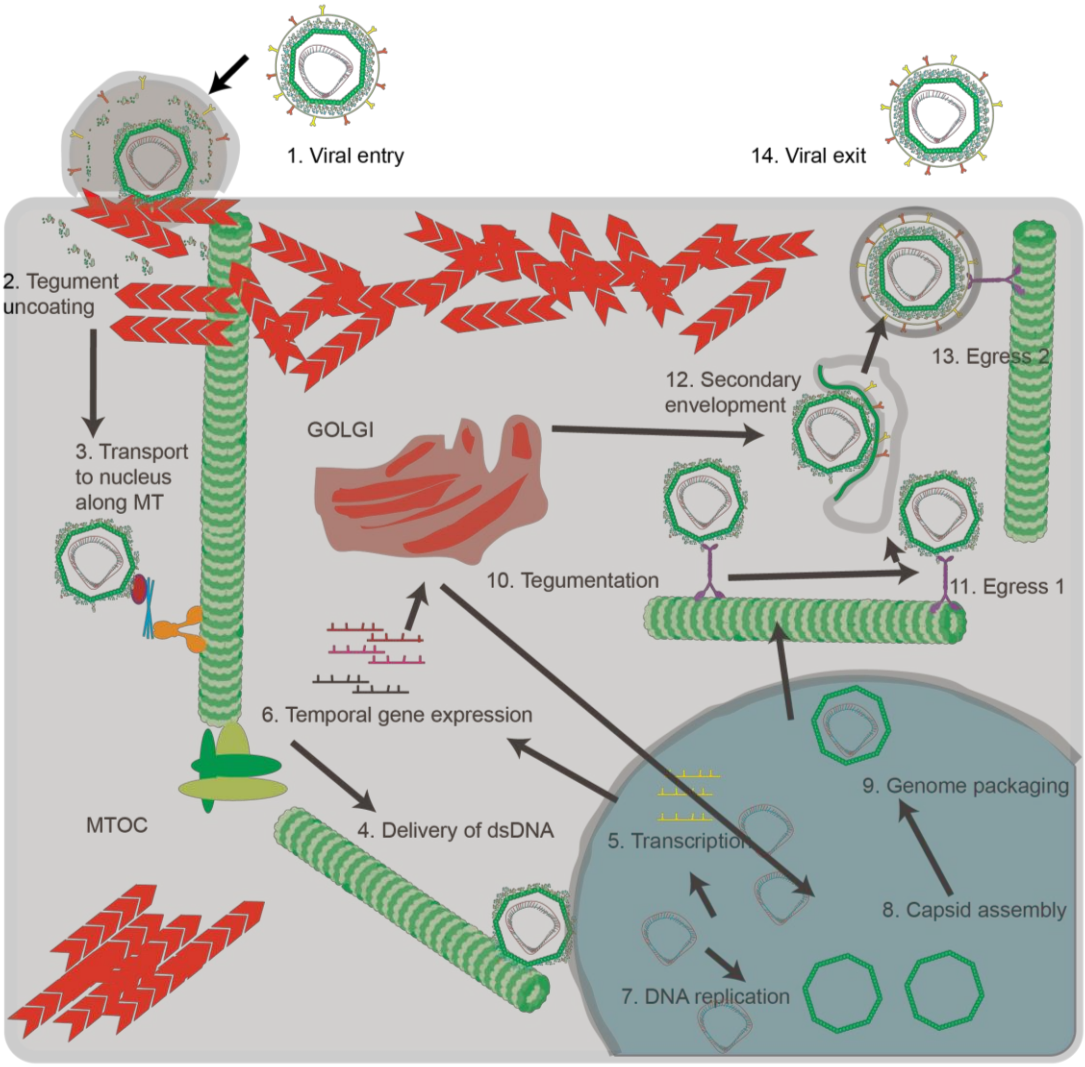


**Figure 1.3: Model of *Alphaherpesvirus* life-cycle in non-neuronal cells**

(1.) A mature virus binds to the host cell surface mediated by viral glycoproteins. Fusion of the membranes delivers the viral capsid and the tegument wrapped around it in to the cytoplasm. (2.) Much of the tegument layer uncoats from the nucleocapsid. (3.) Dynein mediated transport is facilitated by the inner tegument layer towards the MTOC and nucleus. (4.) Upon entry of the viral dsDNA in to the nucleus transcription and replication is initiated in the nucleus. (5/6.) Viral DNA is transcribed and translated in a temporal manner. (7.) DNA replication is carried out in the nucleus. (8.) The viral capsid is assembled in the nucleus. (9.) Newly replicated viral dsDNA is packed in to viral capsids to form a nucleocapsid. (10.) Nucleocapsid leaves the nucleus and acquires an inner tegument layer. (11.) Vial nucleocapsid is then transported to secondary envelopment site. (12.) Secondary envelopment occurs were viral particle gains a viral envelope and is packed in to vesicle at the same time. (13.) Viral particle is then transported to the cell cortex. (14.) Viral particle is released to the extracellular environment via exocytosis.

### 1.2.2: *Alphaherpesvirus* interactions with the host microtubule network

An intact and functioning microtubule network is essential for *Alphaherpesvirus* infection (Mabit et al., 2002, Marozin et al., 2004, Topp et al., 1994). It has long been established that *Alphaherpesviruses* target the host microtubule network during their life cycle (Brzozowska et al., 2010, Dienes et al., 1987, Kotsakis et al., 2001, Pasdeloup et al., 2013a, Pasdeloup et al., 2013b). However, only a handful of viral proteins have been identified to interact with and remodel the microtubule network directly. Most work carried out to identify potential *Alphaherpesvirus* microtubule regulators was carried out in HSV-1 infected cells.

Viral protein US3 from HSV-1 has been shown to phosphorylate a kinase in NHDF cells and inactivate it. This then leads to microtubule stabilisation by +TIP and CLASPs to aid in viral spread (Jovasevic et al., 2015). Infected cell protein 0 (ICP0), which is a viral E3 ligase, has also been observed to destabilise and unbundle microtubules in Vero cells (green monkey kidney epithelial) (Naghavi et al., 2013). From a yeast two-hybrid screening, UL37 and IKAP have been identified as interactors. IKAP has been suggested to stabilise microtubules (Cheishvili et al., 2011, Kelly et al., 2012). HSV-1 infection has also been shown to remodel the microtubule network so that the centrosome is no longer the primary MTOC during egress, but additional mini MTOCs form, hypothesised to direct new progeny towards secondary envelopment sites (Pasdeloup et al., 2013a). These interactions show that during an *Alphaherpesvirus* infection the microtubule network is targeted and remodelled to facilitate viral spread. No evidence has been that MDV infection induces similar changes or effects the microtubule network

## 1.3: Cargo transport in cells

The motor proteins that associate with microtubules belong to two major superfamilies of proteins: dyneins and kinesins (Fig 1.4). Dyneins mediate minus end-directed transport (Allan, 2011, Hook and Vallee, 2006). Kinesin superfamily proteins usually mediate plus end-directed motility (with some members capable of minus end-directed motility) (Hirokawa et al., 2009, Hirokawa and Tanaka, 2015).

Dyneins are categorised in two classes based on their functional and structural roles: axonemal and cytoplasmic dyneins. Axonemal dyneins are involved in the flagella/ciliary beating (Roberts et al., 2013). Cytoplasmic dyneins are multi-subunit proteins with two heavy chains that each contain an N-terminal tail domain (adaptor/cargo binding domain), a motor domain and a microtubule binding domain. The motor domains of dyneins are ATPases associated with cellular activities (AAA+) units that regulate ATP binding, hydrolysis and release of ADP and inorganic phosphates. ATP hydrolysis is coupled to dynein motor movement (Bhabha et al., 2016, Roberts et al., 2013). Three ubiquitous regulators of dynein activity have been identified; the dynactin complex (McKenney et al., 2014, Schlager et al., 2014), nuclear distribution E (NudE) and lissencephaly 1 (Lis1) (McKenney et al., 2011). Cytoplasmic dynein is responsible for transporting many types of vesicles (endosomes, phagosomes, lysosomes, etc.) towards the perinuclear region (Xiang et al., 2015). Many different types of viruses depend upon dynein transport after viral entry and egress (Dodding and Way, 2011).

The kinesin superfamily contains ~15 smaller families ordered by their phylogenic differences, and a total of 45 individual kinesin genes exist in humans (Hirokawa and Tanaka, 2015, Lawrence et al., 2004). The types of kinesins can be determined based on the location of the motor domain, which contains a microtubule binding site and the ATP catalytic domain for motility. N-kinesins have the motor domain on their N-terminus and are responsible for plus-end-directed transport. C-kinesins that have their motor domain on their

C-terminus and drive minus end-directed transport. M-kinesins contain their motor domain in the middle of the protein, and these kinesins are associated with depolymerising microtubules (Hirokawa et al., 2009). Besides the motor domain, kinesins contain a tail region that might contain regions for dimer formation, and domains responsible for binding to regulatory proteins, accessory kinesin light chains and/or cargo (Hirokawa et al., 2009). Kinesins can transport whole organelles, individual proteins, RNA molecules and vesicles (Hirokawa and Tanaka, 2015). They also play an essential role in cargo transport between the TGN to the plasma membrane and endoplasmic reticulum (ER) to the TGN (Hirokawa and Tanaka, 2015). There is also cargo that contains specific binding domains for specific kinesins. Adaptor proteins like JIP1 also aid in the recruitment and subsequent transport of cargo by kinesins (Satake et al., 2013).

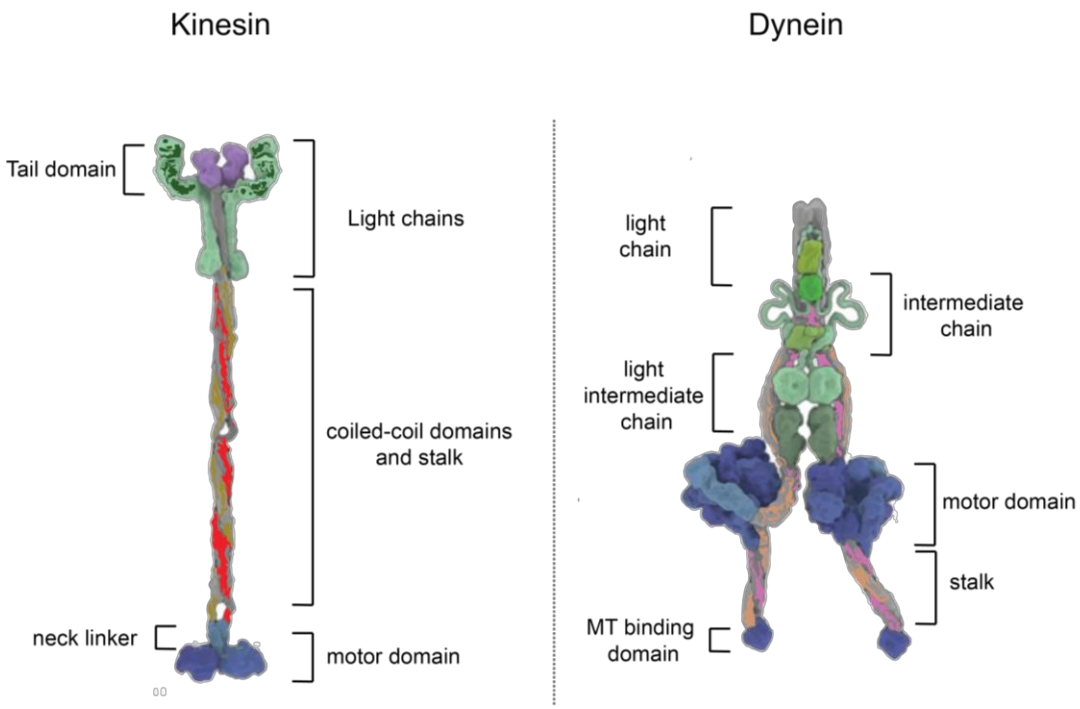


**Figure 1.4: Representative structures of kinesin and dynein motor proteins**

This figure is adapted from Carter (2013). Kinesins are microtubule motors and move towards the plus end of the microtubule (except for kinesin 14). The motor domain (dark blue) binds to the microtubule. The neck linker domain (light blue) along with the coiled-coil domains (red and yellow with grey) facilitate dimerization of two kinesin proteins. Cargo binding is facilitated by the kinesin tail (purple) and the kinesin light chains (green). Dynein is a processive dimeric motor that moves towards the minus end of the microtubule. Dynein binds to microtubules through the microtubule binding domain (light blue) present at the end of the stalk (grey, yellow and purple). The motor domain (dark blue) contains a ring of AAA+ domains. The N-terminal of the stalk associates with light chain, intermediate chain and light intermediate chain (different shades of green).

### 1.3.1: Cargo transporting kinesins

There are three families of kinesins thought to carry out the bulk of the cargo transport needs of the cell; these are Kinesin-1, Kinesin-2 and Kinesin-3 families. Most of what is known regarding kinesins has come from work carried out on Kinesin-1 family members (also known as conventional kinesin) (Lawrence et al., 2004). Minimal kinesin-1 motors that only contain the motor domain and dimerization domains can move processively (taking hundreds of steps without falling of the microtubule), towards the plus end of a microtubule at 8 nm step sizes (this is the distance between each tubulin dimer) at a speed of up to 0.8 $\mu m/s^{-1}$ (Gennerich and Vale, 2009) Processivity is achieved by hand-over-head stepping mechanism in which the two motor domains from the dimer alternate their catalytic cycles (Fig 1.5) (Valentine and Gilbert, 2007).

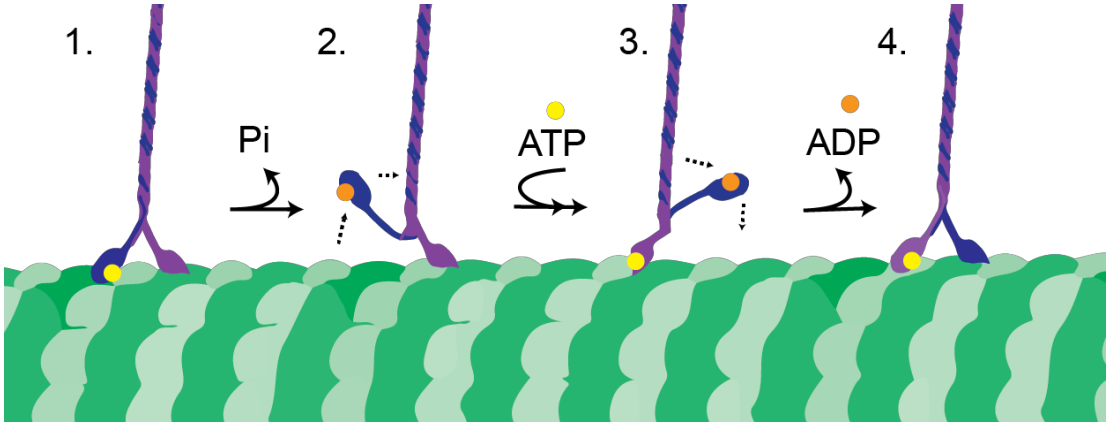


**Figure 1.5: Minimal model of kinesin stepping**

There are four minimal states during the mechanochemical cycle of kinesin stepping. In state 1 both motor domains are bound to the microtubule, the leading motor lacks a nucleotide and the trailing motor domain has a single ATP bound. Upon ATP hydrolysis and release of inorganic phosphate in the trailing motor domain, it detaches from the microtubule (state 2). ATP binding to the leading head results in forward docking of the neck linker, this results in bringing the trailing motor closer to the leading motor domain (state 3). The trailing motor then moves forward and binds on to the next available binding site on the microtubule. This releases the ADP molecule. The trailing motor domain is now the leading motor domain and the cycle continues (state 4). Kinesin is represented by the blue and purple dimers, ATP is a yellow oval and ADP is orange and microtubule in green.

Kinesin-1 holoenzyme is a heterotetramer consisting of two kinesin heavy chains (KHC) and two kinesin light chains (KLC). The KHC contains the motor domain, neck domain, a coiled-coil stalk and a globular tail domain. The neck domain is critical to kinesin-1 processivity and contains a neck linker and neck coil. The coiled-coil stalk contains hinge segments that enable the motor to adopt folded and autoinhibited states and be flexible enough to accommodate multiple molecular motors to work together (Bieling et al., 2008, Coy et al., 1999, Crevenna et al., 2008, Friedman and Vale, 1999, Jaud et al., 2006). The globular tail domain is responsible for regulating motor domain activity and cargo binding (Adio et al., 2006). The KLC subunit contains a heptad repeat region for oligomerisation with the KHC. This is followed by six tetratricopeptide repeat (TPR) motifs that participate in cargo binding. The KHCs are encoded by Kif5A, Kif5B and Kif5C genes and KLC are encoded by four genes (KLC1-4).

The kinesin-2 family contains a further two sub-families that are heterotrimeric or homodimeric. The heterotrimeric kinesin-2 motors are made up of two motor-domain-containing subunits from the Kif3 sub-family and a nonmotor kinesin-associated protein (KAP). The homodimeric sub-family contains Kif17. Both sub-families of kinesin-2 have been implicated in a wide range of transport events: long distance transport during construction and maintenance of cilia and flagella, transport of organelles (mitochondria), melanosomes, mRNA granules, and membrane-bound vesicles (Hirokawa et al., 2009, Scholey, 2008)

Kinesin-3s have been identified as organelle, endosome and vesicle transporters (Siddiqui and Straube, 2017). The kinesin-3 family is comprised of 6 sub-families: Kif1, Kif13, Kif14, Kif16 and Kif28 motors, plus a small group of fungal Kinesin-3 like short proteins (Miki et al., 2005). Kinesin-3 is the largest family of kinesins in humans. Kinesin-3 facilitated transport is essential for neuronal morphogenesis and function. Mutations in Kif1A, Kif13B and Kif1C are known to cause neurological disorders, including spastic paraplegia and multiple sclerosis (Aulchenko et al., 2008, Caballero Oteyza et al., 2014, Dor et al., 2014, Niwa et al., 2008, Yonekawa et al., 1998) For example, Kif13B

(also known as; guanylate kinase-associated kinesin (GAKIN)) has been shown to transport vesicles containing PtdIns(3,4,5)P3 (phospholipid), human discs large (hDlg) tumour suppressor protein, vascular endothelial growth factor receptor 2 (VEGFR 2) and transient receptor potential vanilloid 1 (TPRV1) in rat adrenal gland cells, rat dorsal neurons human endothelial cells (Horiguchi et al., 2006, Xing et al., 2012, Yamada et al., 2007, Yamada et al., 2014).

All kinesin-3 family motors are plus end-directed motors. The defining features of Kinesin-3 motors are the molecular organisation of the neck –region. It contains a β-sheet, a helix and a forkhead-associated (FHA) domain in the tail region (Westerholm-Parvinen et al., 2000). The tail region also contains several short coiled-coil domains and lipid interaction domains thought to mediate cargo binding (Siddiqui and Straube, 2017).

The motor domain of kinesin-3s contains a stretch of positively charged lysine residues termed the K-loop. This loop is positioned to contact the negatively charged glutamate-rich (E-hook) C-terminal tail of β-tubulin. The K-loop in Kif1, Kif13 and Kif16 proteins have been shown to increase microtubule affinity to motor domains, this increases microtubule binding rate and ensures kinesin-3s can effectively work in teams (Matsushita et al., 2009, Rogers et al., 2001, Soppina and Verhey, 2014).

Kinesin-3 does not contain the extended coiled-coils observed in other kinesin families. There are instead smaller predicted coiled-coil regions scattered along the tail domain. With Kif13A, Kif13B and Kif1A, the coiled-coil domains interfere with dimerisation, and the neck coil is sufficient to dimerise kinesin-3s (Hammond et al., 2009, Soppina et al., 2014). The FHA domain found on kinesin-3s has been shown to be important for cargo binding. The FHA domain on Kif13B is essential for binding TRPV1 (Xing et al., 2012). This interaction has been shown to be dependent on phosphorylation of Kif13B at T506 in the FHA domain by cyclin-dependent kinase 5 (Cdk-5) (Xing et al., 2012). Kif1A and Kif13B also have a pleckstrin homology (PH) domain that is important for binding vesicles. This is mediated by phosphatidylinositol 4,5-bisphosphate

(PtdIns(4,5)-P2) (Klopfenstein et al., 2002, Xue et al., 2010). Kif13B also processes a protein interaction domain CAP-Gly thought to bind to sequence motifs at the C-terminus of tubulin and EBs, zinc-finger motifs, and proline-rich sequences (Steinmetz and Akhmanova, 2008). Inactive kinesin-3s are compact and have a crumpled tail (Hirokawa and Noda, 2008). This is termed autoinhibition (Okada and Hirokawa, 1999, Tomishige et al., 2002).

Kinesins are activated by cargo binding. Kif13B is in an autoinhibited state in solution and is activated by cargo binding, e.g., hDlg tumour suppressor. Kif13B is also active during *in vitro* gliding assay – this could be due to the tail region being bound to the glass surface and glass taking over the role of cargo (Yamada et al., 2007). Centaurin α1 (CENTA1) is a cargo adapter for Kif13B. It activates Kif13B from its auto-inhibited state and recruits it to PtdIns(3,4)P2 / PtdIns(3,4,5)P3-containing vesicles. The PH1 domain of CENTA 1 directly interacts with the FHA domain on Kif13B. The FHA domain also interacts with the ArfGAP domain of a second CENTA1 molecule. Kif13B and CENTA1 form a heterotetrameric complex for the transport of PtdIns(3,4,5)P3-rich vesicles (Horiguchi et al., 2006, Tong et al., 2010).

Kinesin-3 has also been suggested to be involved in the bi-directional transport of cargo. When depleting a specific kinesin-3, the transport of cargo towards both ends of the microtubule is impaired (Ally et al., 2009, Theisen et al., 2012, Tien et al., 2011). Kinesin-3s have been suggested to transport cargo together with dynein, but the exact mechanism of this remains unknown (Hancock, 2014). The opposing force/lack of force generated could result in mechanical activation of the partner motor (Ally et al., 2009). It could also be the steric inhibition mechanism where direct interactions between the opposing motors relieve autoinhibition. There could also be a tether mechanism were the opposing motor acts as a weakly bound tether to increase processivity (Hancock, 2014).

A tug-of-war model has also been proposed for bi-directional transport. The motors pull against each other, and generally, the strongest team of motors wins resulting net movement of cargo towards the winning end. The outcome

was determined by the numbers of each motor protein and the force that each motor can produce (Amrute-Nayak and Bullock, 2012, Derr et al., 2012). Potential linkers of both kinesin -3 and dynein could be Hook and Bicaudal proteins as both have been identified to interact with both types of motors (Bielska et al., 2014, Fu and Holzbaur, 2014, Schlager et al., 2010, Splinter et al., 2010). Kinesin binding protein (KBP) could also form the bridge between dynein and kinesin-3 as it has been shown to inhibit Kif1A bi-directional transport and stimulate Kif1B bi-directional transport (Drerup et al., 2016, Kevenaar et al., 2016).

Microtubule based motor proteins are essential for the long-distance transport in eukaryotic cells. They are also essential for the life cycle of many different viruses like adenovirus, vaccinia virus and HSV-1 (Antinone et al., 2010, McDonald et al., 2002, Schepis et al., 2007, Suomalainen et al., 1999). The most detailed image for dynein and virus interaction comes from studies on the role of dynein and microtubules in the adenovirus life cycle. By labelling fluorescently adenovirus particles it was possible to visualise microtubule mediated bi-directional transport during the early phases of adenovirus infection and treating these cells with nocodazole results in significant reduction in adenovirus nuclear targeting (Leopold et al., 2000, Salinas et al., 2009, Suomalainen et al., 1999). Disruption of dynein activity by over expression of dynactin subunit p50/dynamitin or the coiled-coil region of p150glued also results in reduced incidence of virus directed transport towards the nucleus (Engelke et al., 2011, Salinas et al., 2009). Kinesin 1 has been shown to be important for vaccinia virus infections, intracellular enveloped virus (IEV) are transported from the perinuclear region towards the plasma membrane on microtubules (Roberts and Smith, 2008). This transport is dependent on viral protein A36 and in the absence of A36 IEV fail to reach the plasma membrane (Doceul et al., 2010, Smith et al., 2002, Ward and Moss, 2001).

### 1.3.2: *Alphaherpesvirus* interactions with the host molecular motors

The majority of *Alphaherpesvirus* viral proteins that are associated with microtubules in one form or another have been shown to engage not with microtubules directly but with microtubule-dependent molecular motors. Intracellular pathogens generally require kinesin/dynein mediated intracellular transport. Therefore, many pathogens, including *Alphaherpesviruses*, have developed mechanisms of subversion of these molecular motors (Dodding and Way, 2011, Dohner et al., 2005, Smith et al., 2001, Taylor and Enquist, 2015, Ward, 2011).

There are currently two working models for *Alphaherpesvirus* trafficking during egress in neurons. The subassembly model: where naked capsid lacking an envelope is being transported. The second is the married assembly model, where a capsid has undergone secondary enveloping and processes a viral envelope is then transported (Miranda-Saksena et al., 2018). The model of transport chosen reflects which viral proteins are accessible for interaction with host molecular motors during transport. During enveloped capsid transport the tegument and capsid proteins will be inaccessible for interactions with molecular motors, but viral glycoproteins will be accessible for interaction. Both naked and enveloped viral particles have been shown to undergo directional transport on microtubules (Antinone and Smith, 2006, Antinone et al., 2010, Wisner et al., 2011). These models are based in neuronal cells, however the mode of transport exploited by the virus in neurons may also be used as a starting point to try and understand viral capsid transport in non-neuronal cells.

Most of the research into *Alphaherpesvirus* viral protein interactions with host microtubule-associated motors and accessory proteins has been carried out using HSV-1, HSV-2 and PRV viruses. There has been a small number of viral proteins that have been shown to interact with dynein directly or with dynein recruitment proteins (Fig 1.6). UL34 from HSV-1 has been shown to interact with dynein intermediate chain 1a (IC-1a), UL34 has been shown to be a non-structural protein that localises to the nuclear membrane (Loret et al., 2008, Ye et al., 2000). UL35, a viral capsid protein, from HSV-1 has been shown to

interact with dynein light chains Tctex1 and RP3 in a yeast two-hybrid assay. Micro-injection of HSV-1 UL35 enhanced retrograde transport of viral particles. However, deletion studies have suggested that these interactions are dispensable in cells (Antinone et al., 2006, Dohner et al., 2006, Douglas et al., 2004). UL36, a tegument protein, from PRV has also been shown to interact with the dynein/dynactin complex (Zaichick et al., 2013). This interaction was shown to drive active transport of viral particles in the absence of other viral proteins in Vero cells. The viral capsid protein UL25 is also thought to be necessary for this interaction as UL36 is thought to bridge together the dynein/dynactin complex with the viral capsid. The proline-rich domain of UL36 binds UL25 (Zaichick et al., 2013).

Kinesin 1 and 3 family members also facilitate *Alphaherpesvirus* capsid transport (Fig 1.6). US11, tegument protein from HSV-1, has been suggested to interact with kinesin-1 directly. This interaction is achieved by 867-894 residues on kinesin-1 directly binding to the C-terminal domain (RNA binding domain) of US11 (Diefenbach et al., 2002). Additionally, viral protein US9 from HSV-1 has been shown to interact with kinesin-1. Five arginine residues in the basic domain of US9 are thought to facilitate this interaction. This domain was also shown to contribute to the anterograde transport of viral particles in rat dorsal neurons (Diefenbach et al., 2016). RNAi mediated knockdown of kinesin-1 family members Kif5A, 5B and 5C (individually) all halt anterograde transport of enveloped HSV-1 viral particles in neuronal cells (DuRaine et al., 2018)

PRV and HSV-2 viral particles are transported by kinesin-3 family member Kif1A. The viral protein UL56 of HSV-2 has been shown to interact with Kif1A C-terminal transmembrane domain in Vero cells (Daniel et al., 2016, Koshizuka et al., 2005). The US9 protein from PRV has also been shown to interact with Kif1A using a GFP-trap pull-down. This interaction was further solidified by showing that Kif1A interaction with PRV viral particles results in efficient axonal sorting and transport in rat neurons (Daniel et al., 2015, Kramer et al., 2012). UL37 (tegument protein) from HSV-1 recruits dystonin/BPAG1 to viral capsids in human fibroblast cells. Depleting dystonin

has been shown to inhibit plus-end-directed transport of viral particles, and this is thought to be necessary for the transport of incoming viral particles from the centrosome towards the nucleus and during egress (McElwee et al., 2013, Pasdeloup et al., 2013b) Thus, *Alphaherpesvirus* proteins UL36, US9 and US11 are all emerging as viral proteins that interact with host molecular motors to facilitate viral particle transport.

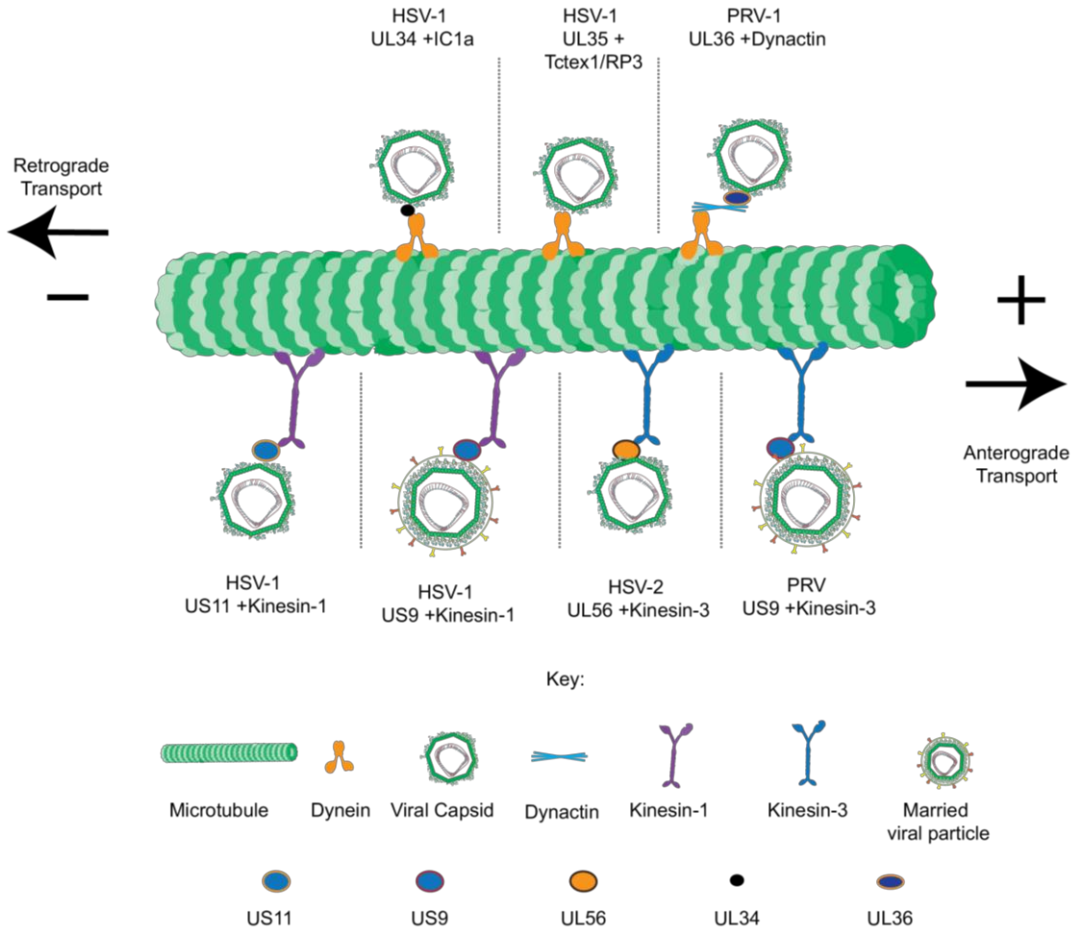


**Figure 1.6: Dynein and kinesin motors transport *Alphaherpesvirus* particles**

*Alphaherpesvirus* viral particles have been suggested to be transported by numerous host microtubule associated molecular motors. These include dynein, kinesin-1 and kinesin-3. HSV-1 uses viral proteins UL34 and UL35 to recruit dynein to the viral capsid during entry. It has also been shown to recruit kinesin-1 motor via US11 and US9 during anterograde transport. PRV recruits dynactin to viral capsids during entry via interaction with UL36 which in turn brings dynein. Kinesin-3 is recruited to PRV viral particles via US9 during anterograde transport. HSV-2 is thought to interact with kinesin-3 via UL56.

## 1.4: Marek's Disease Virus (MDV)

Marek's Disease Virus (MDV) otherwise known as Gallid Herpesvirus 2 (GaHV-2) is an *Alphaherpesvirus* found in the family *Herpesviridae*. MDV is found in the genus *Mardivirus*. MDV is the causative agent of the highly infective lymphoproliferative disease called Marek's Disease (MD) (Nair, 2005). MDV infects many birds that are part of the *Phasianidae* family and results in a high mortality rate in *Gallus gallus domesticus* (Common poultry). This virus was first isolated in 1968 (Churchill, 1968) and Josef Marek first described this virus in 1907 as the causative agent of polyneuritis and as affecting mainly old chickens with low and negligible mortality. However, this is no longer the case as MDV infection mortality has risen drastically with severe symptoms like strong immunosuppression, tumours, and neurological disorders (Gimeno, 2008). The ever-rising virulence of MDV infection is leading to growing concerns over potential outbreaks due to the fact that evolution towards higher virulence in response to vaccine usage has occurred multiple times in the past (Nair, 2005). This is further elevated by the reduced genetic diversity across the poultry industry (Cheng et al., 2008). Novel therapeutic targets are required.

Some of the unique features that differentiate MDV from other *Alphaherpesviruses* is that it is strictly cell-associated (Nazerian et al., 1968), encodes an oncogene (*Meq*) within its own genome (Jones et al., 1992), establishes latency in lymphocytes (Shek et al., 1983) and is able to induce lymphomas (Biggs and Payne, 1967). There are three serotypes of MDV, and each of these serotypes has significant differences both in the genome and biological features. Serotype 1 (RB1B) MDV is a common wild-type virus that includes all oncogenic strains and their attenuated forms. Serotype 2 is the non-oncogenic virus isolated in chickens. Serotype 3 is the non-oncogenic virus isolated from turkeys generally known as herpesvirus of turkeys (HVT) (Gimeno, 2008). Viral cloning, the introduction of overlapping viral genomic fragments into a bacterial artificial chromosome (BAC) vector, has proven to be an indispensable research tool for the MDV field (Zelnik, 2003). The MDV genome is about 175 kb with a circular structure and consists of several

regions, unique long (UL) and unique short (US) regions are flanked by terminal repeats long (TRL), short (TRS) and internal repeats long (IRL) and short (IRS) domains (Zelnik, 2003).

MDV infection starts with inhalation of viral particles shed from the feather follicles of infected birds. Within 24-hours of contact with the lungs, the viral genome can be detected in the spleen, thymus and bursa of the infected bird (Schat et al., 1984). This efficient transmission of the viral infection from the lungs is attributed to infected macrophages in the lung, which transfer the infection to B lymphocytes (Baaten et al., 2009, Barrow et al., 2003, Calnek, 2001). All viral movement throughout the infected bird is achieved via cell-associated viral spread; unenveloped MDV is not infective (Nazerian et al., 1968). MDV infection occurs in four distinct stages, early cytolytic, latent, late cytolytic and transformation (Addinger and Calnek, 1973, Osterrieder et al., 2006). During the early cytolytic infection stage, the virus replicates in macrophages and T and B lymphocytes, and after 7-days latency is established in T-lymphocytes (Arumugaswami et al., 2009, Trapp et al., 2006). Latently infected T-lymphocytes are capable of being transformed by the viral infection, facilitated by the *Meq* viral oncogene 14-21-days post infection. This results in the formation of lymphomas in visceral organs (Burgess and Davison, 2002, Calnek, 2001, Nair, 2005, Osterrieder et al., 2006, Trapp et al., 2006, Witter, 1997). Eventually, the feather follicle epithelium (FFE) becomes infected via peripheral lymphocytes (Johnson et al., 1975). FFE is the only cell type that can produce mature cell-free MDV virions that can persist in the external environment and infect a new host (Calnek, 2001, Osterrieder et al., 2006).

### 1.4.1: MDV interactions with the host cytoskeleton

There are only two papers in the literature that investigate microtubules in the context of MDV infection. The first paper shows that tegument protein VP22 co-localises with microtubules. The N-terminal truncation mutants of VP22 can still co-localize with microtubules (O'Donnell et al., 2002). Schumacher et al. (2005) used a viral plaque assay to conclude that microtubules are

dispensable for MDV viral spread. This conclusion was reached after MDV viral plaque size and plaque number had not changed compared to control after treating a BAC20 (recombinant wild type MDV) transfected CEF monolayer with nocodazole (microtubule depolymerising drug) for five days. This observation is probably the reason why no further research has been carried out on MDV and its possible association with microtubules.

Schumacher et al. (2005) also suggested that US3 from MDV is required for efficient de-envelopment of perinuclear viral particles and plays a role in actin stress fibre breakdown in the late stages of viral infection. This was also shown in HSV-1 infection (Wild et al., 2015). They also used Cytochalasin D (F-actin depolymerising drug) to demonstrate that F-actin is essential for MDV viral spread in a plaque assay. The same group went on to further characterise the role of US3 by generating a point mutation in the BAC20 US3 gene to mutate its kinase domain. Phosphorylation of pp38 (MDV-specific lytic phosphoprotein) was inhibited in this mutant and had the same growth properties as the US3 deletion with primarily enveloped virions found to accumulate at the perinuclear space (Schumacher et al., 2008). However, the mutation of the catalytic domain did not affect the ability of the virus to modulate the actin cytoskeleton. This suggested that US3 modulation of the actin network is independent of US3 kinase activity. Richerioux et al. 2012 have pursued the findings that cytochalasin D treatment of viral plaques results in smaller and fewer MDV plaques. They show that Jasplakinolide which promotes actin polymerisation also significantly reduced viral plaque area. Inhibiting the Rho and ROCK signalling pathways results in smaller viral plaques and inhibiting Rac signalling with inhibitors results in larger viral plaques (Richerioux et al., 2012). Beta-actin mRNA expression is also increased 2-fold during MDV infection (Neerukonda et al., 2016). These papers suggest that microtubules may be dispensable during MDV infection, but that actin is essential and requires fine modulating by the US3 protein. However, many other Alphaherpesviruses rely on the host microtubule network for efficient infection and it is unlikely that an entirely cell-associated virus such as MDV does not depend upon the microtubule network for its life cycle.

## 1.5: Outline of this work

Based on the extensive literature regarding microtubule-based transport of *Alphaherpesviruses* it would be surprising that MDV infection would not be associated with microtubules. Therefore, it was important to reinvestigate the role of microtubules in MDV infection, and to determine if and how MDV particles are transported along them.

The first aim was to establish whether MDV infection depends on microtubules. To achieve this, viral plaque assays with small molecule inhibitors were used to first determine the importance of microtubules. Then, infected cell shape was analysed and the relevance of dynamic microtubules for cell shape was elucidated. The possible role of PTMs during MDV infection was also studied.

In the next step we aimed to determine whether MDV viral particles are associated with microtubules in the cytoplasm. To achieve this, fluorescently labelled viral capsid proteins were used in super-resolution microscopy experiments to show viral capsid transport along microtubules and describe their dynamic characteristics. Electron microscopy was used to determine the native state (i.e., naked or enveloped) of MDV particles in the cytoplasm.

Finally, we attempted to identify the microtubule motor proteins that are responsible for transporting MDV viral particles. This was achieved by using a combination of small molecule inhibitors, shRNA mediated depletion and split kinesin assays.

# Chapter 2: Methods

## 2.1: Molecular Biology

### 2.1.1: Polymerase Chain Reaction (PCR)

PCR amplification was carried out using high-fidelity Phusion Taq or Taq DNA polymerase (NEB, UK) for cloning and gene expression analysis. The PCR mix was prepared to a total volume of 50µl (Table 1) and amplified in a Biometra T3000 thermocycler using conditions in Table 2. Primers used are detailed in Table 3 and combinations of primers used in Table 4. PCR product amplification was confirmed by visualising 10 µl reaction mix with 2 µl 6x Orange G loading buffer on a 1% agarose gel containing safeview (1 µl:20 ml) on a UV table. Product sizes were compared to GeneRuler 1kb ladder (Fermentas). When required, PCR products were purified using PCR purification kit (BioBasic) or spin column gel extraction kit (BioBasic) in accordance with the manufacturer's instructions

| PCR component | Final concentration in 50 µl mix |
|---|---|
| DNA | 50 ng |
| Forward Primer | 10 µM |
| Reverse Primer | 10 µM |
| dNTP | 0.2 mM |
| HF buffer/Taq reaction buffer | 1x |
| Phusion/Taq Polymerase | 1U |

**Table 1: PCR mixture**

| Step | Temperature (ºC) | Time (min) |
|---|---|---|
| Initial Denaturing | 95 | 2 |
| Denaturing<br>Annealing<br>Extension | 95<br>60<br>72 | 0.5<br>0.5<br>0.5/kb |
| Denaturing, Annealing and Extension repeated for 20-35 cycles. | | |
| Final Extension | 72 | 10mins |
| Hold | 4 | Until removed |

**Table 2: PCR cycling conditions**

| Primer Name | Sequence | Experiment used/chapter |
|---|---|---|
| AS701_chKif13B_Fwd(1)<br>Pos: 2966 (nt) | TAT GGG CAC AAG CAG AGT GG | 5.1<br>Confirming shRNA mediated knockdown |
| AS702_chKif13B_Rev(1)<br>Pos: 3179 (nt) | CGA GAT TGC CCC TGT CTG AG | 5.1<br>Confirming shRNA mediated knockdown |
| AS703_chKif13B_Fwd(2)<br>Pos: 4458 (nt) | CTG ATG CAG GTC TGG GTA GC | 5.1<br>Confirming shRNA mediated knockdown |
| AS704_chKif13B_Rev(2)<br>Pos: 4729 (nt) | TGG GCA TCT TTT CGG GAC TC | 5.1<br>Confirming shRNA mediated knockdown |
| AS705_chKif13B_Fwd(3)<br>Pos: 4264 (nt) | TGT GAA TCG GCT TTC TGC GA | 5.1<br>Confirming shRNA mediated knockdown |
| AS706_chKif13B_Rev(3)<br>Pos: 4510 (nt) | TTG GCA TCT GAG GCA CGA AT | 5.1<br>Confirming shRNA mediated knockdown |
| AS707_chGAPDH_Fwd(1)<br>Pos: 833 (nt) | GAG GAC CAG GTT GTC TCC TG | 5.1<br>Confirming shRNA mediated knockdown |
| AS708_chGAPDH_Rev(1)<br>Pos: 1038 (nt) | TCC TTG GAT GCC ATG TGG AC | 5.1<br>Confirming shRNA mediated knockdown |

| | | |
|---|---|---|
| AS709_chGAPDH_Fwd(2) Pos: 51 (nt) | AGG CGA GAT GGT GAA AGT CG | 5.1 Confirming shRNA mediated knockdown |
| AS710_chGAPDH_Rev(2) Pos: 275 (nt) | GGT CAC GCT CCT GGA AGA TAG | 5.1 Confirming shRNA mediated knockdown |
| AS711_chGAPDH_Fwd(3) Pos: 275 (nt) | CTA TCT TCC AGG AGC GTG ACC | 5.1 Confirming shRNA mediated knockdown |
| AS712_chGAPDH_Rev(3) Pos: 429 (nt) | TCA CAA ACA TGG GGG CAT CA | 5.1 Confirming shRNA mediated knockdown |
| AS713_chKif13A_Fwd(1) Pos: 49 (nt) | AGG AGA GAG CTG GAG CTG AA | 5.1 Confirming shRNA mediated knockdown |
| AS714_chKif13A_Rev(1) Pos: 351 (nt) | GAC CCA GCT GCT CTG CAT TA | 5.1 Confirming shRNA mediated knockdown |
| AS715_chKif13A_Fwd(2) Pos: 350 (nt) | GTA ATG CAG AGC AGC TGG GT | 5.1 Confirming shRNA mediated knockdown |
| AS716_chKif13A_Rev(2) Pos: 494 (nt) | CTG CCG ACT CCC TTT TGG AT | 5.1 Confirming shRNA mediated knockdown |
| AS717_chKif13A_Fwd(3) Pos: 370 (nt) | CTG ATC CCA CGG CTC TGT TG | 5.3 Confirming shRNA mediated knockdown |
| AS718_chKif13A_Rev(3) Pos: 492 (nt) | GCC GAC TCC CTT TTG GAT CA | 5.1 Confirming shRNA mediated knockdown |

**Table 3: Primers used in this study.**

### 2.1.2: RNA extraction and RT-PCR

DF-1 cells transfected with pSuper-CherryTub-shKifX plasmids were grown for RNA expression in 6 well plates. Transfection efficiency was checked on Olympus IX71 inverted fluorescence microscope with Deltavsion system (Applied Precision LLC) using mCherry filters. Only when the transfection rate was above 70%, the cells were harvested. Transfected DF-1 cells were trypsinized, and cell pellets were washed with PBS twice at RT by centrifugation at 500xg for 3 minutes. 1.4ml TRIzol reagent (ThermoFisher Scientific) was added to the cell pellet. The pellet was vortexed until entirely re-suspended. After 5 minutes of incubation at RT; 300 µl of chloroform was added to the cell extract. This was vortexed and incubated for 5 minutes at RT. The mixture was centrifuged for 10 minutes at 12,000 xg at RT. The clear top layer was then taken and mixed with 700µl of isopropanol through

inversion and incubated at room temperature (RT) for 10 minutes. RNA was precipitated by 10 minutes of centrifugation at 12,000 xg at RT. The supernatant was discarded, and the pellet was washed with 70% ethanol. This was then centrifuged for 5 minutes at 7,500 xg at RT. The supernatant was discarded, and the pellet was air dried. The pellet was re-suspended in 40 µl nuclease –free dd$H_20$ and then incubated at 50ºC for 20 minutes. RNA was stored at -20 ºC.

Purified RNA was then immediately used to synthesise cDNA. 0.2 µg of random hexamer primers were mixed with 10 mM dNTP mix, and 1 µg of total RNA. This was made up to 12 µl in nuclease free dd$H_2O$ and heated to 65ºC for 5 minutes before quickly chilling for 2 minutes in ice. Next, first strand buffer was added to a final concentration of 1x, along with DTT to a final concentration of 1 mM. This mixture was incubated at RT for 5 minutes, and then 200 U of M-MLV Reverse transcriptase polymerase was added to the mix. This was mixed and incubated at RT for 10 minutes. The mixture was then incubated at 37 ºC for 50 minutes and then heat inactivated at 70 ºC for 15 minutes. This cDNA was then stored at -20ºC until it was used as a template for PCR.

| Primer pairs | Expected band size and source |
|---|---|
| AS701 + AS702 | 233 bp<br>cDNA from DF-1 cells |
| AS703 + AS704 | 291 bp<br>cDNA from DF-1 cells |
| AS705 + AS706 | 266 bp<br>cDNA from DF-1 cells |
| AS707 + AS708 | 173 bp<br>cDNA from DF-1 cells |
| AS709 + AS710 | 245 bp<br>cDNA from DF-1 cells |
| AS711 + AS712 | 174 bp<br>cDNA from DF-1 cells |
| AS713 + AS714 | 313 bp<br>cDNA from DF-1 cells |
| AS715 + AS716 | 164 bp<br>cDNA from DF-1 cells |
| AS717 + AS718 | 142 bp<br>cDNA from DF-1 cells |

**Table 4: Primer pair combinations used and expected product sizes**

### 2.1.3: Cloning

PCR products were digested with restriction enzymes from NEB (used according to manufacturer's instructions), or genes/markers were digested out of previously made constructs. The backbone plasmids were also restriction enzyme digested. These backbone vectors and inserts were separated on an agarose gel bands cut out and DNA fragments were extracted using a spin column gel extraction kit (BioBasic). The fragments were then ligated for 10 minutes at RT using T4 DNA ligase in rapid ligation buffer (Thermo Scientific).

Chemically competent TOP10 cells were made by picking a single colony of TOP10 cells and growing overnight in 3ml DYT media (16 g/L tryptone, 10 g/L yeast extract and 5 g/L NaCl, pH 7). 3ml of culture of TOP10 cells was then added into 600ml fresh DYT media supplemented with 20 mM $MgSO_4$. Culture was grown until $OD_{600}$ = 0.48. At this point onwards, everything was carried out in a cold room and all equipment was precooled. TOP10 cells were then pelleted at 2000 xg at 4ºC. Supernatant was discarded, and pellet was suspended in 180 ml Tfb1 buffer (30 mM KAc, 50 mM $MnCl_2$, 100 mM RbCl, 10 mM $CaCl_2$, 15% v/v glycerol, pH 5.8 (adjusted with HAc)) and incubated on ice for 5 minutes. Cells were then pelleted at 1000 xg for 10 minutes at 4ºC. Supernatant was discarded, and the cell pellet was resuspended in 8 ml Tbf2 buffer (10mM 3-(N-morpholino)propanesulfonic acid (MOPS) (pH 7), 75 mM $CaCl_2$, 10 mM, RbCl, 15% v/v glycerol, pH 7.0 (adjusted with NaoH)) and was incubated on ice for 15 minutes. The TOP10 cells were then aliquoted and snap frozen in liquid $N_2$ and stored at -80ºC.

Chemically competent TOP10 cells were transformed by adding the ligation product to thawed cells. These were incubated on ice for 20 minutes. Then heat-shocked at 42ºC for 45s. The transformed cells were allowed to recover for 1 hour at 37ºC in SOC medium (0.5% Yeast Extract, 2% Tryptone,10 mM NaCl, 2.5 mM KCl, 10 mM MgCl2, 10mM MgSO4, 20 mM Glucose, pH 7). The cells were pelleted at 2000 xg for 5 minutes at RT, re-suspended in 100 µl SOC, and then plated on to LB agar plates containing the appropriate antibiotic. The plate was placed in 37ºC overnight (ON). Single colonies from the plate then picked and grown in 3 ml DYT media overnight. Plasmid DNA

was extracted using Mini-prep spin column kit (BioBasic). The positive clones were further confirmed by restriction digest and sanger sequencing.

### 2.1.4: Construction of shRNA plasmids

Firstly, target sites were determined using RNAi Central (http://cancan.cshl.edu/RNAi_central/RNAi.cgi?type=shRNA). Then 19 base pairs from the start of the site was used to design forward and reverse oligos using the following template (see table 5 for actual sequences):

Forward oligo:
5':gatcccc(sense_target_sequence)ttcaagaga(antisense_target_sequence)ttttc:3'
Reverse oligo:
5':tcgagaaaaa(sense_target_sequence)tctcttgaa(antisense_target_sequence)ggg:3'

The matching pairs were then annealed by mixing 5 mM final concentration of each oligo along with 1x T4 ligase buffer in 30 µl total volume. The mixture was then incubated at 94ºC for 4 minutes then cooled down to 60 ºC at 0.01 ºC/s and then to 4 ºC at a rate of 0.03 ºC/s. To phosphorylate ends, 1x Polynucleotide Kinase (PNK) buffer, 0.5mM ATP and 20U PNK final concentrations were added in a final volume of 50 µl. The mixture was incubated at 37ºC for 1 hour. These double-stranded DNA fragments were then cloned into pSuper_NeoGFP expression plasmid (Oligoengine) digested with BglII and XhoI restriction enzymes (NEB). Colonies were picked and screened using restriction enzymes BglII and NcoI (NEB). The successful insert was checked using Sanger sequencing.

The Neo_GFP tag was replaced with a mCherry Tubulin tag. This was achieved by digesting both the newly made pSuper_shKifx_NeoGFP and pSuper-mCherryTubulin_EB3 (Straube and Merdes, 2007) plasmids with BamHI and NheI restriction enzymes. The 2089 base pair (bp) band from pSuper_mCherryTubulin_EB3 and 3718 band from pSuper_shKifx_NeoGFP

plasmids were then ligated. The correct insert was confirmed by restriction enzyme digest using XhoI (NEB), Sanger sequencing, and transfection of CEFs to visualise microtubules.

| Plasmid name | Description | Experiment used/ chapter |
|---|---|---|
| pBa-Kif5c 559-tdTomato-FKBP | Kif5C motor domain with a tdTomato and FKBP tag Provided by Banker Lab (OHSU) | Split kinesin assay / 5.1 |
| pBa-FRB-3myc-Kif 1a 395-1695 | Kif1a tail domain with 3myc and FRB tag Provided by Banker Lab (OHSU) | Split kinesin assay / 5.1 |
| pBa-FRB-3myc-Kif 1B alpha tail | Kif1Ba tail domain with 3myc and FRB tag Provided by Banker Lab (OHSU) | Split kinesin assay / 5.1 |
| pBa-FRB-3myc-Kif 1b Beta 386-1770 | Kif1Bb tail domain with 3myc and FRB tag Provided by Banker Lab (OHSU) | Split kinesin assay / 5.1 |
| pBa-FRB-3myc-Kif 5c tail | Kif5C tail domain with 3myc and FRB tag Provided by Banker Lab (OHSU) | Split kinesin assay / 5.1 |
| pBa-FRB-3myc-Kif 17 400-1038 | Kif17 tail domain with 3myc and FRB tag Provided by Banker Lab (OHSU) | Split kinesin assay / 5.1 |
| pBa-FRB-3myc-Kif 21B tail | Kif21B tail domain with 3myc and FRB tag Provided by Banker Lab (OHSU) | Split kinesin assay / 5.1 |
| pBa-FRB-3myc-mmKif 13A tail | Kif13A tail domain with 3myc and FRB tag Provided by Banker Lab (OHSU) | Split kinesin assay / 5.1 |
| pBa-FRB-3myc-mmKif13B tail | Kif13B tail domain with 3myc and FRB tag Provided by Banker Lab (OHSU) | Split kinesin assay / 5.1 |
| pSuper_shKif13A(1)_mCherryTub | A plasmid expressing shRNA against target sequence: AGCCAGTGAAGCTTCTTCA (Kif13A) with mCherryTub expressed independently Target start position: 1713 bp | RNAi Knockdown experiments / 5.3 |
| pSuper_shKif13A(2)_mCherryTub | A plasmid expressing shRNA against target sequence: GAAGTCTGGAAGTCATGGA (Kif13A) with mCherryTub expressed independently Target start position: 2561 bp | RNAi Knockdown experiments / 5.3 |
| pSuper_shKif13B(1)_mCherryTub | A plasmid expressing shRNA against target sequence: CCACACACTTTATGATGTG (Kif13B) with mCherryTub expressed independently Target start position: 696 bp | RNAi Knockdown experiments / 5.3 |
| pSuper_shKif13B(2)_mCherryTub | A plasmid expressing RNAi against target sequence: GATGACTTTAGCTCCCAAG (Kif13B) with mCherryTub expressed independently Target start position: 3541 | RNAi Knockdown experiments / 5.3 |
| pSuper_shLuciferase(1)_mCherryTub (Straube and Merdes 2007) | A plasmid expressing shRNA against target sequence CGTACGCGGAATACT TCGA (Luciferase) with mCherryTub expressed independently | RNAi Knockdown experiments / 5.3 |
| pSuper_shKif1B(1)_mCherryTub | A plasmid expressing shRNA against target sequence: AGCCAGTGAAGCTTCTTCA (Kif1B) with mCherryTub expressed independently Target start position: 647 bp | RNAi Knockdown experiments / 5.3 |

| | | |
|---|---|---|
| pSuper_shKif1B(2)_mCherryTub | A plasmid expressing shRNA against target sequence: TGGGCCAGAGTGTGAGCAA (Kif1B) with mCherryTub expressed independently Target start position: 3383 bp | RNAi Knockdown experiments / 5.3 |
| pSuper_shKif13A/B(1)_mCherryTub | A plasmid expressing shRNA against target sequence: AAGTATCCTACATGGAGAT (Kif13A+B) with mCherryTub expressed independently Designed to knock down both Kif13A and B Target start position: 440 bp | RNAi Knockdown experiments / 5.3 |
| pSuper_shKif13A/B(2)_mCherryTub | A plasmid expressing shRNA against target sequence: ATCCTACATGGAGATATAC (Kif13A+B) with mCherryTub expressed independently Designed to knock down both Kif13A and B Target start position: 666 bp | RNAi Knockdown experiments / 5.3 |
| pSuper_shKif21B(1)_mCherryTub | A plasmid expressing shRNA against target sequence: TCCCAGACAATCTCGTGTC (Kif21B) with mCherryTub expressed independently Target start position: 3630 bp | RNAi Knockdown experiments / 5.3 |
| pSuper_shKif21B/B(2)_mCherryTub | A plasmid expressing shRNA against target sequence: ACCCAAATAATGTCGTTTC (Kif21B) with mCherryTub expressed independently Target start position: 4055 bp | RNAi Knockdown experiments / 5.3 |

**Table: 5 Plasmids used in this study**

### 2.1.5: Western Blotting

Western blotting was carried out by running whole cell extracts on polyacrylamide gels (see Table 6 for full details). The gels were cast between two glass slides. First the separating gel was poured, allowed to polymerise and then followed by the stacking gel. A comb was inserted, and the gel was allowed to polymerise for 30 minutes at RT. Each well was loaded with whole cell extracts containing 1x Laemmli protein buffer (2% SDS, 62.5mM Tris-HCl pH 6.8, 25% glycerol, 0.01% Bromophenol Blue and 5% β-mercaptoethanol) The gel was ran at 16 mA per gel in the tank for 90 minutes at RT in gel running buffer (25 mM Tris, 192 mM glycine, 0.1% SDS). The proteins on the gel were then transferred to a nitrocellulose membrane by electroblotting at 400mA for 90 minutes in transfer buffer (25 mM Tris, 192 mM glycine, 10% methanol). The membranes were then blocked with 5% milk in PBS and then incubated in primary antibody overnight at 4$^{o}$C in 0.5% milk in 0.1%Tween in PBS (PBST). The membrane was then washed with PBST three times, 10 minutes each. The membrane was then treated with each species-specific secondary antibody conjugated to horseradish peroxidase (HRP) for an hour at RT. The

membrane was washed with PBS 3x, 10 minutes each. The membrane was then developed with pico or femto chemiluminescence kit and exposed to film for 1-10 minutes and developed using Xograph, Compact X4 film developer.

| **Separating gel** | | | | |
|---|---|---|---|---|
| Separating gel percentage | 8 | 10 | 12 | 15 |
| dd$H_20$ (ml) | 5.3 | 4 | 3.3 | 2.3 |
| Seperation buffer (Tris-HCL (1.5 M, pH 8.8 , 10% SDS) (ml) | 2.5 | 2.5 | 2.5 | 2.5 |
| 30% Acrylamide/Bis-Acrylamide solution (ml) | 2.67 | 3.33 | 4 | 5 |
| 10% Ammonium Sulphate (APS) (µl) | 200 | 200 | 200 | 200 |
| *N*,*N*,*N*′,*N*′-tetramethylethylene-diamine (TEMED) (µl) | 10 | 10 | 10 | 10 |

| **Stacking gel** | | | | |
|---|---|---|---|---|
| dd$H_20$ (ml) | Stacking buffer (Tris-HCL (0.5 M, pH 6.8 , 10% SDS) (ml) | 30% Acrylamide/ Bis-Acrylamide solution (ml) | 10% Ammonium Sulphate (APS) (µl) | *N*,*N*,*N*′,*N*′-tetramethylethylene-diamine (TEMED) (µl) |
| 2.7 | 1.13 | 0.6 | 80 | 8 |

**Table 6: Details of acrylamide gel composition**

| Antibody name / clone / source | Dilutions | Target |
|---|---|---|
| DM1A a-Tub (mouse), Alexa Flour 647, Sigma<br>Cat#: T6199<br>Lot#: 2949133 | IF 1:1000 | Anti a –tubulin with Alexa Flour 647 congregate |
| DM1A a-Tub (mouse), Sigma<br>Cat#: T6199<br>Lot#: 037K4772 | IF1:1000<br>WB 1:10,000 | Anti a -tubulin |
| 6-11B-1 Ace-Tub (mouse), Sigma<br>Cat#: T7451<br>Lot#: 025K4794 | IF 1:300<br>WB: 1:4000 | Anti-Acetylated Tubulin modification |
| GT335 Poly-Glut-Tub (rabbit), Adipogen<br>Cat#: AG-20B-0020-C100<br>Lot#: A20631002 | IF 1:2000<br>WB 1:8000 | Anti Poly Glutamate modification tubulin |
| IN105 PolyE-Tub (mouse) Adipogen<br>Cat#: AG-25B-0030-C050<br>Lot#: A26381411 | IF 1:1000<br>WB 1:4000 | Anti poly Glutamate chains |
| GFP- 1020 Chicken IgY<br>Aves labs<br>Cat#: GFP-1020<br>Lot#: 0511FP12 | IF 1:5000 | Anti GFP antibody from chicken |
| Goat anti mouse IgG<br>Promega W402B | WB 1:4000 | Secondary antibody from goat anti mouse with a HRP conjugate |
| Goat anti rabbit IgG<br>Promega W401B | WB 1:4000 | Secondary antibody from goat anti rabbit with a HRP conjugate |
| Donkey anti rabbit IgG Alexa 488<br>Molecular Probes A-21206 | IF 1:500 | Secondary antibody anti rabbit with Alexa 488 label |
| Donkey anti rabbit IgG Alexa 594<br>Molecular Probes A-21207 | IF 1:1000 | Secondary antibody anti rabbit with Alexa 594 label |
| Donkey anti rabbit IgG Alexa 647<br>Molecular Probes A-31573 | IF 1:300 | Secondary antibody anti rabbit with Alexa 647 label |
| Donkey anti mouse IgG Alexa 488<br>Molecular Probes A-21202 | IF 1:500 | Secondary antibody anti mouse with Alexa 488 label |
| Donkey anti mouse IgG Alexa 594<br>Molecular Probes A-21203 | IF 1:1000 | Secondary antibody anti mouse with Alexa 594 label |
| Donkey anti mouse IgG Alexa 647<br>Molecular Probes A-31571 | IF 1:300 | Secondary antibody anti mouse with Alexa 647 label |
| Goaf anti chicken IgY –CF488A<br>Sigma SAB4600039 | IF 1:1000 | Secondary antibody anti chicken with CF488A label |

**Table 7: List of antibodies used in this study**

## 2.2: Cell Biology

### 2.2.1: CEF harvesting and maintenance

Chicken embryo fibroblasts (CEFs) were obtained from 10-day old chicken embryos (*Gallus gallus domesticus*, *Bovans Brown*, Henry Stewart and Co. Ltd) according to a standardized protocol (Lam, 1995). Ethics was obtained by Animal Welfare and Ethical Review Body (AWERB) and project reference is 29/15-16. Eggs were kept at 37 ºC at 80 % humidity until day 10 after fertilization. Briefly, 10-day old fertilised chicken eggs were opened, embryos decapitated and separated from the yolk. Embryo bodies were then cut into small pieces using scissors, washed in warm PBS and covered with 0.025% trypsin-EDTA (Sigma) for 2 minutes at room temperature (RT). Supernatant was transferred into 10 volumes of FBS. The digestion process was repeated four times, each time covering the embryo pieces with trypsin. The cells were pelleted out of FBS by centrifugation at 500 xg for 5 minutes and re-suspended in complete CEF media (1x Medium 199 (Sigma), 10% Tryptose phosphate broth (Sigma), 2.3 g/l sodium bicarbonate (Sigma), 1 mM L-Glutamine (Sigma), 100 U/ml penicillin and streptomycin (Sigma) and 10% FBS (Sigma)). The cells were subsequently passed through a 40µm filter to remove any large clumps. The cells were then pelleted by centrifugation at 500 xg for 5 minutes and re-suspended in freezing media (90% FBS + 10% DMSO (99.9%)). Aliquots were frozen using Mr. Frosty freezing containers cooling at 1 ºC/min until -80 ºC and stored in liquid nitrogen.

For routine cell culture, a frozen aliquot of CEFs was thawed at 37 ºC and transferred to 5ml CEF media. The CEF were spun briefly at 500 xg, and the pellet was re-suspended in pre-warmed 5 ml CEF media and transferred to a T25 flask. The cells were incubated in a humidified incubator at 38.5 ºC and 5% $CO_2$. During cell passaging, CEFs were first washed with PBS once and subsequently treated with 0.025% trypsin-EDTA (Sigma) for 3-5 minutes at 38.5 ºC. Detached cells were then re-suspended in CEF media to inhibit the trypsin-EDTA, and transferred to a new T25 flask at a 1:2 ratio split. The

number of splits per batch of frozen cells was kept to a maximum of 4 passages

### 2.2.2: Other cell line maintenance

Prof. Venugopal Nair's group kindly provided DF-1 cells, these are an immortalised chicken fibroblast cell line. Frozen aliquots of passage 10 DF-1 cells were thawed in DF-1 complete media (High Glucose (4500ml/l) DMEM (D6429, Sigma) supplemented with 10% FBS and 100U/ml penicillin and streptomycin (Sigma)) and transferred to T25 flasks. The cells were incubated in a humidified incubator at 38.5 ºC and 5% $CO_2$. During cell passaging, DF-1 cells were first washed with PBS once and subsequently treated with 0.025% trypsin-EDTA (Sigma) for 3-5 minutes at 38.5 ºC. Detached cells were then re-suspended in DF-1 media to inhibit the trypsin-EDTA, and transferred to a new T25 flask at a 1:10 ratio split. The number of splits was kept to a maximum of 10 passages after thawing cells.

### 2.2.3: Transfections

Transfection of expression plasmids into cells was carried out with FuGENE-6 transfection reagent (Promega). Briefly: 1-2ug of plasmid DNA was added into 50µl of OptiMEM (Sigma) medium. This mixture was vortexed for 5 seconds, and 4.5 µl/per µg of DNA of FuGENE 6 transfection reagent was added. The transfection solution was mixed by pipetting for 1min. The mixture was incubated at RT for 15 minutes. Fresh media was added to dishes prior to drop-wise addition of the transfection mixture into each FluoroDish quadrant (FisherScientific). Transfected cells were at 80 % confluence. More significant volumes of transfection were scaled up accordingly. In the case of multiple plasmid transfections; the plasmids were mixed well, before mixing with OptiMEM media.

### 2.2.4: Establishment and maintenance of virus infection

Viruses used in this study:

RB1B UL35-GFP: Wild type strain of MDV that has had GFP fused to the small capsid protein UL35. This tag allowed visualisation of individual viral particles in the nucleus and the cytoplasm. The GFP tag resulted in attenuation of infection and the virus spread 50% slower than the parental virus used to generate tagged virus in a cell monolayer (Kut and Rasschaert, 2004).

RB1B TK GFP: Wild type strain of MDV that expresses GFP from a TK promotor. This allowed visualisation of infected cells and to follow viral spread. No attenuation of virus spread was detected with this tag compared to the parental virus used to generate this fluorescent virus (Shimojima et al., 1997).

RB1B EGFP-UL49: Wild type strain of MDV that expresses EGFP tag on the N-terminal of UL49 gene product. This tag allowed visualisation of UL49 protein in an MDV infected cell. This virus has attenuated viral spread in a monolayer at 60% compared to the parental virus (Remy et al., 2013).

CEF cells were transfected with BAC DNA of RB1B UL35-GFP (kindly provided by V. Nair's group) (Kut and Rasschaert, 2004) or RB1B TK GFP (Shimojima et al., 1997) (also kindly provided by V. Nair's group) or RB1B EGFP UL49 (Remy et al., 2013) (kindly provided by C. Denesvre group) using Lipofectamine 2000. Briefly: Fresh CEFs were seeded into six-well plates when cells reached 80% confluence, 2 µg of BAC DNA was added to 180 µl of OptiMEM, mixed by very gently pipetting then 20 µl of Lipofectamine 2000 was added to the mixture. The transfection solution was mixed by inversion and incubated for 20 minutes at RT. 800 µl of OptiMEM was added to the mixture. 1ml of transfection mix was added to CEFs by completely replacing media. The cells were then returned to the incubator. The transfection mixture was replaced with 2 ml complete CEF media after 6 hours.

Once transfection had occurred, the virus infection spread in the CEF monolayer. Maximal infection is usually reached after 5-6 passages – fresh

CEFs are added after three passages. After infection reaches around 30-50%, the cells are frozen in freezing media (90% FBS and 10% DMSO) and stored at -80ºC. Plaque forming units/ml (PFU/ml) were calculated from each harvested batch using plaque assays. Here, infected cells were thawed, diluted and seeded onto a monolayer of uninfected CEFs. The new infection was initiated by co-culturing with uninfected CEFs. The number of plaques per well were counted. Infection was maintained by passaging infected CEFs onto new CEFs for a maximum of 10 passages.

### 2.2.5: Immunofluorescence staining

CEFs or infected CEFs were seeded onto 16mm round coverslips at 10,000 cells per coverslip. Once cells adhered, incubated for 12 hours, they were fixed using Fixation buffer (4% Paraformaldehyde (PFA) (Electron Microscopy Sciences), and 0.1% Glutaraldehyde (GA) (Electron Microscopy Sciences) in MRB80 (80mM PIPES pH 6.9, 1mM EGTA, 4mM MgCl) and adjusted to pH 7.5) for 10 minutes. PFA and GA were then reduced with 0.1% $NaBH_4$ for 7 minutes. Cells were blocked and permeabilised with 3% BSA and 0.2 % Triton X100 (Sigma) in PBS at room temperature (RT) for 1 hour prior to incubation with primary antibodies/cell stains (e.g., DM1A (1:1000) or 647-phalloidin (1:1000)) for 1 hour in 3% BSA (Sigma) and 0.2 % Triton X100 in PBS in a humidified chamber. Cells were washed 1x in 0.3% BSA, 0.02% Triton X100, followed by 2x PBS, prior to incubation with the appropriate species-specific secondary antibodies (anti-mouse Alexa 561 (1:500) for DM1A). Coverslips were washed with PBS and stained with DAPI (0.1 µg/ml) for 1 minute. The coverslips were washed with PBS x3 and mounted onto glass slides using Vectashield (H-1000) and sealed with nail varnish. Slides were visualised using a spinning disk confocal system (Ultraview Vox, Perkin Elmer) with a 100x 1.4 NA oil-immersion objective.

Cells were fixed with methanol by removing media on cells and replacing with ice-cold methanol and placed in -20ºC for 1 hour. Methanol fixed cells were prepared for immunoflouresence by removing the methanol from the wells and washing with PBS at RT 3x, 5 minutes each. The cells were then blocked right

away using with 3% BSA in PBS for 1 hour at RT. Cells were then incubated with primary antibodies/cell stains (e.g. DM1A (1:1000) or 647-phalloidin (1:1000)) for 1 hour in 0.3% BSA (Sigma) in PBS in a humidified chamber. Cells were washed with PBS 3x 5 minutes at RT, prior to incubation with the appropriate species-specific secondary antibodies (i.e. anti-mouse Alexa 561 (1:500) for DM1A) for 1 hour. The coverslips were washed with PBS x3 and mounted onto glass slides using Vectashield (H-1000) and sealed with nail varnish. Slides were visualised using a spinning disk confocal system (Ultraview Vox, Perkin Elmer) with a 100x 1.4 NA oil-immersion objective.

### 2.2.6: Plaque Assays

Confluent CEFs were infected with 100 plaque forming units (PFU) of RB1B TK GFP. Twenty-four hours post infection each well was treated with varying concentrations of either, Nocodazole, Cytochalasin D, Taxol or DMSO. 48 hours post infection the dishes were imaged live using an Olympus IX71 inverted fluorescence microscope with Deltavision system (Applied Precision LLC) in a stage-top incubator (Tokai Hit) at 37 ºC and 5% $CO_2$. The acquisition was controlled by Softworx (Applied Precision LLC) with 10x 0.40 NA air objective. The GFP channel was imaged for every plaque detected. The area of each plaque was measured manually using the free line tool in Fiji (Image J). Three independent replicates were carried out for each experiment with a minimum of 60 plaques analysed for each replicate. Statistical significance was determined using a one-way ANOVA.

### 2.2.7: Cold treatment assay

CEFs were seeded onto 16mm round coverslips in 12 well plates at 30-50% confluence and incubated in a humidified incubator at 38.5 ºC and 5% $CO_2$. The next day, the plate was taken out of the incubator and directly placed on ice for 10 minutes, ensuring the plate was covered with ice. The media was then completely removed, and cells were fixed in -20ºC methanol for 1 hour. The coverslips in each well were then prepared for immunofluorescence (see immunofluorescence section for detailed protocol) with antibodies against α-tubulin and acetylated α-tubulin. Slides were visualised using a spinning disk

confocal system (Ultraview Vox, Perkin Elmer) with a 100x 1.4 NA oil-immersion objective. Complete cell Z-stacks were taken for 10 cells at each condition. Stacks were then Z projected using Fiji and mean intensity of microtubule density was measured in the cytoplasm. The experiment was repeated 3 times. Statistical significance was determined using a two-sample t-test.

### 2.2.8: Viral capsid transport assay

CEFs infected with RB1B UL35-GFP were seeded into fluorodishes (40,000 cells per dish). After 24 hours, the cells were treated with 5 μM Nocodazole or 500 pM Taxol or 100 μM Celiobrevin D or DMSO in imaging media (L-15 with 5% FBS, 1 mM L-Glutamine (Sigma), and 100 U/ml penicillin and streptomycin (Sigma)) for 1 hour in a humidified incubator at 38.5 ºC and 5% $CO_2$. Infected cells were imaged using a spinning disk confocal system at 37 ºC (Ultraview Vox, Perkin Elmer) with a 100 x1.4 NA oil-immersion objective, 3 x Z-stacks at 0.75μm step size and at 2.6 frames per second (FPS) for 3 minutes using 488 nm laser. Movies were then Z-projected using Fiji. Viral capsids were tracked semi-automatically using Image-Pro Analyzer. Viral capsid dynamics were determined by first tracking all viral capsids that were 5 μm away from the closest nucleus. The greatest distance each viral capsid travelled from its point of origin was then determined. If this was greater than 5 μm then that viral capsid was marked and shown as a 'run' suggesting active transport. Any viral capsid track lasting fewer than 100 frames was not considered for analysis. For all experiments 10 cells of each condition were tracked and every experiment was repeated 3 times. Statistical significance was determined using a two-sample t-test.

### 2.2.9: Split-Kinesin Assay

The plasmids pKif5C$^{559}$-tdTM-FKBP and pFRB-3myc_KifXtail (Kif5C, Kif17, Kif1A, Kif1Ba, Kif1Bb, Kif13A, Kif13B and Kif21B) (detailed in table 5), provided by G. Banker's Lab (Jenkins et al., 2012), were both transfected into CEFs using FuGENE6. Only a single kinesin tail construct was transfected along with the Kif5C plasmid. Therefore, there was be 8 kinesin tails

investigated during each experiment. Transfections were carried out in one quadrant of a fluorodish that has been separated into four quadrants (Fisher Scientific). The negative controls for this experiment were CEFs transfected with Kif5C motor domain plasmid only, and cells that had not undergone any transfection. Transfected cells were subsequently infected with RB1B UL35-GFP virus by co-culturing with infected CEFs. Two days post-transfection a small population of transfected cells would also be infected with RB1B UL35 GFP virus (0.5-1%). A single cell was imaged per quadrant. Using the spinning disk microscope, transfected and infected cells were selected and imaged with 3 x Z planes at 0.75μm step size at 2.6 FPS for 1 minute using a 488nm laser at 5% power. A 561nm image was taken to confirm transfection. Rapamycin (2nM final concentration) was then added, and after 10 minutes the same cell was imaged again using the same imaging conditions. Movies were then Z-projected using Fiji. Viral capsids were semi-automatically tracked using Image-Pro Analyzer. The greatest distance each viral capsid has travelled from its point of origin was then determined. If this was greater than 1.5 μm then that viral capsid was marked and shown as a 'run' suggesting active transport. Any viral capsid track lasting fewer than 50 frames was not considered for analysis. For all conditions between 4-10 cells were tracked. Statistical significance was determined using a paired t-test.

### 2.2.10: shRNA mediated depletion

The plasmids pSuper-CherryTub-shRNAKifX (Kif21B, Kif13B Kif13A, Kif13A/B and Kif1B) were each transfected individually into RB1B UL35-GFP infected CEFs using FuGENE6 according to the manufacturer's instructions and as described above. The transfected cells were subsequently infected by co-culturing with RB1B UL35-GFP infected CEFs. Two-days post transfection, cells that were both transfected and infected were selected and imaged with 3 x Z planes at 0.75μm step size at 2.6 FPS for 3 minutes using 488nm laser at 5%. A 561nm image was taken to confirm transfection. Movies were then Z-projected using Fiji. Viral capsids were semi-automatically tracked using Image-Pro Analyzer. The greatest distance each viral capsid has travelled from its point of origin was then determined. If this was greater than 3 μm then

that viral capsid was marked and shown as a 'run' suggesting directional movement. Any viral capsid track lasting fewer than 100 frames was not considered for analysis. For all conditions 6 cells were tracked at least per experiment and experiments were repeated 3 times independently. Statistical significance was determined using a two-sample t-test.

### 2.2.11: Cell Shape assay using Shape Space Explorer

CEFs infected with RB1B TK GFP virus were seeded at low density (10,000 cells) into fluorodishes. These cells were either treated with DMSO or 500 pM Taxol. Low-density seeding ensured that single cells could be imaged for a long time without interference from neighbouring cells and sequential cell shapes were obtained. Cells were imaged live using an Olympus IX71 inverted fluorescence microscope with Deltavsion system (Applied Precision LLC) in a stage-top incubator (Tokai Hit) at 37 ºC and 5% $CO_2$. A 20x air objective with 0.75 NA was used. The acquisition was controlled by Softworx (Applied Precision LLC) at 10 min/frame for 24 hours. GFP and bright-field images were taken. The GFP signal was used to confirm infected cells, and bright-field images were used to manually draw around each cell using the polygon tool in Fiji. For each cell at every time point in a sequential manner the cell shape was extracted until it was not possible to define cell shape due to interference from other cells or 20 time points had been reached. Using a custom macro each cell shape was saved. The saved cell shapes were then used in Shape Space Explorer (Jefferyes and Straube, unpublished) to visualise and quantify the morphology of cells in the data set. Ten cells per condition per experiment were analysed. Experiments were repeated 3 times independently.

### 2.2.12: STORM

CEFs were prepared for Stochastic optical reconstruction microscopy (STORM) by fixation in 4% PFA, 0.1% GA in MRB80 pH 7.5 for 10 minutes. PFA and GA were then reduced with 0.1% $NaBH_4$ for 7 minutes, and washed thrice with PBS (5 minutes each). Cells were then blocked and permeabilised with 3% BSA and 0.2 % Triton X100 in PBS pH 7.5 at RT for 1 hour.

Immediately after blocking, cells were incubated in primary antibody DM1A (1:1000 in 3% BSA and 0.2% Triton X100 in PBS (p.H 7) in a humidified chamber for 1 hour. Cells were washed 3x 5 minutes with PBS. The secondary antibody used was anti-mouse Alexa 647 (1:1000). Cells were incubated in secondary antibody diluted in 3% BSA and 0.2% Triton X100 in PBS pH 7 in a humidified chamber for 50 minutes. Cells were washed thrice in PBS (10 minutes each). Cells and antibodies were post-fixed using 4% PFA, 0.1% GA, MRB80 pH 7.5 for 5 minutes. After post-fixing, cells were washed 3x 5 minutes in PBS. PBS was replaced with STORM/OxEA buffer (Nahidiazar et al., 2016) (50 mM β-mercaptoethylamine hydrochloride (MEA, Sigma-Aldrich), 3% (v/v) OxyFlour (Oxyrase Inc.) and 20% (v/v) sodium DL-lactate solution (L1375, Sigma-Aldrich) in PBS, pH 8–8.5) prior to imaging.

STORM images were acquired using the Warwick Open Source Microscope (WOSM) TIRF system using an oil-immersion 100x 1.46 NA objective. 20,000 frames at 10ms exposure were acquired with 40-60 kW/cm$^2$ 647 nm laser power in combination with 1-5 kW/cm$^2$ of 405 nm laser. The sample was bleached with 100 kW/cm$^2$ laser power for 30s before acquisition. Reconstruction was performed using the Image J plugin ThunderSTORM (Ovesny et al., 2014). The parameters used were as follows: Image filtering: Wavelet filter (B Spline), Approximate localization at local maximum with 3*std(Wave.F1), Sub pixel localization at PSF: Integrated Gaussian with 3 pixel fitting radius and visualisation with average shifted histograms and 5x magnification. Further post processing was carried out after image generation, this were removing uncertainty (nm) values over 10, removing duplicates based on uncertainty values and correcting for drift based on cross correlation.

STORM staining using microfluidics was carried out by a simple microfluidics system that involved; a 2ml syringe connected to 10 cm long 0.1 mm thick tubing that lead to the chamber where the cells were growing. On the other side of the chamber was the output tubing that lead to a waste beaker. Flow was controlled using gravity. Chambers were made using PDMS 184 (Scientific laboratory Supplies). Chamber designs were cut from double sided tape using an electronic cutting tool (Silhouette Portrait). The positive chamber

designs were attached to the bottom of a 10cm petri dish and PDMS was poured to over to cover the moulds. PDMS was then de-gassed and baked at 60 ºC over night. Each chamber design was carefully removed from the mould to reveal a chamber underneath. The PDMS was then bound to a 50 mm x 24 mm glass coverslip using a bench top plasma generator (Henniker Plasma) for 3 minutes at 40W to charge the glass. The cut PDMS was then bound to the cover slip creating a chip. Input and output openings were created using a needle and tubing was inserted. CEFs were then seeded into the chamber with gravity flow and treated the same way as described above.

During this experiment, the viral capsids were imaged live for 1 minute in the chamber using the TIRF capabilities of the WOSM, and then cells would be fixed by flowing fixation buffer into the chamber. The fixed cells in the viewing chamber would then be stained for STORM by flowing in the buffers and then same cell imaged live previously would be processed for STORM imaging. By performing live imaging of viral capsids and the STORM imaging of the same cell on the same microscope mean no correlation between the two images was be required.

Correlative spinning disk confocal microscopy and STORM were carried out by using a girded glass bottom dish (MatTek), the infected cells were imaged live for 30s using a spinning disk microscope (Ultraview Vox, Perkin Elmer) with a 100x 1.4 NA oil-immersion objective and an environmental chamber. The cells were then fixed on the microscope stage using 2x fixing buffer to compensate for the media already in the dish during imaging. Imaging continued until all viral capsids stopped moving. The cells were then processed for STORM staining in the dishes, and the same cell was subsequently found again using the coordinates etched on to the dish on the WOSM. The cell was imaged using the WOSM with TIRF settings for viral capsids and microtubules. Then the STORM procedure was carried out. The two separate images were then correlated back together using the final frame of the dynamic viral capsid movie from the confocal and static viral capsid image from the WOSM. Correlation in X and Y, was achieved by using ICY

(image analysis software) and a plugin called eC-CLEM (Paul-Gilloteaux et al., 2017).

### 2.2.13: SRRF Microscopy

Super-resolution radial fluctuations (SRRF) images were obtained using an Inverted Marianas Microscope (3i, Denver, USA) with CSU-X1 spinning disk confocal (Yokogawa, Japan) and a sCMOS 95B Prime Camera (Photometrics) with a 100x 1.46 NA oil-immersion objective (Zeiss, Jena, Germany). Encased in a 37ºC degree incubator (Okolab, Italy). The acquisition was controlled by Slidebook 6.0 software (3i) using stream mode. CEFs cells infected with RB1B UL35-GFP were seeded onto fluorodishes. Prior to imaging, CEF media was replaced with SRRF imaging media (L-15, 5% FBS, P/S, L-Glut, 1% Oxyrase, 1 µM Verapamil) and treated with 1 µM SiR-tubulin dye (Lukinavicius et al., 2013) for 1 hour. Images were collected by direct streaming to the hard-drive to obtain 50 FPS acquisition rates using 647nm laser line with a single frame of 488nm every 50 647nm frames. Using the NanoJ-SRRF plugin (Gustafsson et al., 2016) in Fiji, movies of super-resolution microtubules were constructed at 1 FPS, and this was correlated with the 488 nm capsid image.

Viral capsid event occurrence was determined using the SRRF movies. These were scored with a 0 for absence or 1 for the presence for 9 different events. Three different categories describe capsids that are not associated with microtubules and are: (i) stationary (>500 nm), (ii) diffusing far from microtubule (>500 nm), and (iii) diffusing near microtubule (<500 nm) but appear to ignore the microtubule. The other 6 categories describe different types of association of viral capsids with microtubules: (iv) Diffusing near microtubule (<500 nm) and occasionally binding, (v) viral capsid switching tracks, (vi) viral capsid diffusing along a microtubule, (vii) viral capsid bound to microtubule but stationary, (viii) viral capsid running along microtubule and (ix) viral capsid showing bi-directional movement along microtubule. A total of 19 cells from 3 independent experiments and a total of 385 viral capsids were characterized. Mean and standard deviation of the percentages each event occurrence is presented.

### 2.2.14: Electron microscopy (EM)

CEFs infected with RB1B UL35 GFP were seeded in to 6 well plates at full confluence and prepared for EM the following day. The rest of the protocol was carried out by Nick Clarke. CEFs were trysinised and all the cells were pooled together to form a single pellet by centrifugation at 300 xg for 2 minutes at RT. Cells were then re-suspended in cryoprotectant (DMEM with 10% FBS, and 10% BSA). Cells were loaded into an aluminium type B carrier (approx. 1-2 ul). A second type B carrier was placed, flat side down, on top of the cells and then immediately frozen in the HPM100 High Pressure Freezer. Frozen carriers were transferred to the AFS2 (Low temperature resin embedding system), pre-cooled to -130 °C, and cells were embedded in resin (HM20). This was carried out by placing cells into a flow through chamber (cell side up). Cooled freeze substitution (FS) media (2% Uranyl acetate (UA), 5% $dH_2O$ in acetone) was added to each chamber (UA diluted from a 10% stock in methanol). The following program then ran in the AFS2 ( freeze substitution processor):

| Program | Step | T-start (°C) | T-end (°C) | Time | Reagent | UV |
|---|---|---|---|---|---|---|
| **Freeze substitution** | 1 | -130 | -90 | 02:00 | FS media | |
| | 2 | -90 | -90 | 06:00 | FS media | |
| | 3 | -90 | -45 | 09:00 | FS media | |
| | 4 | -45 | -45 | 03:00 | FS media | |
| **Wash** | 5 | -45 | -45 | 01:00 | Acetone (x4 wash) | |
| **Infiltration** | 6 | -45 | -45 | 02:00 | 25% HM20 in acetone | |
| | 7 | -45 | -45 | 02:00 | 50% HM20 in acetone | |
| | 8 | -45 | -45 | 02:00 | 75% HM20 in acetone | |
| | 9 | -45 | -45 | ON | 100% HM20 | |
| | 10 | -45 | -45 | 02:00 | 100% HM20 | |
| | 11 | -45 | -45 | 02:00 | 100% HM20 | |
| | 12 | -45 | -45 | 02:00 | 100% HM20 | |
| | 13 | -45 | -45 | 02:00 | 100% HM20 | |
| **Polymerization** | 14 | -45 | -45 | 48:00 | 100% HM20 | x |
| | 15 | -45 | 25 | 16:00 | | |

**Table 8: Resin embedding programme**

Polyermized blocks were removed from the flow through chamber and the aluminium carrier was removed using a razor blade to expose the resin-embedded cell pellet. Sections of 200 nm were collected on (0.3%) formvar

coated finder grids. Sections were imaged on the Jeol 2100Plus this is a 200kV LaB6 instrument fitted with a Gatan OneView IS camera. Infected cells were found by scanning at low magnification. Cell infection was confirmed by looking for viral particles inside the nucleus. All found viral capsids in the cytoplasm was imaged at high magnification. Analysis was carried out by first determining if viral capsid had a viral membrane and if it was in a vesicle. Next all the microtubules in each image was determined and the distance of each viral particle to the closest microtubule (edge to edge) was measured using the line tool in Fiji. As a control, each image containing a viral capsid was split into even quadrants. Each viral capsid in the quadrant was shifted 200nm towards the opposite quadrant in a diagonal manner. In the new location distance to the nearest microtubule was measured again. This experiment was only carried out once. Statistical significance was determined using a Kolmogorov-Smirnov test.

### 2.2.15: Statistics

One-way analysis of variance (ANOVA) was used to determine statistical significance in the viral plaque assays. LSD post-hoc test was used with comparing 3 means or below and Turkey's HSD was used to compare 4 or more means. Statistical significance is shown above all conditions on relevant figures using asterisks (*= $p<0.05$ ** = $p<0.005$ *** = $p<0.0005$ ****=$p<.00005$). Two-sample T-test was used when comparing only two conditions (e.g., cold treatment assays). Samples were first checked for normal distribution using F-test. If unequal distribution was suggested from the F-test then a Mann–Whitney U test was carried out. Paired T-test was used for the split kinesin assay analysis. Both populations were tested for distribution and T-test was adjusted according to F-test results to take in to account normal distribution in the two populations. Kolmogorov-Smirnov test was used to determine differences in distribution between large populations (e.g., viral capsid speeds with and without nocodazole). All statistical analysis was carried out on GraphPad Prism 8.

# Chapter 3: MDV infection requires the host cytoskeleton

Schumacher et al. (2005) suggested that microtubules are dispensable for the viral spread of MDV and that actin filaments are essential. This is surprising given that many *Alphaherpesviruses* depend on active transport along microtubules to move within the cytoplasm of the host cell (Mabit et al., 2002, Marozin et al., 2004, Topp et al., 1994). To determine the requirement of the cytoskeletal elements; actin and microtubules during MDV infection, the effects of cytoskeletal depolymerising drugs on viral spread were investigated.

## 3.1: Cytoskeleton depolymerising/stabilising small agents effect efficiency of MDV viral spread

To determine the requirement of microtubules and actin, the two main components of the cellular cytoskeleton, for the viral life cycle, a modified plaque assay was designed. Plaque assays are used for determining the concentrations of viral particles harvested from previously infected cells (Baer and Kehn-Hall, 2014). By modifying the classical plaque assay, it is possible to determine the effects that various drugs/small molecules might have on viral spread in a cell monolayer. Plaque assays represent viral spread in a monolayer. Any condition that effects viral spread can be seen as a smaller or larger viral plaque phenotype. Any defects induced from treatment to the viral cycle or replication defects and to structural defects can be monitored and viral plaque size is only and output of the assay. Briefly, the modified plaque assay involved seeding a monolayer of CEFs prior to infection with MDV RB1B virus that expresses cytoplasmic GFP under the control of the thymidine kinase (TK) promoter. Infection was allowed to establish for 24 hours and then was treated with various cytoskeleton modifying drugs for 48 hours. Each plaque from every condition was imaged at the end of the 48 hours. It is difficult to get a synchronised infection with MDV as it does not produce any cell-free viral particles and infection is started with infected cells. This means that a mixture of infected cells at different stages of infection are used for these experiments.

RB1B TK GFP virus compared to the parental wild type virus showed no change to viral kinetics in a plaque assay (Shimojima et al., 1997). Therefore, this fluorescent virus was used to track viral spread in these plaque assays.

Nocodazole, which is a microtubule depolymerising agent (Lee et al., 1980), was used to determine the requirement of microtubules during the viral life cycle. Taxol, which is a microtubule stabilising drug (Wani et al., 1971, Weaver, 2014), was used to determine the requirement of microtubule dynamics during the viral life cycle. Cytochalasin D (CytoD) is a drug known to depolymerise actin filaments (Goddette and Frieden, 1986). This drug was used to determine the necessity of actin filaments to the viral life cycle. Concentrations of the small molecule inhibitors used in this study was based on the literature showing the same small molecule inhibitors used in the same cell types. No toxicity of these small molecule inhibitors was tested on the CEFs used here. The small molecule inhibitors and the concentrations used are well established in the literature (Richerioux et al., 2012, Schumacher et al., 2005).

Treatment of CEFs with nocodazole had drastic effects on the size of viral plaques (Fig 3.1). Two different concentrations of nocodazole were used: 5 μM nocodazole, a 70% reduction in viral plaque size can be observed, and a 50% reduction at 0.5 μM suggesting a dose-dependent effect (Fig 3.1C). The use of nocodazole efficiently removes microtubules but does not remove actin (Fig 3.1B). This suggests that microtubules are required for efficient viral spread during the MDV life cycle in contrast to published findings (Schumacher et al., 2005).

Treatment of a CEF monolayer with Taxol had a dose-dependent effect on the size of viral plaques (Fig 3.2). Four different concentrations of Taxol were used, and the highest concentration of 5 μM reduced average plaque size by 75% (Fig 3.2A, C). This concentration of Taxol resulted in re-organisation of the microtubule network to form large bundles (Fig 3.2B, D). At 0.5 nM the microtubule network appeared unaltered compared to DMSO-treated cells, however there was still a 40% reduction in viral plaque size (Fig 3.2C). These

findings suggest that dynamic microtubules are required for efficient viral spread.

Treatment of CEFs with CytoD had potent effects on reducing the size of viral plaques (Fig 3.3). Two different concentrations of CytoD were used, 0.5 µM of CytoD caused a 90% reduction in viral plaque size. 0.05 µM CytoD resulted in 10% reduction suggesting a dose-dependent effect (Fig 3.3C). The use of CytoD did not affect microtubules but efficiently removed actin bundles (Fig 3.3B). This effect suggests that actin bundles are required for efficient viral spread during the MDV life cycle and are in line with previous findings (Schumacher et al., 2005).

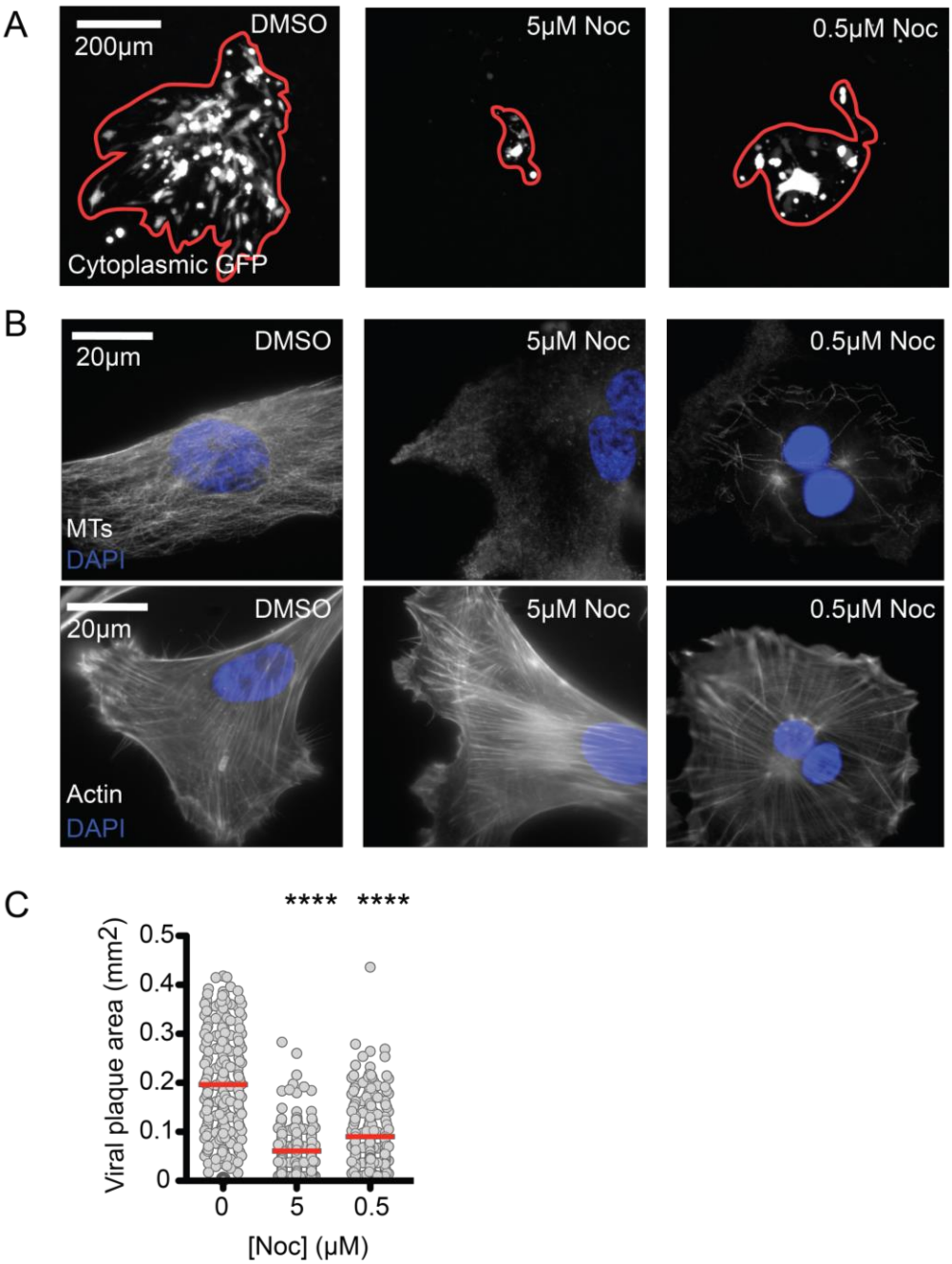


**Figure 3.1: Effects of nocodazole on viral plaque size.**

(A) Representative images of plaques of MDV infected CEFs treated with different concentrations of nocodazole (Noc). GFP highlights infected cells. The red outline indicates the boundaries of each viral plaque. Scale bar is 200 µm (B) CEFs treated with nocodazole and stained with DAPI and anti-α-tubulin antibodies or phalloidin-561 to visualise the effects of nocodazole on the cytoskeleton. Scale bar is 20 µm. (C) Graph showing plaque areas pooled from three independent experiments (n=180-240 plaques for each condition). Red line indicates the mean of the data. Statistical significance **** p=<0.0001 (LSD post-hoc test).

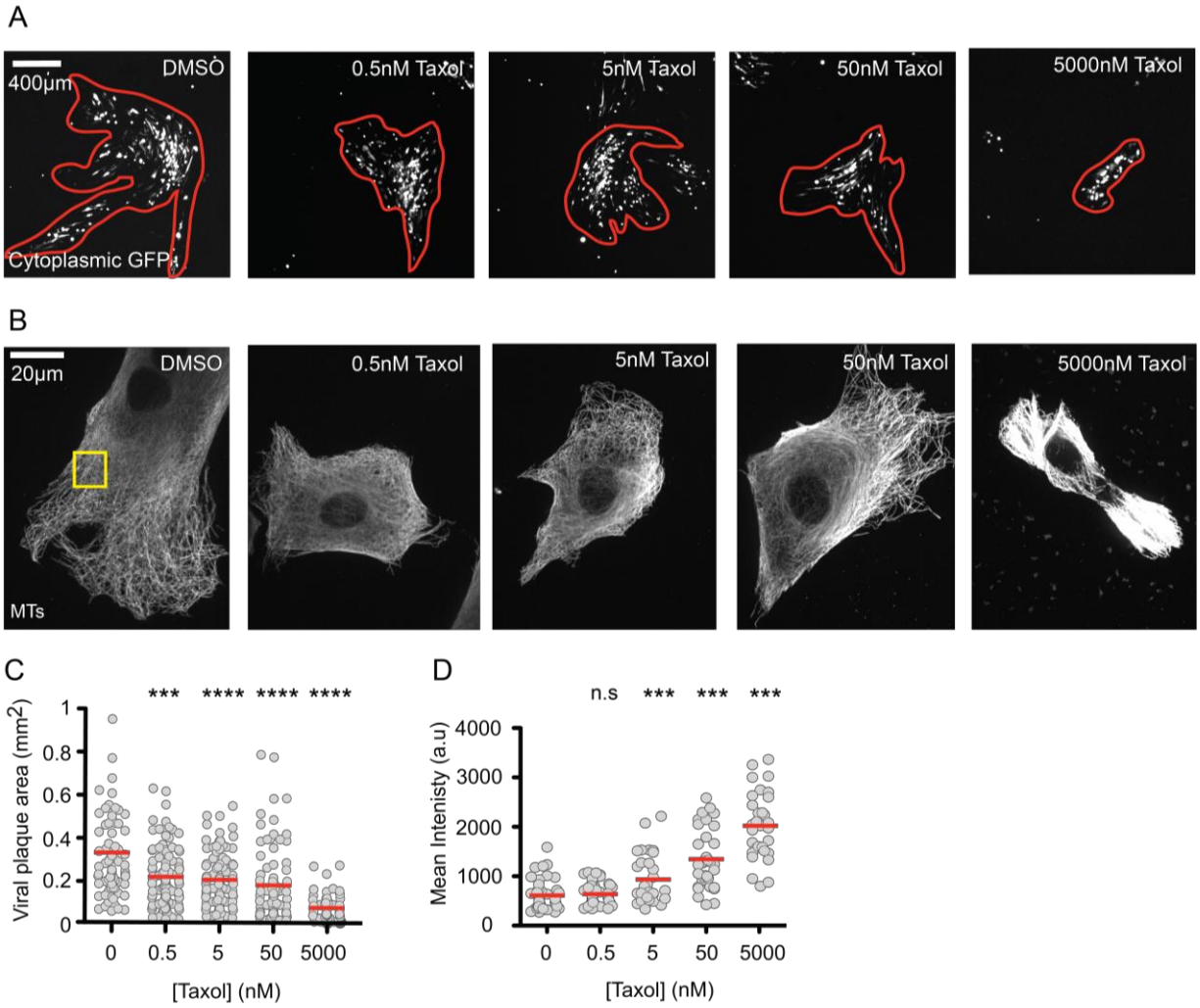


**Figure 3.2: Effects of Taxol on viral plaque size.**

(A) Representative images of plaques of MDV infected CEFs treated with different concentrations of Taxol. GFP highlights infected cells. The red outline indicates the boundaries of each viral plaque. Scale bar is 400 µm. (B) CEFs treated with Taxol and stained with DAPI as well as anti-α-tubulin antibodies to visualise the effects of Taxol on the cytoskeleton. Scale bar is 20 µm (C) Graph showing plaque areas pooled from three independent experiments (n=100-120 for each condition). Red line indicates the mean of the data. Statistical significance *** p =0.0001, **** p =< 0.0001 (Turkey's HSD post-hoc test). (D) The graph is showing data of mean intensities of α-tubulin staining taxol-treated cells (n=>20). A red line indicates the average. Statistical significance *** p =0.0001, n.s. = not significant (Turkey's HSD post-hoc test).

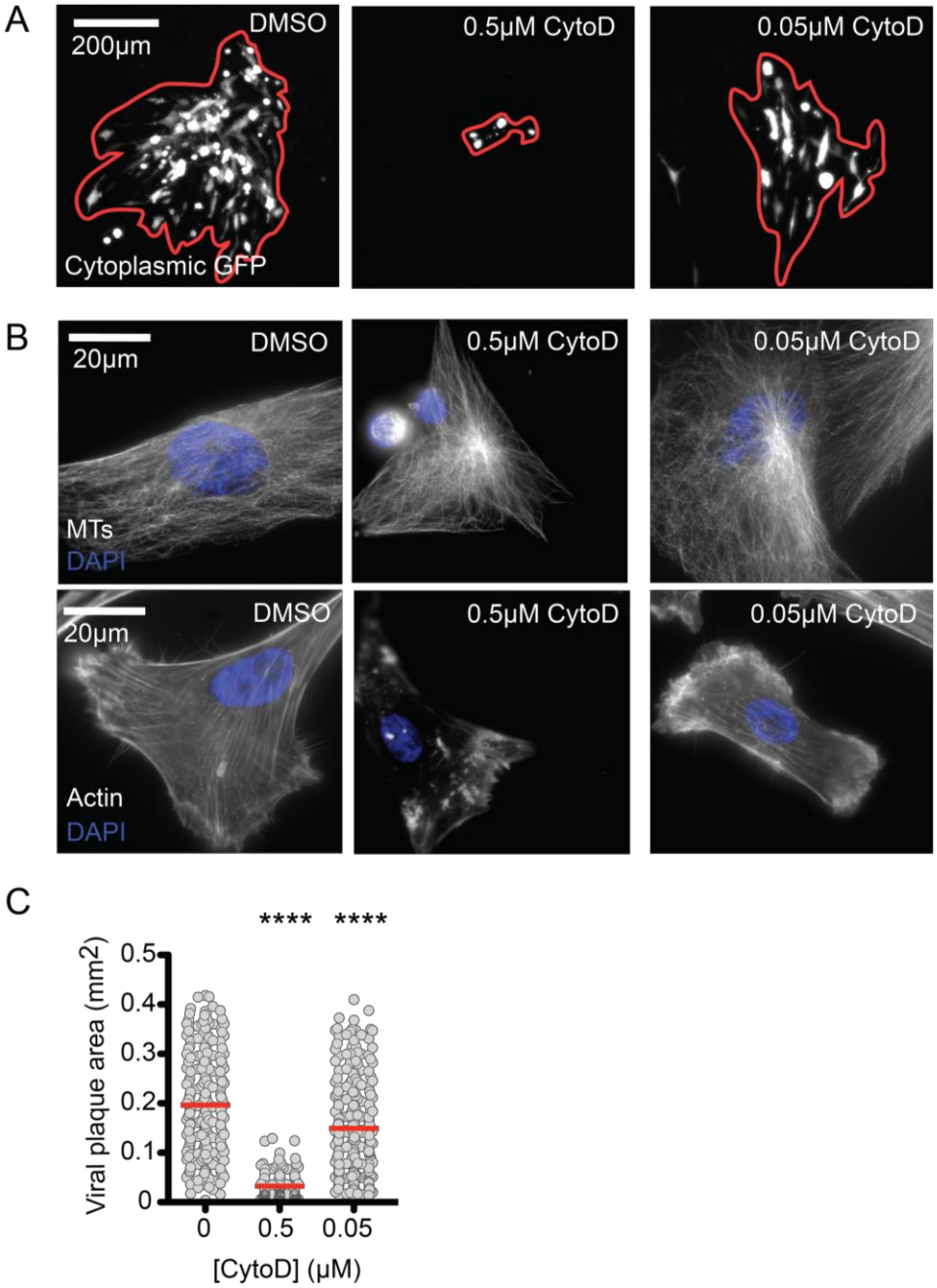


**Figure 3.3: Effects of Cytochalasin D on viral plaque size.**

(A) Representative images of plaques of MDV infected CEFs treated with Cytochalasin D. GFP highlight infected cells. The red outline indicates the boundaries of each viral plaque. Scale bar is 200 µm. (B) CEFs treated with Cytochalasin D and stained with DAPI as well as anti-α-tubulin antibodies or phalloidin-561 to visualise the effects of Cytochalasin D on the cytoskeleton. Scale bar is 20 µm (C) Graph showing plaque areas pooled from three independent experiments (n=150-200 for each condition). Red line indicates the mean of the data. Statistical significance **** p =< 0.0001 (LSD post-hoc test).

## 3.2: Dynamic microtubules are required for cell shape changes induced during MDV infection.

Both, depolymerisation as well as stabilization of the microtubule network had drastic effects on viral plaque size. As MDV is a strictly cell-associated virus (Ahmed and Schidlovsky, 1968, Churchill and Biggs, 1967, Solomon et al., 1968), the infected cell needs to make direct contact with target cells in order for intracellular viral spread to occur. An important observation made when investigating the cytoskeletal arrangement of MDV infected cells was the appearance of extended protrusions that form from infected cells towards uninfected cells when sparsely seeded in culture. This observation was brought to attention by Prof. Nair's group initially (unpublished). Other *Alphaherpesviruses* have been reported to induce cytoskeletal rearrangements and cell extensions during the late stages of infection (Dixit et al., 2008, Favoreel et al., 2005, Oh et al., 2010).

This observation prompted the investigation of the role of microtubules on infection-induced cell shape changes. To facilitate this, a custom MatLab package developed in Straube Lab called Shape Space Explorer (unpublished) was used. This script can analyse manually drawn or auto-detected shapes within a data set and represent these in a 2D shape space based on their morphology. Therefore, the closest shapes in shape space will be very similar to each other and the further away the shapes are the more different they are.

Based on the exemplar shapes observed and plotted (Fig 3.4A), a wide range of shapes were detected within our data set from: almost perfectly round cells to elongated cells and to 'irregularly shaped' cells with multiple protrusions. For visualisation purposes of the entire shape space, each shape is represented as a location in shape space. Infected CEFs and CEFs occupy different locations in shape space (Fig 3.4B). Treating these cells with 500 pM Taxol results in further separation from the untreated cells in shape space.

This suggests that infected cells produce different shapes compared to uninfected CEFs. Taxol treatment also results in cellular cell shape changes.

To be able to quantify these observed differences, a shape space area analysis was performed. Based on the types of shapes in the shape space the data was divided into four distinct regions. Each cluster represents a general shape. Region 1 represents elongated shapes, region 2 round shapes, region 3 are slightly elongated with single protrusions and region 4 containing irregular shapes with multiple protrusions (Fig 3.5A).

When the fraction of shapes in each region is plotted for each condition significant differences in cell shape can be observed (Fig 3.5B). CEFs predominantly have slightly elongated shapes with single protrusions. When treated with 500 pM Taxol this shifts to many more elongated cellular shapes. MDV-infected CEFs mainly showed cell shapes with multiple protrusions. When infected cells were Taxol-treated, these became predominantly round. These data suggest that the loss of dynamic microtubules during infection results in a loss of cytoskeletal changes induced during MDV infection. Dynamic microtubules are also required for required for intracellular viral spread (Fig 3.2)

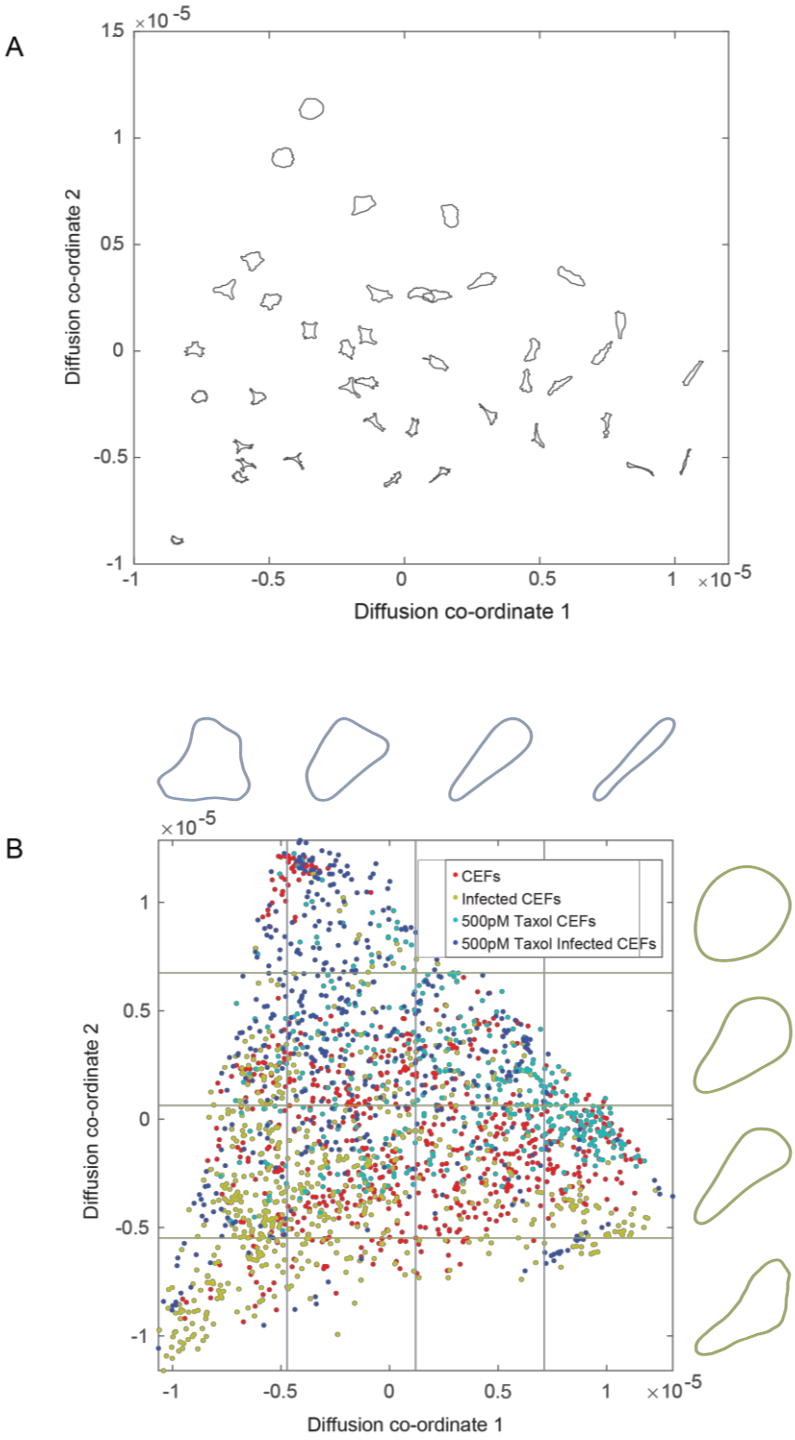


**Figure 3.4: Shape Space Explorer: exemplary shapes and diffusion map slicing.**
(A) Exemplar shapes in shape space. This plot shows the first two coordinates in the diffusion map embedding (B) Shape space showing locations of all shapes recorded in each condition – CEFs, CEFs infected with RB1B TK GFP and Taxol treated infected and uninfected cells. In blue is the average cell shape in each slice of shape space for co-ordinate 1. In green is the average cell shape in each slice of shape space for co-ordinate 2. N= 30 cells per condition.

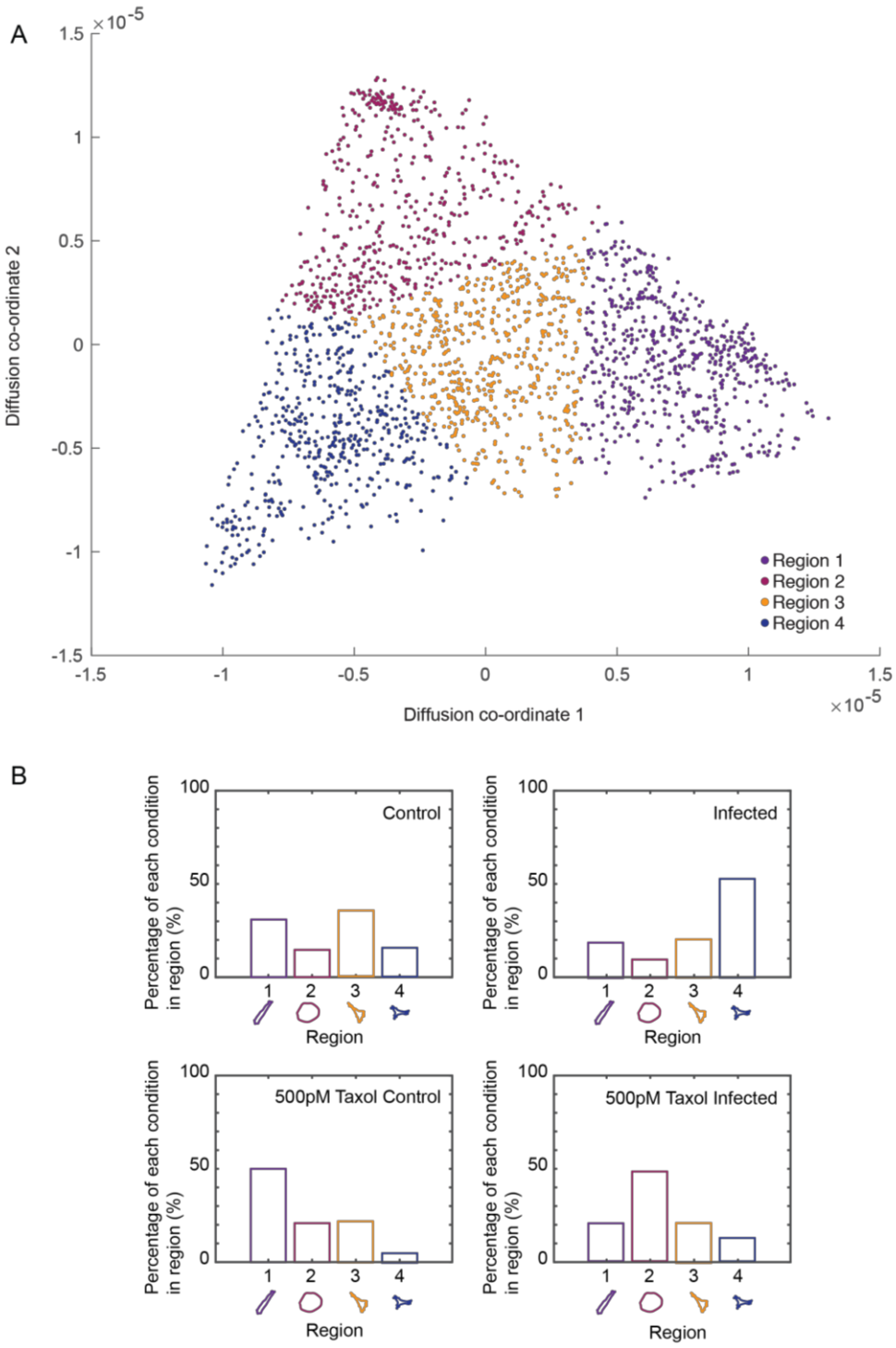


**Figure 3.5: Shape Space Explorer: Area analysis.**

(A) Area analysis in shape space. The shape space is separated into four distinct regions. (B) Bar charts show the percentage of shapes located within each region. Below are representative images to highlight the typical cell shape in each region. N=10 cells per experiment, repeated 3 times.

## 3.3: MDV infection does not result in changes to the post-translational modifications of microtubules

Results from the cell shape analysis and plaque assays suggested that microtubules are required during MDV infection. The microtubule network may be targeted during the MDV infection (O'Donnell et al., 2002). There is a possibility that MDV infection may stabilize microtubules to provide a transport network for viral capsids during egress. HSV-1 and another *Alphaherpesvirus* have been shown to stabilize microtubules through various viral proteins like US3 that interacts with CLASPs (Naghavi and Walsh, 2017), VP22 that directly binds microtubules (Elliott and O'Hare, 1998) and UL37 that interacts with dystonin (Pasdeloup et al., 2013b).

Post translational tubulin modifications like acetylated tubulin provide a marker to identify highly stable microtubules (Perdiz et al., 2011, Takemura et al., 1992). Highly stable microtubules will in turn be used preferentially by some molecular motors for vesicle trafficking (Janke and Bulinski, 2011, Naghavi and Walsh, 2017). For example, kinesin-1s use poly-glutamylated microtubules while kinesin-2s prefer detyrosinated microtubules (Sirajuddin et al., 2014). Investigating any changes that occur to PTM's of tubulin can provide insights into how viral capsids are transported during infection and if the virus modifies microtubules.

Immunofluorescence allowed visualization of the microtubule network, specifically, tubulin post-translational modifications, in CEFs and MDV-infected CEFs. CEFs were infected with a virus that expresses a GFP tagged UL49 protein. The reason for the change from using RB1B TK GFP virus to RB1B UL49 EGFP virus is that when RB1B TK GFP virus is fixed using methanol the cytoplasmic GFP is washed away making it difficult to determine infected cells when imaging. UL49 EGFP remains visible with methanol fixation. Therefore, this virus was used to identify infected cells when screening for infection and any changes to the microtubule network. Acetylated tubulin, polyglutamate modifications and longer polyglutamate

chains were analysed. No visual change in each of the modifications investigated was observed between uninfected CEFs and CEFs infected with RB1B UL49 EGFP (Fig 3.6A).

The levels of each protein were also analysed by Western blotting. CEFs infected with RB1B TK GFP or uninfected CEFs were investigated and were harvested for whole cell lysate. Acetylated tubulin, polyglutamate chains and α-tubulin were detected using specific antibodies. Based on the levels from the western blots, no change in the levels of microtubule modifications was observed (Fig 3.6B). A draw back with this experiment is that a control band for infection, such as a specific viral protein, is not present making it hard to determine if infection was present. However, before lysing the cells the dishes were checked for infection using a widefield microscope and infection was at 45 % before lysis. Therefore, both approaches suggest that any changes induced to the microtubule network during MDV infection do not result in changes to post-translational modifications like acetylation and polyglutamate chains of microtubules.

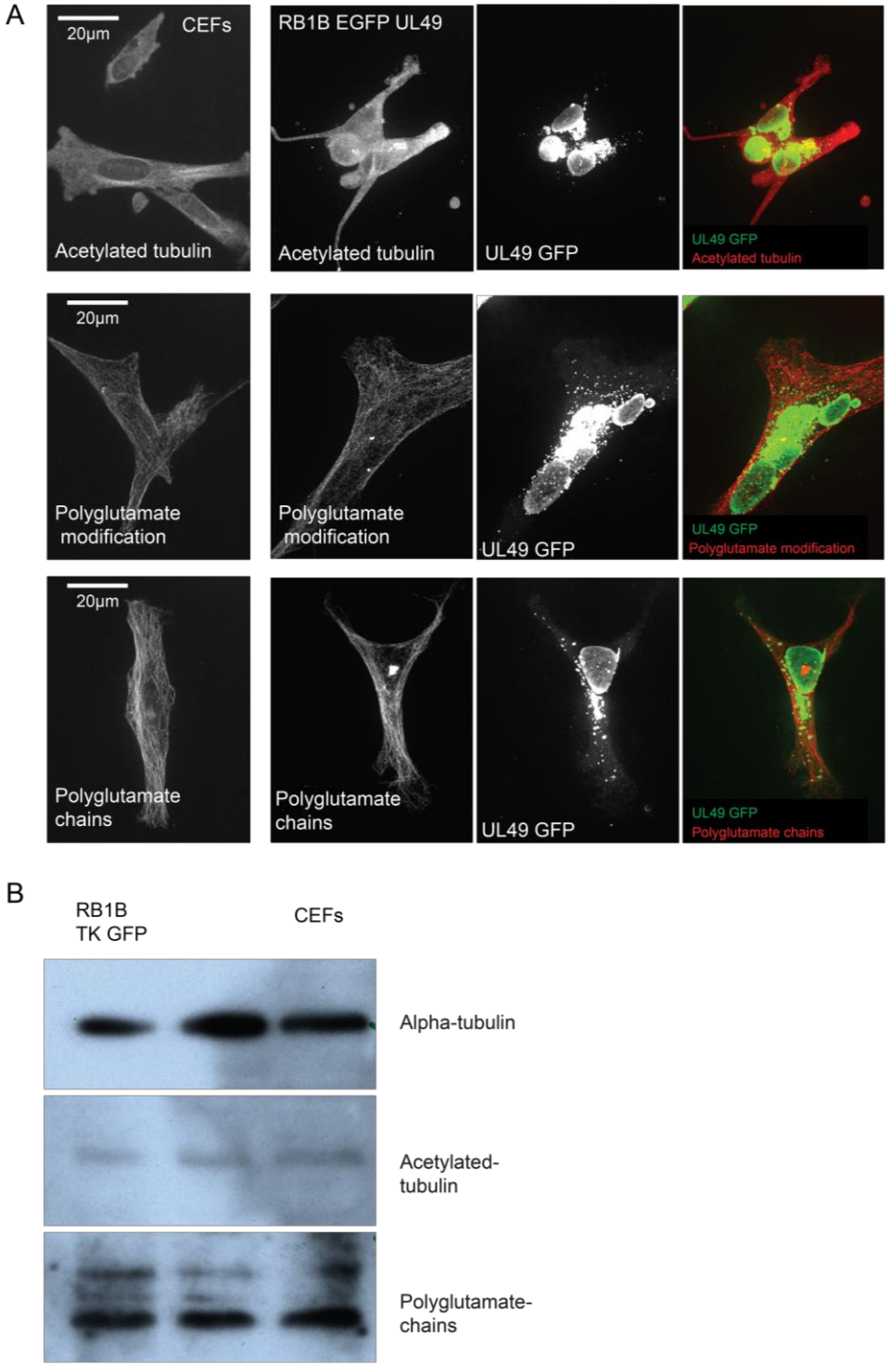


**Figure 3.6: Post-translational modifications of microtubules during MDV infection.**
(A) Immunofluorescence images show acetylated tubulin, polyglutamate modifications and polyglutamate chains on microtubules in grey. These were detected using antibodies specific to each modification. CEFs infected with RB1B EGFP UL49 are in green. Merge of all channels together is also shown, green is UL49 GFP and red is each modification. Scale bar is 20 µm. N= 3 independent experiments (B) Western blot showing levels of α-tubulin, acetylated tubulin or polyglutamate chains on microtubules from whole cell protein extracts.

## 3.4: CEFs have highly stable microtubules.

Analysis of microtubule modifications revealed that CEFs have a high number of acetylated microtubules (Fig 6A). Acetylation of tubulin is thought to indicate increased stability of microtubules (Takemura et al., 1992), suggesting that microtubules in CEFs could be highly stable. To test this, a cold treatment assay was employed. This assay is generally used in the mitosis community to remove unstable microtubules outside of k-fibers (DeLuca et al., 2006). Thus, in interphase CEFs, unstable microtubules introduced to low temperatures should largely depolymerise. CEFs were treated on ice for 20 minutes and then fixed using methanol and processed for immunofluorescence probing for α-tubulin and acetylated tubulin.

The dense microtubule network is obvious in CEFs. Many of the microtubules are heavily acetylated. When treated on ice the microtubule network is not affected (Fig 3.7A). When the density of microtubules is quantified before and after cold treatment, there seems to be a slight increase in mean intensity levels (Fig 3.7B). There is no change in the intensity of microtubules that have been acetylated (Fig 3.7B). This observation suggests that cold treatment of CEFs does not depolymerise microtubules. This further implies that CEFs have a naturally stable pool of microtubules and, that the MDV infection may not need to stabilise the microtubule network further.

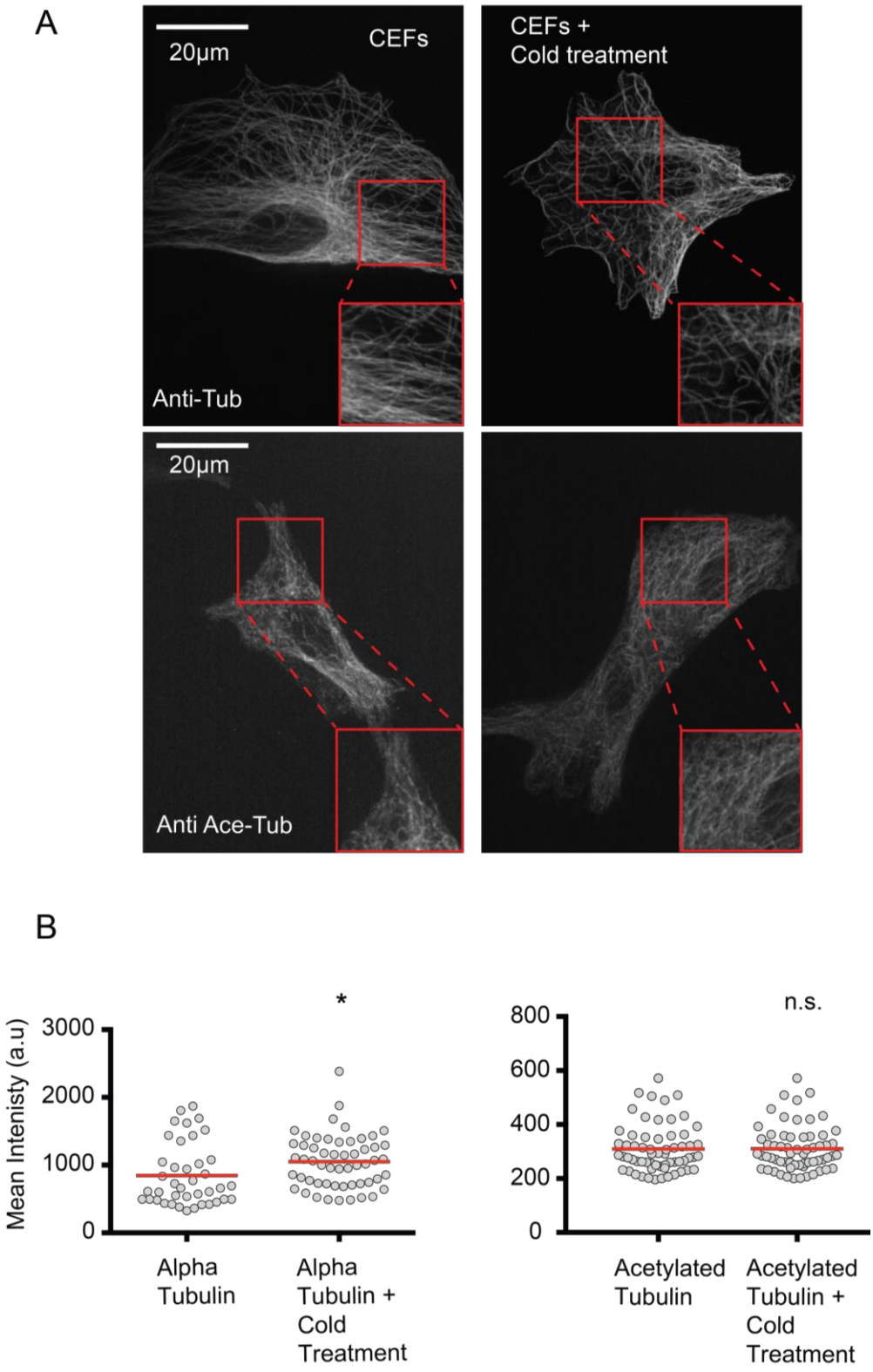


**Figure 3.7: Microtubules in CEFs are highly stable.**

(A) Immunofluorescence images showing α-tubulin and acetylated tubulin in grey. Red box indicates area in insert. (B) The graphs show mean intensities of α-tubulin and acetylated tubulin staining (n=>30, 3 independent experiments). A red line indicates the average. Statistical significance * p= < 0.05, n.s not significant (two-sample t-test).

## 3.5: Discussion

### 3.5.1: Microtubules are essential for efficient MDV viral spread

The finding that microtubules are essential to MDV viral spread contradict Schumacher *et al.* (2005), who suggest that microtubules are dispensable. Schumacher *et al*. (2005) used plaque assays to show that CytoD reduces plaque sizes significantly but nocodazole treatment does not. There could be several reasons for the discrepancy with our results. The first reason could be that fact that using 5 μM nocodazole all microtubule structures were depolymerized in this study, however, the same concentration of nocodazole has clearly not depolymerized all microtubule structures in the immunofluorescence (IF) images presented by Schumacher *et al.* (2005). This suggests that microtubules are present during their plaque assay and could explain the lack of plaque size reduction compared to the control.

Further reasons could be the differences in experimental design. For the plaque assays used during this study frozen infected cells were thawed directly on to the CEF monolayer. Nocodazole was introduced to the cells after infection was established, and no media was changed during the 48 hours of incubation with inhibitors. Schumacher *et al.* (2005) transfected the cell monolayer with BAC20 viral plasmid and then added drugs 8 hours after transfection. Fresh media with drugs was added every 12 hours for 5 days. With these differences, there could be a difference in the outcome of the experiment. Transfection versus seeding infected cells on to a confluent monolayer could result in different dynamics of viral spread. Seeding cells more closely represents physiological conditions when compared to transfections to start a viral spread assay. As an infecting viral particle brings in a tegument layer shown to be important for viral infection establishment (Diefenbach, 2015). A BAC20 DNA transfected cell that is then subjected to nocodazole treatment after 8 hours – before the onset of the late phase replication (McPherson and Delany, 2016) – could result in changes to the viral life cycle that would not normally occur. Additionally, the rounding up of

cells when treated with nocodazole described by Schumacher *et al.* (2005) could also mean the long-distance transport within cells that is facilitated by microtubules may no longer be required as the cell cortex is much closer to the nucleus.

In this study, however, an already infected batch of cells at known plaque forming units (PFU) were introduced to the cell monolayer for 24 hours, allowing the establishment of infection before the introduction of depolymerising drugs. This incubation allows for a complete viral life cycle to occur and the infection to be established. Measuring viral plaque size after two and not five days also meant that the immediate effect of nocodazole on viral spread could be determined, rather than determining long-term effects of nocodazole treatment as infection may adapt to a lack of microtubules. It has been previously shown that when fibroblast cells (and RPE-1 cells) are constantly exposed to nocodazole they remain in mitosis for 10-48 hours and then arrest in G1 phase without a microtubule cytoskeleton but not undergo apoptosis (Uetake and Sluder, 2007). This suggests that after the initial shock of nocodazole treatment the cell will essentially carry on. This may also be true for an MDV infected cell that is treated with nocodazole for 5 days.

Moreover, the incubation temperatures of cell culture were different in our studies. CEFs in this study were incubated at 38.5 ºC throughout cell maintenance. Schumacher et al. (2005) used 37 ºC. The natural body temperature of *Gallus gallus* is 41 ºC (Bolzani et al., 1979). Our cell culture conditions represent physiological conditions more than the conditions used by Schumacher *et al.* (2005). Temperatures different to physiological conditions could have drastic effects on intracellular *Alphaherpesvirus* viral spread (Cole, 1992).

To conclude the difference in experimental design, and the fact that not all microtubules were depolymerized by Schumacher *et al.* (2005) could account for the discrepancy seen between the two studies. The findings that microtubules are essential for MDV viral spread opens a new avenue of study regarding the MDV life cycle. Understanding how microtubules are important

to the MDV life cycle could lead to new potential drug targets to treat MDV in the future.

### 3.5.2: Cell Shape changes occur to MDV infected cells

This study shows that cellular shape changes occur in MDV infected cells and depend on dynamic microtubules. Cell shape change during MDV infection has been studied previously in the context of viral plaques (Richerioux et al., 2012). MDV viral plaques tend to spread in an organized manner following the regulated microenvironment created by the cellular monolayer. The microenvironment created by the cell monolayer is structured and favours actin stress fibre preservation and elongated cellular shape (Richerioux et al., 2012). Similar viral plaque organisations were also seen in this study. However, in a sparse environment without the microenvironment-dictated boundaries of a confluent monolayer, MDV infected cells show drastic changes to the cell shape that are dependent upon dynamic microtubules.

There are many differences between cells in 3D tissue and our 2D culture setup. Within tissues, cells are contained in a structured environment made up of the extracellular matrix (ECM). Neighbouring cells impose boundary conditions on each other that influence cell architecture, mechanics, cell polarity and function (Ingber, 2003, Ingber, 2006, Thery, 2010). In our 2D cell culture setup, cell shape is dictated much more by the adhesions cells make with the glass surface and ECM than outside influences from neighbouring cells (Duval et al., 2017) It may be much more relevant to study MDV viral spread in a 3D environment in the future to take in to account the restrictions imposed on to tissue architecture as a whole.

The cell shape changes seen in this study could also be relevant to viral infection *in vivo* as macrophages are one of the main targets of MDV infection (Barrow et al., 2003). Macrophages go through stages of cellular shape changes when stimulated with cytokines to induce the M1 and M2 stages of activation (McWhorter et al., 2013). Macrophage shape is independent of

those cells around them as they can move freely between cells and depend upon short lived interactions with the ECM (Pixley, 2012). The cell shape changes induced during an MDV infection might play an important role during MDV viral spread *in vivo* as the many interactions macrophages have with cells in tissue could facilitate its rapid viral spread. Bringing together 3D cell culture and macrophage dependent MDV spread could be the next experiment to try to fully understand the cell shape changes induced, and how this relates to the larger picture of MDV pathogenesis.

Other viruses like HIV-1 have been described to change cell shape and promote the formation of membrane extensions to facilitate cell-to-cell virus propagation (Nikolic et al., 2011). HSV-1 viral spread has also been shown to depend upon cell-to-cell contact, where viral capsids arrive at epithelial cell junctions from the TGN to infect neighbouring cells without having to leave the host (Akhtar and Shukla, 2009, Farnsworth and Johnson, 2006b). HSV-1 and HIV-1 are also able to produce viral particles that leave the host, unlike MDV that is entirely dependent upon cell-to-cell contact for viral spread (Nazerian et al., 1968, Solomon et al., 1968, Johnson et al., 1975). Therefore, MDV could have evolved to initiate changes to the cytoskeleton of the host to facilitate efficient and rapid viral spread.

### 3.5.3: MDV infection does not require stabilized microtubules

Other *Alphaherpesviruses,* such as HSV-1, have been shown to alter the host microtubule network, presumably to assist in viral spread (Brzozowska et al., 2010, Dienes et al., 1987, Kotsakis et al., 2001, Kuhn et al., 2005, Mingo et al., 2012, Pasdeloup et al., 2013b). Viral proteins including US3 – a viral Akt mimic – stabilise microtubule arrays from the TGN towards the cell cortex and recruit +TIPs to capture microtubules at the cell periphery (Favoreel et al., 2005, Naghavi et al., 2013). Other viral proteins like VP22 and have also been suggested to aid in the formation of acetylated microtubule arrays to stabilise existing microtubule structures further (Elliott and O'Hare, 1998). Cytoplasmic linker-associated proteins (CLASPs) are also recruited during

*Alphaherpesvirus* infection to encourage microtubule growth towards specific viral- glycoprotein-enriched regions of the plasma membrane (Hogue et al., 2014b, Mingo et al., 2012). Stabilising and acetylating microtubules originating from the TGN and directing microtubule polymerisation towards specific sections of the plasma membrane could result in a stable and reliable method of transporting newly produced viral particles to the cell periphery.

CEFs used during this study appear to have highly stable microtubules, with cold treatment assays resulting in none to very little change in the number of microtubules. Cold- stable microtubules have been described before, for example in mouse embryonic cells where suppressing the cold-stable properties of microtubules has been shown to disrupt synapse formation (Andrieux et al., 2002). It can also be seen that the microtubules in CEFs are highly acetylated, which is thought indicate microtubule stability. This could be the reason why no changes to microtubule modifications were seen in MDV infected cells, as microtubules are already stable.

## 3.6: Summary

Based on the plaque assays performed, nocodazole treatment of MDV infection resulted in smaller plaque formation in a dose-dependent manner. Taxol treatment of MDV infection also results in significantly reduced viral spread in a dose-dependent manner. Using 500 pM Taxol does not obviously affect the microtubule network in individual CEFs but causes a significant reduction to viral spread suggesting viral infection requires dynamic microtubules. This suggests that microtubules are vital to the efficient spread of MDV to neighbouring cells. The effect of low dose Taxol on cellular shape showed that dynamic microtubules are instrumental to the cellular shape changes caused during infection. Treating MDV-infected CEFs with low dose Taxol results in dampening of the cell shape changes caused during infection. MDV infection does not result in changes to post-translational modifications on microtubules. CEFs have highly stable microtubules that are resistant to cold treatment.

# Chapter 4: MDV capsids travel along microtubules

One of the principal roles of microtubules is the facilitation of long-distance directional transport within the cell. Like other *Alphaherpesviruses*, MDV capsids that leave the nucleus must be trafficked to various sites (Wild et al., 2017). Further transport from these sites to the cell cortex and cellular protrusions is also necessary for the spread of infection. Additionally, newly infecting virus also needs to be trafficked to the perinuclear region (Ward, 2011). To investigate whether MDV viral capsids are transported via microtubules, a viral strain with a C-terminal GFP tag on the UL35 gene (RB1B UL35-GFP) (Kut and Rasschaert, 2004) was used. The UL35 gene encodes a small viral capsid protein that is incorporated into the outside of the viral capsid. This tag allows the visualisation of individual viral capsids within an infected cell.

## 4.1: MDV viral capsids are transported on microtubules

First, it was necessary to establish the requirement of microtubules for individual viral capsid transport. To do so, RB1B UL35-GFP infected CEFs were treated with 5 μM nocodazole (microtubule depolymerisation drug) for an hour prior to imaging. The bottom 1.5 μm of the cell was imaged as this is where most viral capsids and microtubules are located. The individual capsid dynamics in nocodazole treated cells were compared to those in DMSO-treated cells. Movies generated were 3 minutes long. Viral capsid dynamics were determined by first tracking all viral capsids that were 5 μm away from the closest nucleus. The greatest distance each viral capsid travelled from its point of origin was then determined. If this was greater than 5 μm then that viral capsid was marked and shown as a ‘run’ suggesting active transport. Any viral capsid track lasting fewer than 100 frames was not considered for analysis unless the viral capsid had travelled more than 5 μm in that time frame. The reason for this cut-off was to ensure that viral capsids that moved out of focus during acquisition would not affect analysis.

CEFs infected with RB1B UL35-GFP have a very distinct appearance: the nucleus is packed with individual viral capsids, whereas the cytoplasm contains individual viral capsids that occasionally show directional movement or no movement, but mostly show diffusion-like behaviour (Fig 4.1A). When infected cells are treated with 5 μM nocodazole, directional movement is lost, and viral capsids mostly show diffusive behaviour (Fig 4.1A).

Tracking each capsid individually revealed that on average ~10% of viral capsids travel over 5 μm in 3 minutes in DMSO treated cells. Active transport was largely lost when cells were treated with 5 μM nocodazole (Fig 4.1B). Nocodazole treatment resulted in a decrease in the average velocity of a viral capsids from 0.15 μm/s to 0.06 μm/s (Fig 4.1C). This suggests that microtubules are absolutely required for the active transport of MDV viral capsids.

Next, the effect of stabilising microtubules and impairing microtubule dynamics and its effects on viral capsid transport was investigated. RB1B UL35-GFP infected CEFs were treated with 500 pM Taxol (MT stabilising drug) for 1 hour prior to imaging. Viral capsids were then imaged and analysed in the same way as the nocodazole data set. Viral capsids treated with Taxol showed very similar dynamics to the DMSO control (Fig 4.2A). Quantification revealed no differences between the percentage of viral capsids travelling more than 5 μm in 3 minutes in Taxol-treated versus DMSO-treated cells (Fig 4.2B). This suggests that MDV viral capsids do not require dynamic microtubules for transport. The presence of microtubules alone is enough to facilitate active capsid transport.

To confirm by visualisation that viral capsids are transported along microtubules, the cell permeable dye SiR-Tubulin was used on RB1B U35-GFP infected cells (Lukinavicius et al., 2013). This dye allows visualisation of microtubules without the need for transfection (Fig 4.3A). Imaging both microtubules and viral capsids live revealed that viral capsids do move on microtubules (Fig 4.3).

The directional transport of viral capsids along microtubules is visible in areas of the cell with a relatively sparse microtubule network (Fig 4.3B). However, these areas are limited and are usually found near the cell cortex. In areas where the microtubule network is denser, individual microtubules can no longer be separated due to the resolution limitations associated with spinning disk microscopy. This caused problems with matching individual capsid transport with single microtubules in these dense microtubule areas of the cell (Fig 4.3B). A much higher resolution of at least 3-fold is required to characterise and follow viral capsids on microtubule bundles successfully.

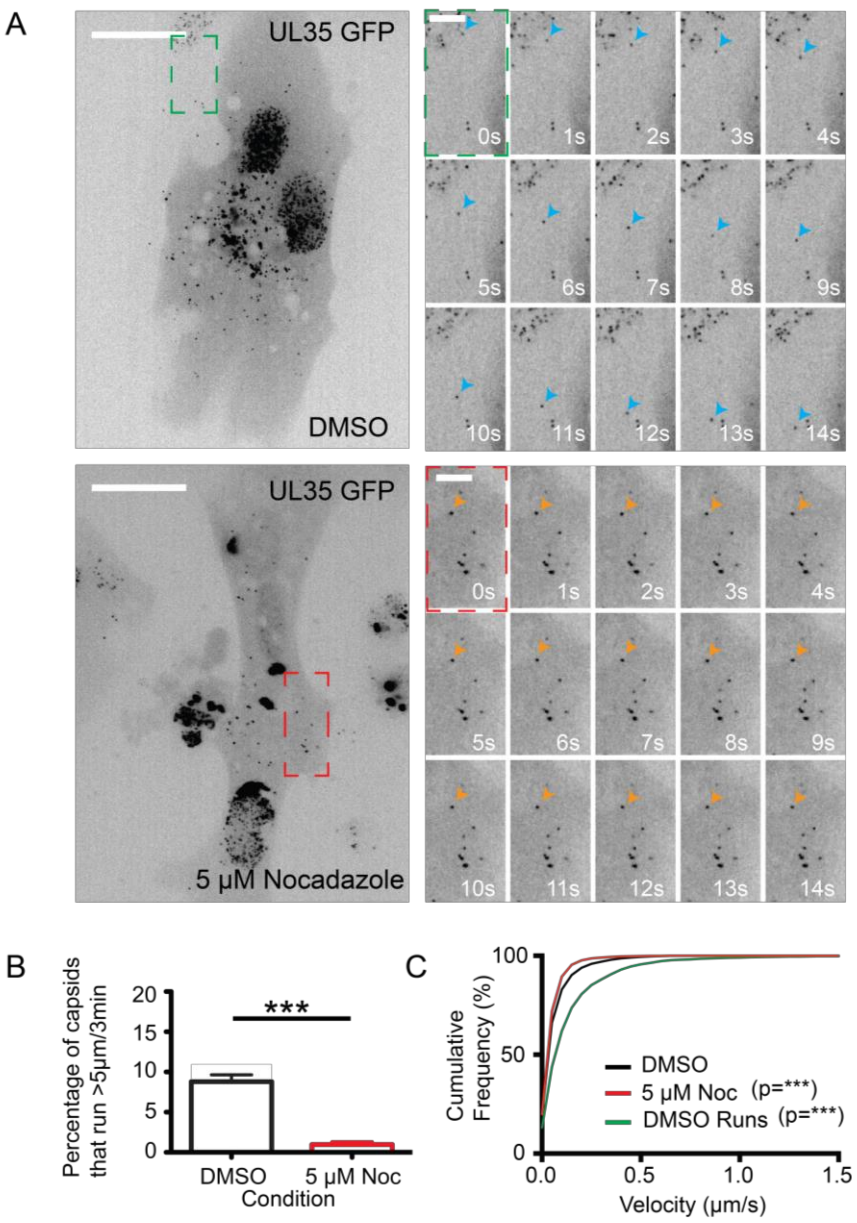


**Figure 4.1: Microtubules are required for viral capsid dynamics**

(A) Representative images of RB1B UL35-GFP infected CEFs, and nocodazole-treated RB1B UL35-GFP infected CEFs. GFP labels individual viral capsids. Scale bar is 20 μm. The green box indicates the area shown in the montage for DMSO treated cells. The red box indicates the area shown in the montage of 5 μM nocodazole-treated cells. Blue arrow indicates a viral capsid that travels over 5 μm. The orange arrow indicates a static viral capsid. Scale bar is 5 μm. (B) Quantification of the percentage of capsids that ran over 5 μm in 3mins. Data pooled from 3 independent experiments (n=30 cells for each condition total). Data shows mean ± standard deviation. Statistical significance *** p= <0.001 (two sample t-test). (C) Cumulative frequency plot shows the distribution of instantaneous velocities. DMSO and 5 μm Noc data show instant velocities from all cells at every time point. DMSO Runs data show instantaneous velocities of viral capsids that ran over 5 μm in 3min. Statistical significance *** p= <0.001 (Kolmogorov–Smirnov test).

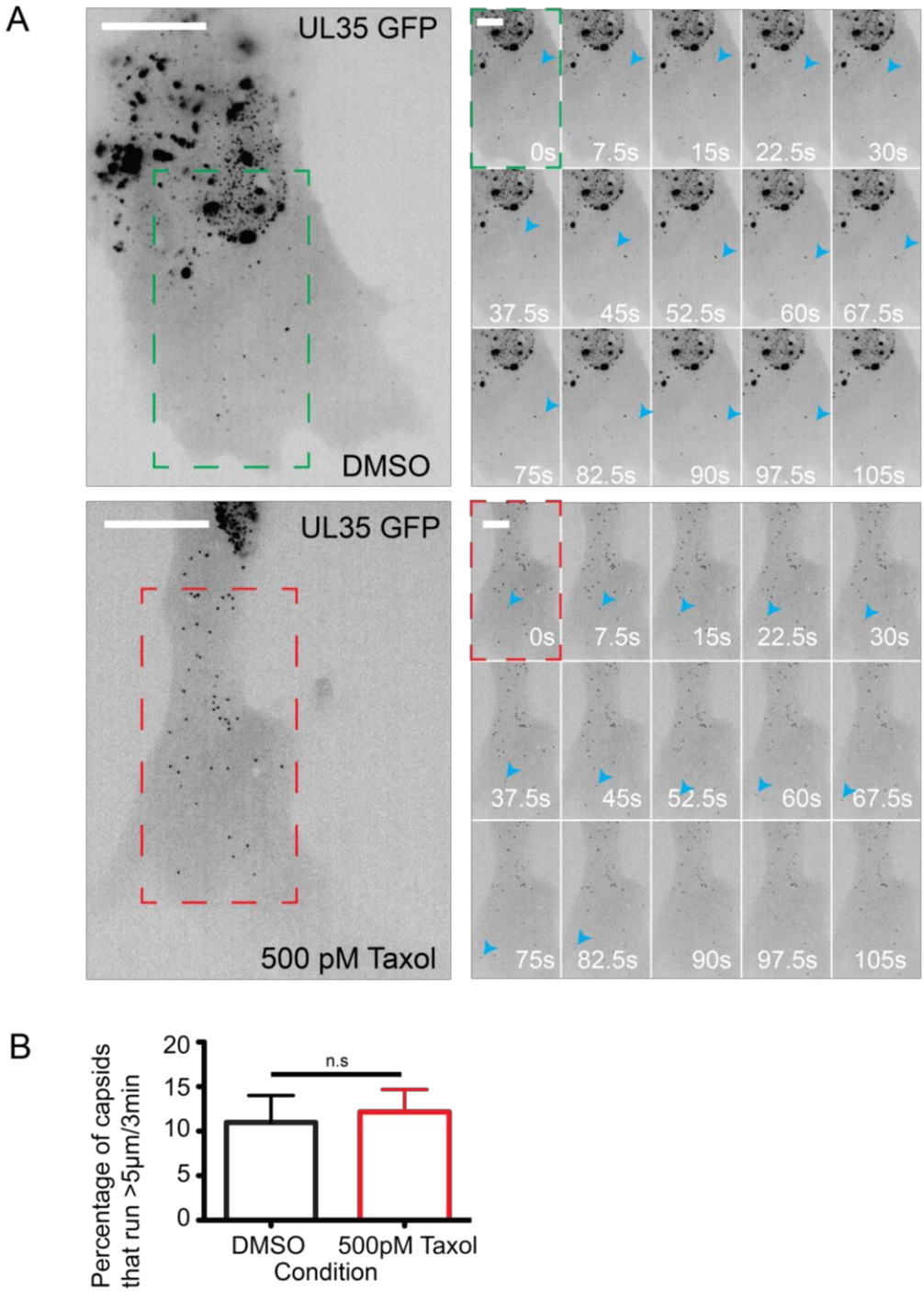


**Figure 4.2: Dynamic microtubules are not required for viral capsid transport**

(A) Representative images of control RB1B UL35-GFP infected CEFs and Taxol-treated RB1B UL35-GFP infected CEFs. The green box indicates the area shown in the montage of DMSO-treated cells. The red box indicates the area shown in the montage of 500 pM taxol-treated cells. Blue arrow indicates a viral capsid that travels over 5 µm. Scale bar is 20 µm. (B) Quantification of the percentage of capsids that ran over 5 µm in 3mins. Data pooled from 3 independent experiments (n=30 cells for each condition). Data showing mean ± standard deviation. Statistical significance, p= 0.3102 (two sample t-test), not significant (n.s.).

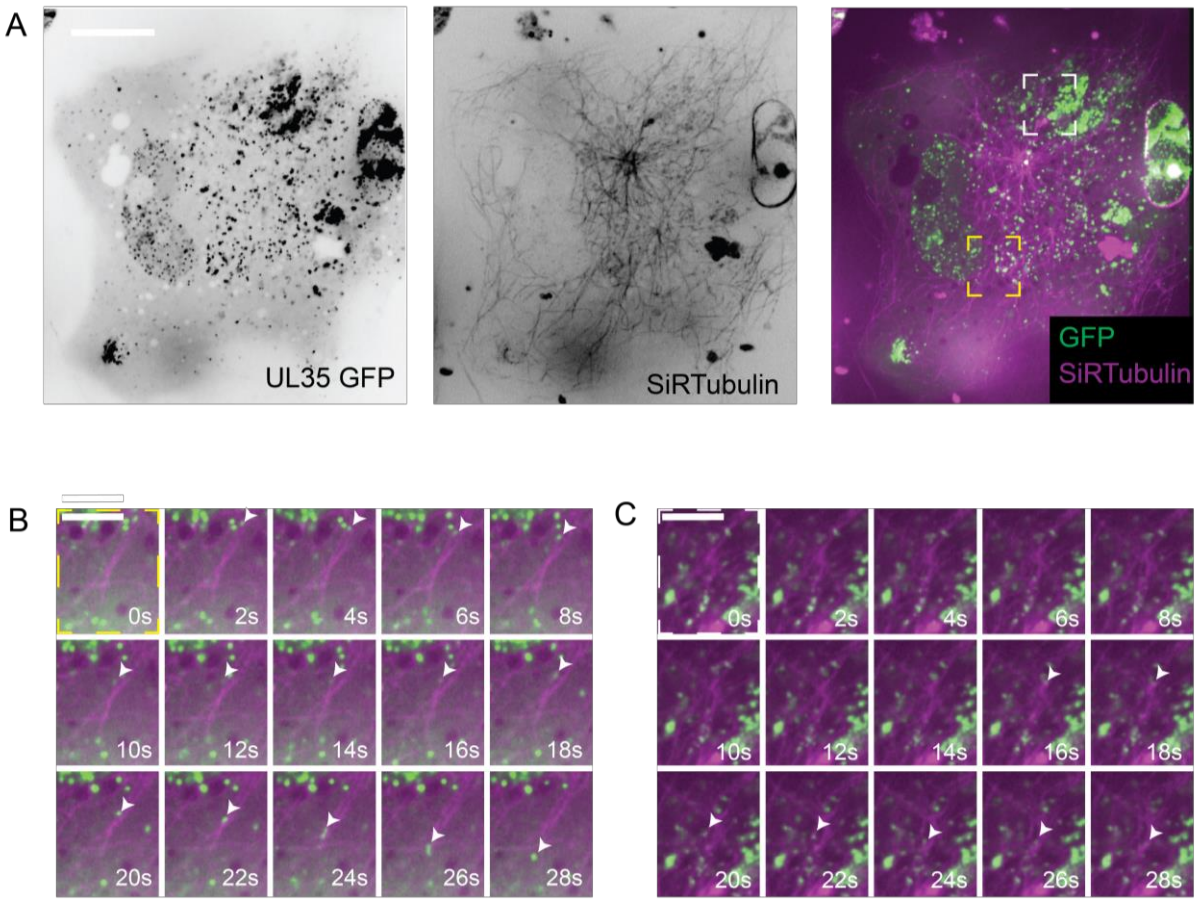


**Figure 4.3: Viral capsids are transported along microtubules**

(A) Representative image of CEF infected with RB1B UL35-GFP and stained with SiR-Tubulin dye. Viral capsids shown in green and magenta shows microtubules. The yellow box highlights an area with low microtubule density, and white box indicates an area with high microtubule density. Scale bar is 20 µm. (B) Montage of the yellow box showing a viral capsid moving along a microtubule. White arrow indicates a viral capsid. Scale bar is 5 µm. (C) Montage of the white box showing viral capsid moving. White arrow indicates movement of a viral capsid. Scale bar is 5 µm.

## 4.2: Viral capsids are transported along microtubules

To fully characterise viral capsid behaviour on microtubules, a temporal resolution high enough to capture the fast movement of directional capsid movement and a super-resolution image of microtubules is required. MDV viral capsids are approximately 125 nm in diameter, and a fully mature virus with a tegument and envelope is ~200 nm in diameter (Ahmed and Schidlovsky, 1968). Super-resolution images of viral capsids are not required as capsids are usually singular outside the nucleus (Fig 4.1A) and their large size means they can be resolved using approaches such as total internal reflection fluorescence (TIRF) microscopy and spinning disk confocal microscopy

Super-resolution microscopy is required, however, to resolve individual microtubules. Microtubules have a diameter of approximately 25 nm (Mandelkow and Mandelkow, 1989), Techniques that can be employed to resolve them are Electron Microscopy (EM), Photoactivated localisation microscopy (PALM) (Zhang et al., 2017), live Stimulated Emission Depletion Microscopy (STED), Structured Illumination Microscopy (SIM) (Wegel et al., 2016) and Stochastic Optical Reconstruction Microscopy (STORM) (Rust et al., 2006). STORM relies on the natural stochastic ‘blinking' of fluorophores usually used in fluorescence microscopy (Fig 4.4). However, this technique requires fixing samples, and therefore dynamic microtubule data cannot be obtained. Based on the limitations of each technique, combining confocal/TIRF microscopy with STORM was determined to be the best approach to try and address capsid dynamics on microtubules. This combination would provide the high temporal resolution required for characterising viral capsid dynamics and provide a super-resolution image of the microtubules to correlate with capsid dynamics.

During standard STORM with our setup cells are directly seeded on to coverslips. Once ready cells are prepared for STORM and then a simple chamber is created directly on the coverslip containing the cells using motor grease and another coverslip. Then, STORM buffer is flown directly in to the

chamber containing stained cells and sealed. This chamber is directly mounted on to the microscope and STORM imagining is carried out on the coverslip containing the cells (Fig 4.4). This is a very straight forward and effective way of getting high resolution STORM images.

Combining TIRF and STORM had to introduce changes to our standard protocol for STORM. The changes included the use of a gravity flow microfluidics chip system built on the in-house Warwick Open Source Microscope (WOSM) system capable of both TIRF and STORM (Fig 4.5) (see methods for greater detail). This was loosely based on a much more sophisticated microfluidics system developed previously (Tam et al., 2014).

Three different generations of chambers were tested. Generation 1 was a simple design that had an output and input insert at each end for flow and a large viewing chamber for cell growth and imaging (Fig 4.5B). Using this chamber produced poor STORM reconstructions and the resolution obtained was no different to confocal microscopy (Fig 4.5C-D). Generation 2 chambers were slightly more complex and were designed to reduce the rate of flow into the viewing chamber by restricting flow into smaller channels before liquid reached the viewing chamber (Fig 5B). This produced much better staining of microtubules where they could be seen, but the resolution obtained for STORM was still poor (Fig 4.5C-D). Generation 3 chambers were designed to further slow down the flow of liquids into the viewing chamber to a rate of 50 µl/s (Fig 4.5B). Also, bi-directional flow of fluids was used in this chamber: antibody-containing solutions were moved back and forth in the chamber during incubation. Of all the chamber designs tested, Generation 3 chambers provided the best STORM reconstructions, with a resolution of 160 nm (Fig 4.5C-D). However, this resolution was still not close enough to the 30-50 nm resolutions achieved with our standardised STORM protocol (Fig 4.4). A second limitation with this approach was the lack of an environmental chamber, meaning the live imaging aspect of the experiment was carried out at room temperature, therefore not reflecting physiological conditions.

To address these issues correlative confocal spinning disk and STORM was carried out (Fig 4.6A-B) (see methods for further details). This addressed the environmental chamber issue and the low resolutions achieved with microfluidics. However, there were also some drawbacks to this approach, these being that the two images used for correlation could not be correlated accurately in the Z dimension. X and Y dimension correlations were achieved simply by using viral capsids as markers for a reliable correlation. However, it is not possible to determine whether the live capsid movies and the STORM images were taken in the same Z. This caused some capsids to appear to run in areas where no microtubules were present. Another limitation was that the super-resolution microtubule image was static from the end point of the movie and no information regarding the position of the microtubule during the movie could be obtained. Growth and shrinkage of microtubules could affect the viral capsid dynamics, and there was not a way of determining whether either had occurred with this approach. Therefore, super-resolution imaging of live microtubules along with live capsid dynamics is required.

To achieve live super-resolution imaging, the newly developed Super-Resolution Radial Fluctuations (SRRF) microscopy technique was employed (Gustafsson et al., 2016). This approach allows the use of conventional microscopes including widefield, confocal and TIRF to generate super-resolution images from live (or fixed) cells. The achievable resolution is stated at 60 nm (Gustafsson et al., 2016) , although only 100 nm resolutions were obtained during this study. This was still a significant increase in resolution compared to the correlative super-resolution and confocal microscopy attempted previously and was sufficient to study viral capsid dynamics in live cells. Individual viral capsids were matched to microtubules reliably using this method (Fig 4.7A-C) This was achieved by separating the two channels imaged, generating SRRF images for the microtubules and then recombining the super resolution microtubule image to the capsid images (see methods for more detail).

Using SRRF microscopy to correlate individual viral capsid runs to single microtubules provided insights into the characteristics of viral capsid

behaviour. All SRRF movies were a minute long. Viral capsids outside the nucleus showed that 89.4 % are associated with microtubules. Within this, 56.6% (±13.6 %) are stuck or pausing and showing little or no directional transport. Directional transport was observed with 11.8 % (± 4.8 %) of viral capsids outside the nucleus. Bi-directional transport was observed with 3.7 % (±1.6 %) capsids suggesting multiple motors transporting viral capsids. Microtubule track switching was observed with 9.1 % (±6.6 %) of viral capsids outside the nucleus. Diffusion of capsids along microtubules was observed with 5.1 % (±1.8 %) of viral capsids. Occasional binding of capsids to microtubules but not being transported was observed with 3.1% (±2.8 %) of capsids (Table 9). Together, these findings suggest that the majority of viral capsids outside the nucleus are engaging with microtubules even though only a fraction of them are actively transported at any given time.

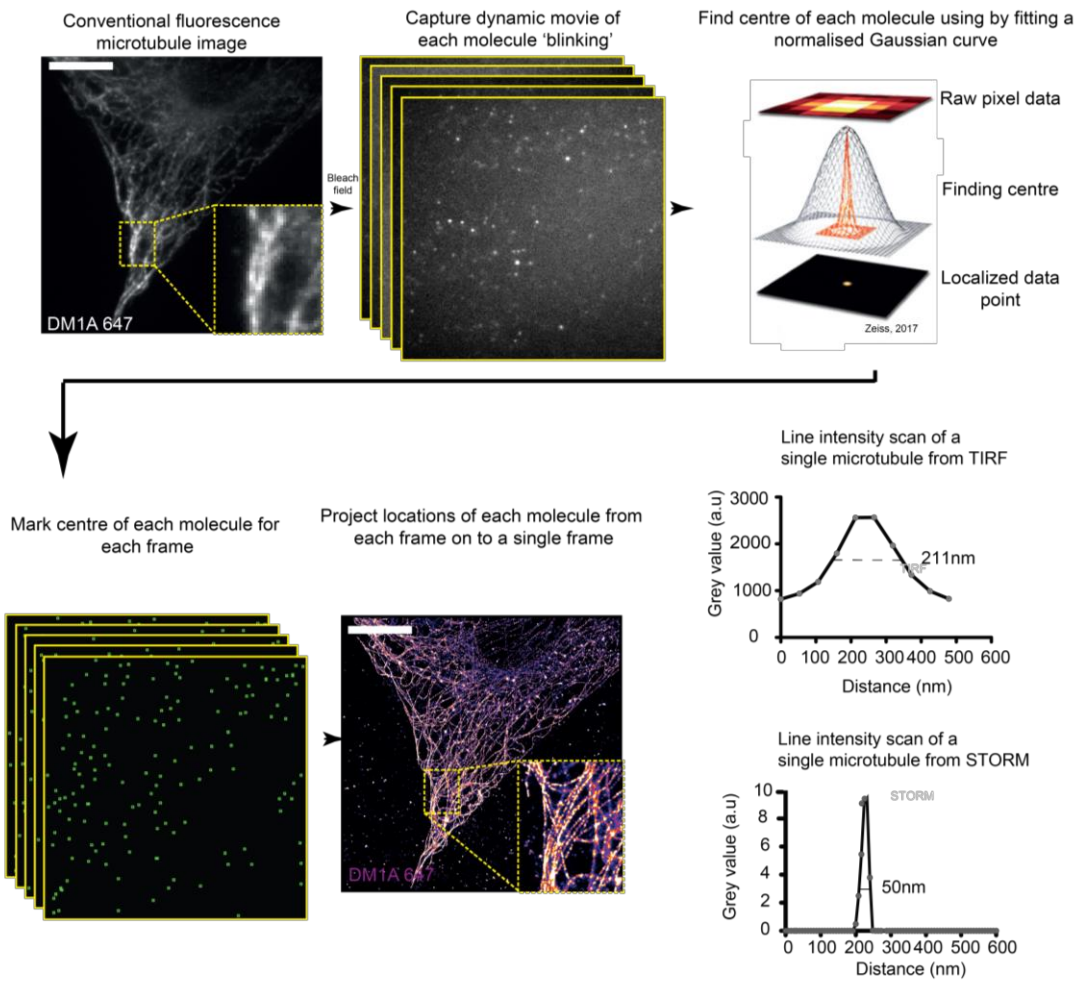


**Figure 4.4: Workflow of STORM**

Schematic workflow of STORM. The cell of interest was imaged using conventional microscopy first as a reference image. Using 100 kW/cm$^2$ 647 nm laser power all the fluorophores were forced into a dark state. Once sufficiently bleached, 647 nm laser power was reduced to 40-60 kW/cm$^2$ to promote stochastic blinking of the fluorophores. 1-5 kW/cm$^2$ of 405 nm laser was also used to promote blinking events. The acquisition is started at this point. After a sufficient number of frames (~20,000) are taken, the acquisition is stopped. Then the localised point of each 'blink' from each frame is calculated using a normalised Gaussian curve. Each point is then superimposed on to a single image to form a reconstructed STORM image. By fitting each molecule to an exact position, the diffraction limit is eliminated, and resolution can be increased up to 10 times.

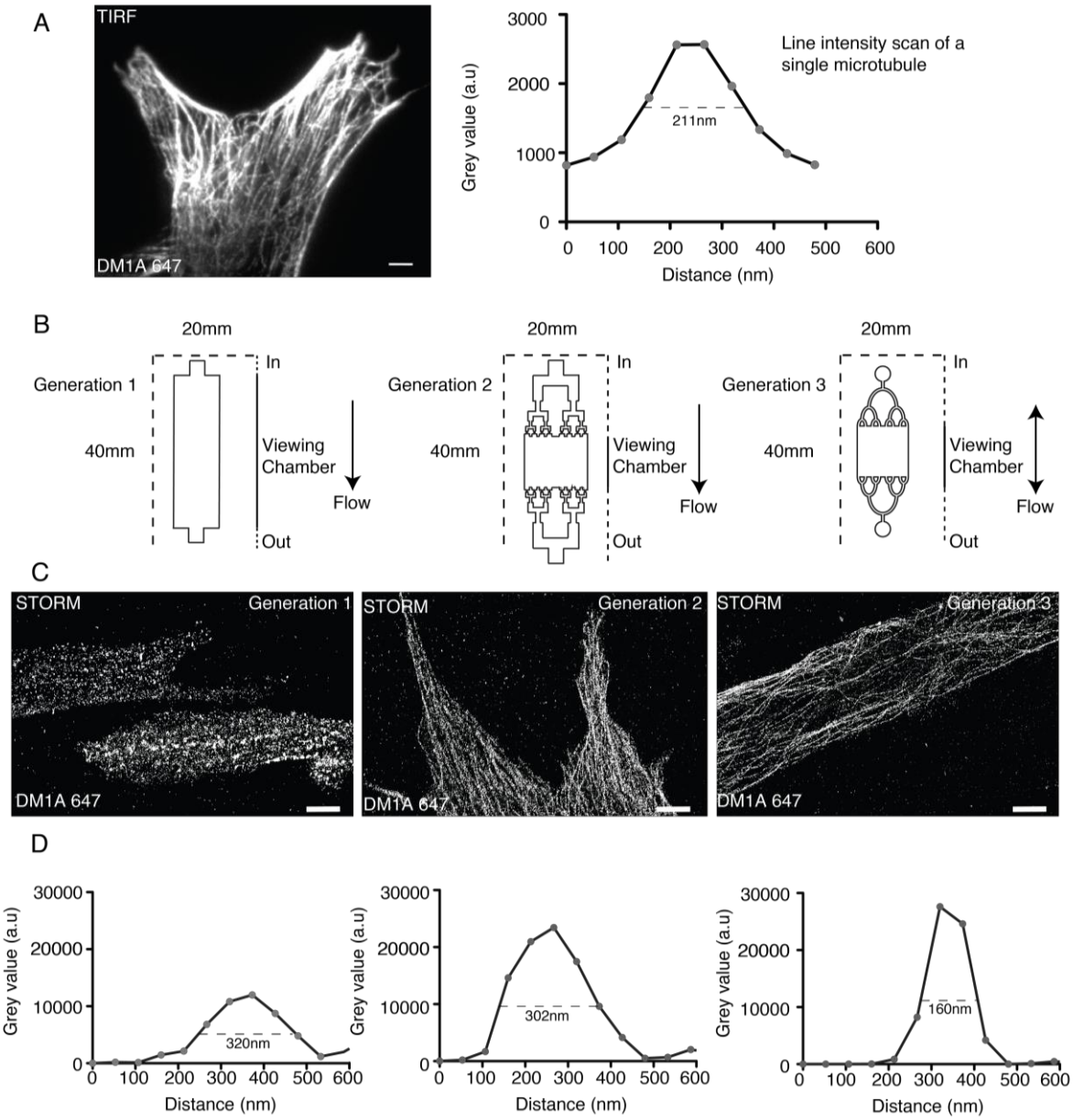


**Figure 4.5: Microfluidic STORM**

(A) Representative image of TIRF microscopy showing microtubules and a line intensity scan of a single microtubule demonstrating the width of a microtubule which is the resolution achieved with TIRF microscopy. (B) Schematics of the chambers designed and used. Arrows indicate the direction of flow in each generation. Viewing chamber is where the cells were seeded, grown and imaged. (C) STORM reconstructions of microtubules from each chamber. Images show the best STORM images obtained from each chamber generation. (D) Line intensity scans showing the width of a single microtubule to demonstrate the resolution obtained from each chamber.

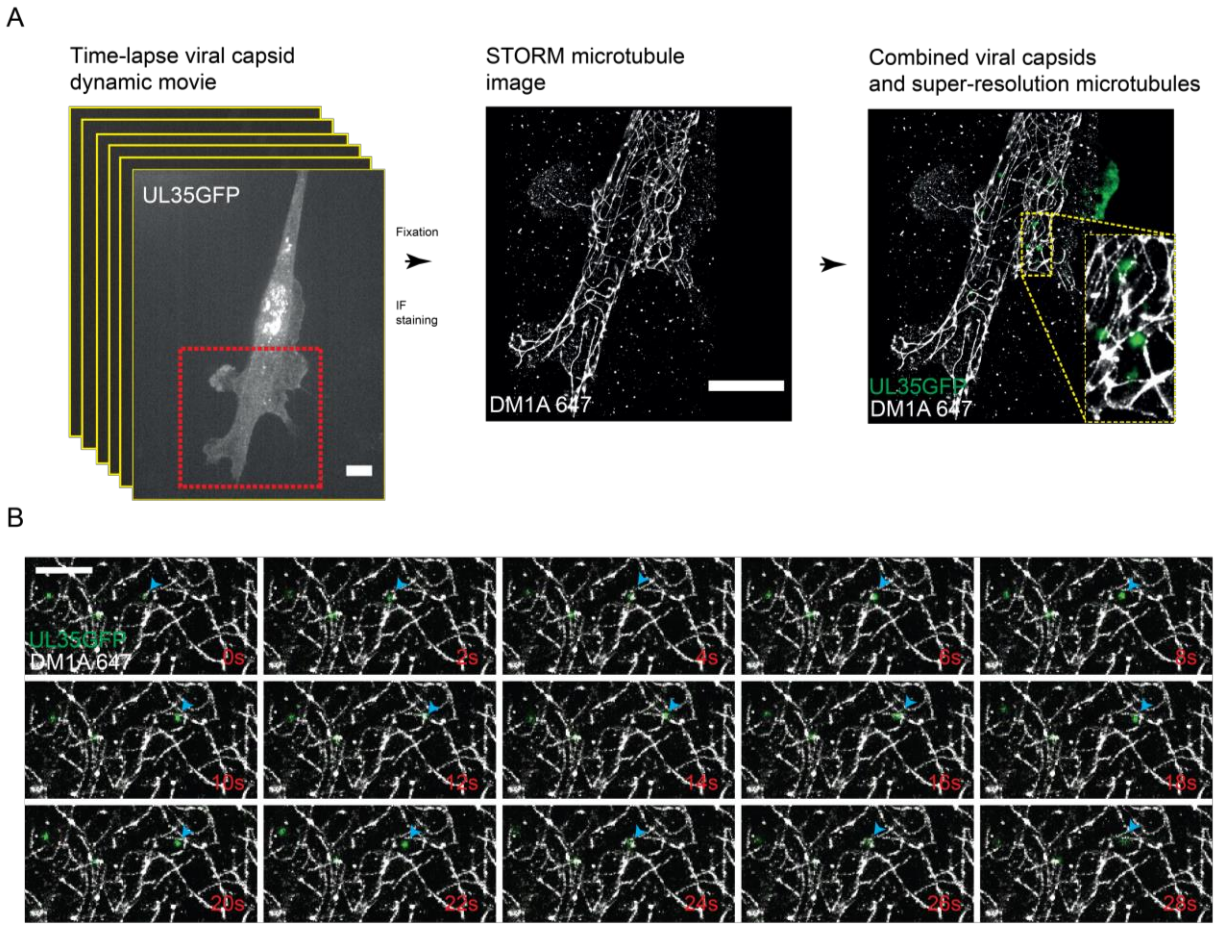


**Figure 4.6: Correlative spinning disk confocal microscopy and STORM**

(A) Schematic representation of the workflow for correlative confocal and STORM microscopy. First, the infected cells are imaged live, fixed on stage and then prepared for STORM. A STORM image of the microtubules is then generated. The movie of viral capsids and the STORM image is then correlated in X and Y using the viral capsids as landmarks. The red box indicates the area that was used for STORM. (B) Montage of viral capsid showing directional transport on microtubules. Blue arrow indicates and follows a single viral capsid. Each frame of the montage is 2s. Scale bar is 5 µm.

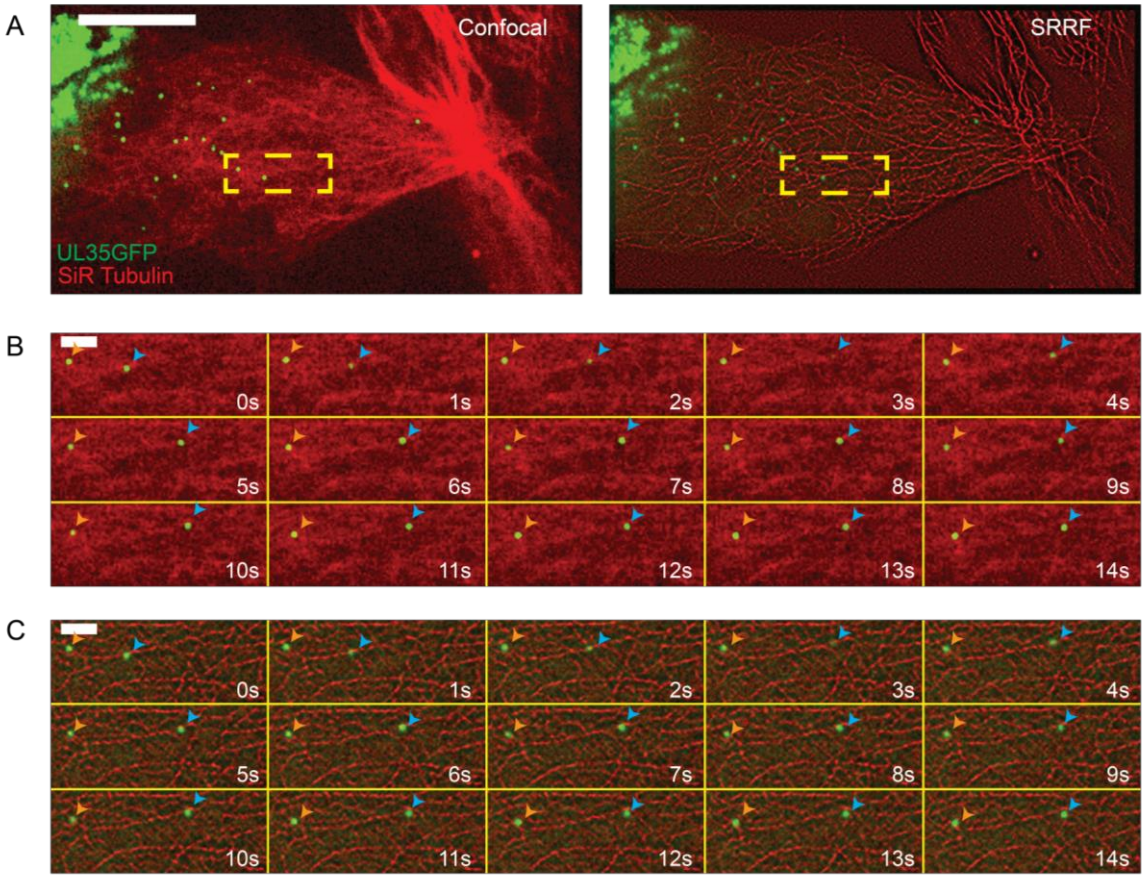


**Figure 4.7: Live SRRF microscopy and viral capsid dynamics**

(A) Representative images comparing spinning disk confocal microscopy (left) and SRRF microscopy (right) images of the same cell. The image shows viral capsids in green and microtubules in red. The yellow box indicates the area shown in the montages. Scale bar is 20 µm. (B-C) Montage of viral capsid moving along microtubule from confocal microscopy/SRRF microscopy. Orange arrow indicates static viral capsid and blue arrow indicates viral capsid that has directional movement along a microtubule. Scale bar is 5 µm.

| Illustration | Event name | Description | Percentage of event occurrence |
|---|---|---|---|
| **Microtubule-independent events** | | | |
| 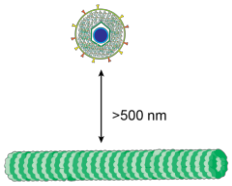 | Stationary | Viral capsid that is not associated with a microtubule and is not showing any signs of diffusion | 7.1 % (± 4.7 % (s.d.)) |
| 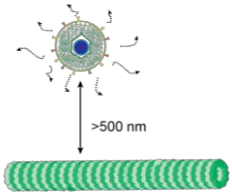 | Diffusing far from Microtubule | Viral capsid that is diffusing and is more than 500 nm away from the nearest microtubule | 0.9 % ((± 0.3 % (s.d.)) |
| 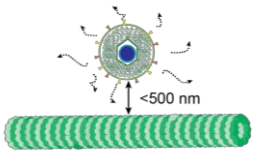 | Diffusing near microtubule | Viral capsid that is diffusing and is less than 500 nm away from the nearest microtubule and not binding to it | 2.7 % ((± 0.3 % (s.d.)) |
| **Microtubule-associated events** | | | |
| 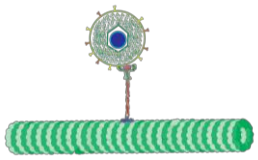 | Pausing or stuck | Viral capsid that is clearly on a microtubule and is not showing any movement | 56.6 % ((±13.6 % (s.d.)) |
| 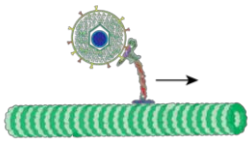 | Directional movement | Viral capsid that is directionally travelling on a microtubule and travels over 500 nm in distance | 11.8 % ((± 4.8 % (s.d.)) |
| 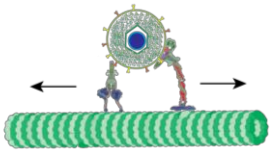 | Bi-directional movement | Viral capsid that is showing directional movement in both directions on the same microtubule | 3.7 % ((± 1.6 % (s.d.)) |
| 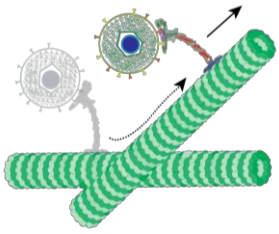 | Track switching | Viral capsid that is switching microtubules – usually multiple times during the acquisition | 9.1 % ((± 6.6 % (s.d.)) |

| | | | |
|---|---|---|---|
| 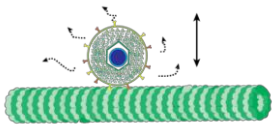 | Diffusing near microtubule and binding | Viral capsid that is diffusing and is less than 500 nm away from the nearest microtubule and binding to it | 5.1 % ((± 1.8 % (s.d.)) |
| 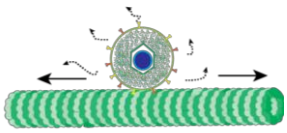 | Diffusing along microtubule | Viral capsid that is travelling on a microtubule in a non-directional manner and travels under 500 nm in distance | 3.0 % ((± 2.8 % (s.d.)) |

**Table 9: Summary of viral capsid dynamics**

Quantification from SRRF movies. Total of 385 capsids were analysed from 19 cells from 3 independent experiments. Note: a single viral capsid can be attributed to multiple events, i.e. a running capsid that is directionally transported over 500 nm then stops and then switches microtubules would be marked as directional movement and track switching.

## 4.3: Viral capsids are in very close proximity to microtubules in the cytoplasm

Using super-resolution microscopy to identify viral capsid interactions with microtubules has shed light on capsid dynamics. However, the nature of these viral capsids is not known and whether these capsids possess an envelope is a question that remains to be addressed. Determining whether viral capsids poses an envelope in the cytoplasm can help understand how viral capsids are transported. To attempt to understand at which stage of maturation these capsids are, e.g., if they have a viral membrane or are they in vesicles, EM was employed. RB1B UL35-GFP infected CEFs were pelleted, high-pressure frozen, stained with heavy metals, embedded in resin, sectioned and then imaged. Infected cells were first identified by searching for a nucleus that contained viral capsids. Various cytoplasmic regions that contained viral capsids were then imaged (Fig 4.8).

Infected cells are easily identifiable as viral capsids are electron dense and have a distinct structure. In infected cells, the nucleus contained many viral capsids, and some capsids could also be seen in the cytoplasm (Fig 4.8A). Investigating cytoplasmic capsids further revealed three distinct states for viral capsids; the naked capsid that lacks an envelope and is approximately 125 nm in diameter (Fig 4.8B); the fully enveloped viral capsid with an approximate diameter of 200 nm (Fig 4.8C); or the naked viral capsid/ fully enveloped virus within a vesicle of varying sizes (Fig 4.8D). Most viral capsids observed outside the nucleus were naked viral capsids (31/36). Enveloped viral capsids comprised only a small fraction of total capsids observed (5/36). A small percentage of viral capsids were in vesicles (4/36) and of that population, 75 % (3/4) were naked capsids and 25 % (1/4) were enveloped.

The distance between each viral capsid and the closest microtubule was also measured. As a negative control each viral capsid was shifted by 200nm and the distance to the nearest microtubule was measured again. This method ensured that if microtubules were randomly near viral capsids then there would

be no difference between the shifted viral capsid and actual viral capsids distance a microtubule. The median distance of viral capsid to a microtubule is 143 nm whereas when shifted this increased to 179 nm in the negative control suggesting viral capsids are close to microtubules. However, statistically this is insignificant, possibly due to low n numbers present in our study.

There are other studies that have shown that *Alphaherpesvirus* capsids from HSV-1 infection are also in close proximity to microtubules using electron microscopy techniques. Immunoelectron microscopy was used to show that cytosolic capsid transport of HSV-1 particles in Vero cells is mediated by microtubules and that viral capsids are indeed in very close proximity to microtubules (Sodeik et al., 1997). Additionally, immunoelectron microscopy targeting Kinesin-1 has shown that HSV-1 particles are being transported along microtubules in neurons (Miranda-Saksena et al., 2009). Therefore, our findings are in line with the consensus that *Alphaherpesvirus* particles are in close proximity to microtubules.

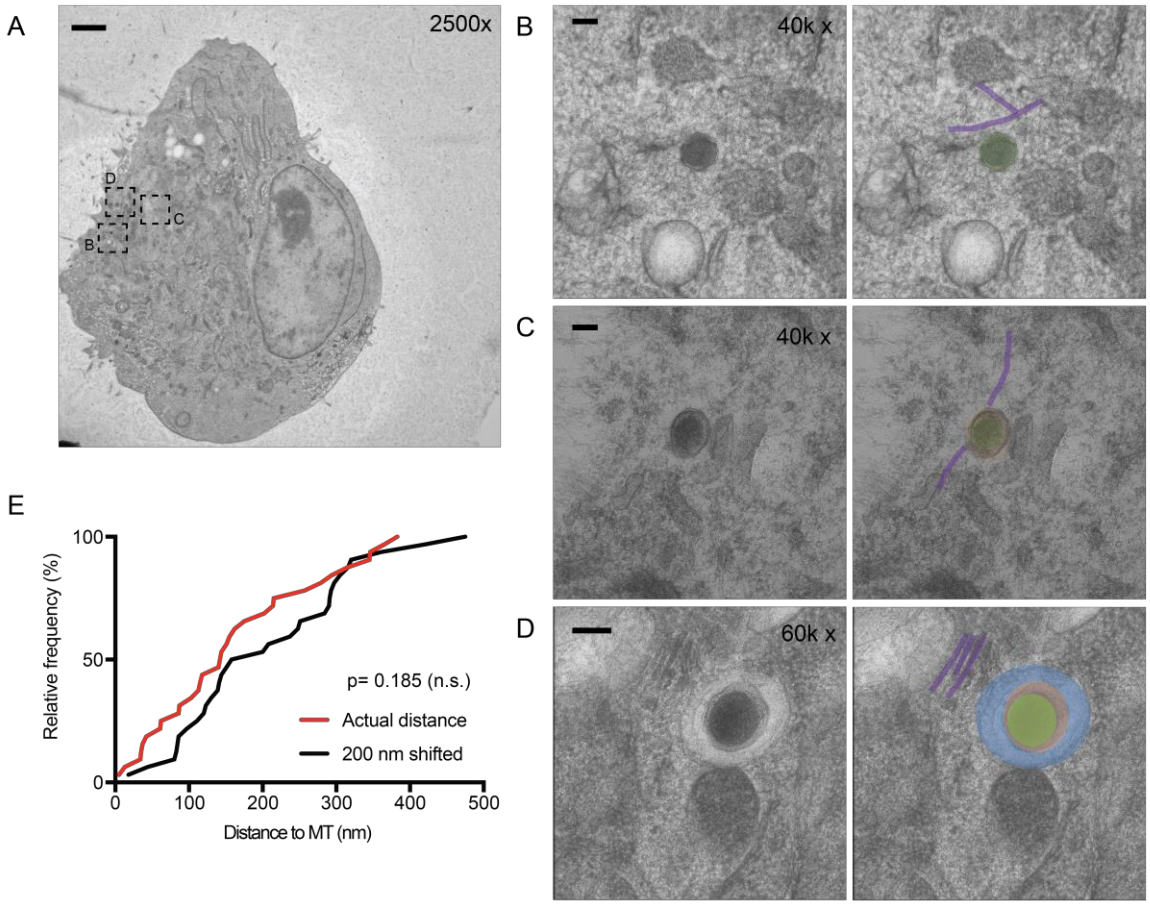


**Figure 4.8: Viral capsids are very close to microtubules and lack viral envelopes**

(A) CEF cell infected with RB1B UL35-GFP. The cell was stained with heavy metals and sectioned into 200 nm thick sections. This is a 2500 x magnification. Scale bar is 1 µm. The black boxes indicate from where the images in B, C and D are derived. (B) A naked viral capsid in the cytoplasm. 40k x magnification. Scale bar is 100 nm. (C) A viral capsid with an envelope. 40k x magnification. Scale bar is 100 nm. (D) A enveloped viral capsid inside a vesicle. 60k x magnification. Scale bar is 100 nm. For all inserted images, a raw image and an annotated image is shown. Green is a viral capsid. Orange is a viral envelope. Blue is a vesicle. Purple is a microtubule. (E) Cumulative frequency plot showing distribution of the distances measured of viral capsids to the closest microtubule. In red is the actual distance to the closest microtubule for each viral capsid. In black is the 200 nm shifted viral capsid distance to the closest microtubule. N = 32 viral capsids and 3 cells. Statistical significance is p=0.185 (not significant) (Kolmogorov- Smirnov test).

## 4.4: Discussion

### 4.4.1: Super-resolution microscopy

Recent advances in super-resolution microscopy have enabled the visualisation of subcellular structures that are too dense to be separated with classical optical techniques. However, super-resolution approaches such as STORM can only be applied to fixed samples or live samples that require very low (minutes) temporal resolutions. To overcome this, we attempted correlative live cell imaging of viral capsids and STORM imaging of microtubules. Combining live imaging and STORM had been achieved before with the use of a computer-controlled fluid injection system and multi-channelled flow switching system (Tam et al., 2014). The system used in this study was a single channel gravity flow-controlled microfluidics chip, which was a much simpler approach.

Established protocols were used in the microfluidics chips for seeding cells, immunostaining and STORM imaging. This resulted in poor STORM images. One of the first problems that needed addressing with this approach was the low number of cells adhering in the viewing chamber of the chip. This effect is common and usually seen in blood cells flowing through capillaries: the Fahraeus-Lindqvist effect (Lindqvist, 1931). This effect describes how fluids become less viscous as the diameter of tubing gets smaller. This results in lower density of cells flowing though the tubing and therefore fewer cells being seeded. This problem was overcome by increasing the number of cells seeded by 20-fold. The second problem with this approach was the poor quality of the STORM images obtained. This was be attributed to the fact that most sample preparation protocols are optimised for materials like polystyrene and glass. These have very different material properties compared to PDMS (Berthier et al., 2012). PDMS tends to absorb small molecules (Toepke and Beebe, 2006) and can change the local concentrations of some reagents unpredictably. These characteristics of PDMS could have resulted in the poor STORM reconstructions obtained from the microfluidic chips used in this study.

Previous studies have overcome this problem by going through a stepwise optimization procedure for each chip (Tam et al., 2014). Carrying out a similar procedure was not possible within the limited time-frame of this study.

In order to overcome the poor STORM reconstructions, the method was changed to correlative spinning disk and STORM microscopy. This approach used an established STORM protocol that would provide the resolution required to resolve microtubules. Correlative spinning disk and STORM proved to provide the temporal and optical resolution required for addressing viral capsid dynamics on microtubules. However, significant limitations with this approach were also encountered. The main issue was the lack of reliable Z correlation between the spinning disk image and the STORM image, as these were obtained from two different microscopes. Correlating in the Z dimension was near impossible without obtaining 3D movies of viral capsids and STORM images. 3D movies were not possible as viral capsid transport is a very rapid process and at least 2-3 Hz is required for reliable tracking. Lattice Light Sheet Microscopy (LLSM) could be used to achieve the 3D temporal resolution but finding the same cell again on the WOSM would be near impossible. Also obtaining 3D STORM images was not possible at the time while using the WOSM system. This resulted in abandoning this approach.

Recently, other studies were able to correlate live and super-resolution images (Xiang et al., 2018). This was achieved by using 3D live imaging and STORM images to achieve correlation not only in X and Y also in the Z dimension. No fiducial markers were required during their study as the object of study; replication domains produce distinct structures that was be used instead.

SRRF microscopy was the super-resolution microscopy technique that was able to finally meet the criteria required to associate MDV viral capsid dynamics to microtubules. This was a much simpler approach compared to all the correlative work that was attempted previously and proved to be an indispensable tool to finally study viral capsid dynamics. SRRF has been used to study a wide range of cellular functions (Khan et al., 2017, Retzer et al.,

2017, Weihs et al., 2018) but this is the first time it has been used to study viral infection to the best of our knowledge.

### 4.4.2: Viral capsids are associated with microtubules

Microtubules and their associated motor proteins are involved in *Alphaherpesvirus* capsid transport (Dohner et al., 2002, Mabit et al., 2002, Pasdeloup et al., 2013a, Pasdeloup et al., 2013b, Sodeik et al., 1997). However, MDV capsid transport has not previously been associated with microtubules. The only reference to MDV infection associating with microtubules was the suggestion that MDV VP22 from MDV is associated with microtubules (O'Donnell et al., 2002), and only shown via immunofluorescence. To the best of our knowledge this study is the first to show that MDV viral capsids are not only associated with microtubules but are actively and directionally transported along them.

Viral capsid behaviour was characterised in this study, with many viral capsids observed showing very little directional transport during image acquisition. This was surprising as viral capsids on microtubules would be expected to be transported along rather than statically bound to microtubules. Other studies have also reported stalled/stationary capsids bound on microtubules. PRV viral capsids that are transported along microtubules via Kif1A during egress included up to 30% of viral capsids that were stationary but remained bound to the microtubules (Kramer et al., 2012). Therefore, having a high number of stationary capsids may be expected. This phenomenon could be a result of limited imaging time, as only a snapshot of time is taken from an infected cell and catching all viral capsids undergoing directional transport during this time is not possible. The fact that these viral capsids are bound to microtubules and remain bound to microtubules during image acquisition also indicates the possibility that these viral capsids will undergo directional transport eventually.

Bi-directional transport of MDV viral capsids was also observed in this study. HSV-1 and PRV viral particles have both also been described to be

transported in a bi-directional manner (Antinone and Smith, 2010, Smith et al., 2001, Smith et al., 2004). This bi-directional transport is probably a result of viruses avoiding obstacles on microtubules, such as other cargo and may occur to ensure that they are trafficked to the right cellular location. This model was suggested for general cellular cargos and can be applied to viruses as they are essentially considered cargo by the host (Welte, 2004). The fact that viruses employ bi-directional transport raises several questions regarding a net direction of viral transport towards the cell periphery and how is this controlled during viral entry and egress. Few models are proposed for bi-directional transport. The first is that a tug-of-war exists between plus end and minus end-directed motor proteins that transport viral capsids. It is thought that the number of motors and their competing activities define the direction of travel (Akhmanova and Hammer, 2010, Hendricks et al., 2010, Muller et al., 2008, Shubeita et al., 2008, Soppina et al., 2009, Verhey et al., 2011). The second model is that the opposite polarity motors regulate the activity of each other as they are usually coupled together (Akhmanova and Hammer, 2010, Ally et al., 2009, Encalada et al., 2011, Gennerich and Vale, 2009). Other models are the microtubule tethering state and the steric disinhibition models (Hancock, 2014). It would be essential to address how bi-directional MDV capsid transport is regulated in the future. This can be achieved by either purifying entire MDV viral particles with motors and adaptors still bound to them or tagging potential motors and adaptors with fluorescent markers and visualizing interactions in cells, or by rebuilding the entire transport system with viral capsids *in vitro*.

### 4.4.3: Most MDV viral capsids in the cytoplasm lack an envelope

This study has shown that most MDV viral capsids in the cytoplasm lack an envelope. This suggests that there is a large population of viral particles present in the cytoplasm awaiting secondary envelopment. In other *Alphaherpesviruses* such as HSV-1 and PRV there has been some controversy as to whether viral capsids observed with directional movement possess a viral envelope or a tegument layer. Using fixed cell imaging, it was

not possible to determine whether the viral capsid possesses a viral envelope and has undergone transport (Saksena et al., 2006, Snyder et al., 2006). However, with live cell imaging, 70% of viral capsids undergoing directional transport were determined to have a viral envelope (Antinone and Smith, 2006, Antinone et al., 2010, Feierbach et al., 2007). It was also determined that the majority of HSV-1 and PRV particles were found within vesicles (Avitabile et al., 1995, Huang et al., 2011, Maresch et al., 2010, Negatsch et al., 2010). However, only a small fraction of MDV viral capsids were in vesicles.

There are some significant differences from the studies already carried out with HSV-1 and PRV, and this study. Firstly, the cell types employed: the majority of HSV-1 and PRV work is carried out in cultured neurons and Vero cells, whereas all the work in this study was carried out in primary chicken cells (mainly embryonic fibroblasts) due to the fact the wild-type MDV only infects primary cells in culture. Different cell types may result in different secretory pathways to be exploited resulting in changes to the viral life cycle (Huang et al., 2005). Therefore, the viral membrane could be obtained much later resulting in a higher percentage of viral capsids waiting for secondary envelopment. Additionally, although MDV is in the same family as HSV-1 and PRV, there could be critical differences in viral capsid maturation and secondary envelopment, and it would be interesting to investigate these in the future. Determining that most MDV viral capsids lack an envelope needs to be verified with the use of viral envelope markers, which would also allow correlation of enveloped viral particles with microtubules during transport.

## 4.5 Summary

MDV Viral capsids are shown to be transported on microtubules: removal of microtubules prevent the directional transport of MDV capsids. However, artificially stabilising microtubules with Taxol did not affect viral capsid transport, suggesting that microtubule dynamicity is not required for active transport. Super-resolution microscopy reveals that the majority of viral capsids outside the nucleus associate with microtubules and are transported on them. Electron microscopy suggested that most viral capsids in the cytoplasm lack a viral envelope and are very close to microtubules.

# Chapter 5: Kinesin-3 transports viral capsids

Based on the findings that MDV viral capsids are transported directionally along microtubules, the molecular motors responsible for transporting viral capsids were investigated. *Alphaherpesvirus* capsids undergo directional trafficking, and the molecular motors dynein and kinesins are responsible for this (Antinone and Smith, 2006, Antinone et al., 2010, Hirokawa et al., 2009, Radtke et al., 2010). Dynein is a minus end directed molecular motor responsible for transporting a wide range of cargo towards the centre of the cell (Flores-Rodriguez et al., 2011, Roberts et al., 2013, Rogers et al., 2001, Rogers et al., 2010). Kinesin-3s are fast organelle, endosome and mitochondria transporters (Siddiqui and Straube, 2017, Yamada et al., 2014, Yue et al., 2013).

## 5.1: Kif13B transports MDV viral capsids.

To identify promising candidates for viral capsid transport from the 45 possible kinesins, a split kinesin assay was employed. This assay, developed by the Banker Lab (Jenkins et al., 2012), is dependent upon a chemical dimerisation inducer – rapamycin (Choi et al., 1996). During this assay, CEFs are transfected with two plasmids. The first plasmid expresses a Kif5C motor domain with a tdTomato marker and an FRB domain on the C-terminus. Kif5C motor domains can bind and travel on microtubules, however, this protein is not able to bind to cargo as it lacks all cargo binding domains found on the tail region of kinesins. The lack of a tail means that the protein is constantly active: once on a microtubule it will continue to travel towards the plus end with minimal regulation, which is usually provided by the tail region. The second plasmid expresses the tail domain of a kinesin of choice (see methods – split kinesin assay) that lacks a motor domain but has an FKBP domain on the N-terminus. This tail can bind to its native cargo but lacks the motor domains to bind to microtubules and transport them. These two truncated proteins remain independent until the addition of rapamycin to bring the FRB and FKBP

domains together to form a chimeric kinesin, that is capable of binding both to MTs and to cargo.

The approach taken was to individually express a different kinesin tail with the Kif5C motor domain in CEFs. These cells were seeded in co-culture with infected cells. After 2 days, 0.5-1% of the transfected cells became infected. The kinesin tail expressed in an infected cell might bind to the viral capsid, enveloped virus or a vesicle containing the viral particle but be unable to transport it. Upon addition of rapamycin a chimeric kinesin bound to the viral capsid might be formed and transport the viral capsid along microtubules. In this case, a detectable change in viral capsid dynamics was observed after introducing rapamycin. If the expressed kinesin tail does not associate with the viral capsid, no change in dynamics was observed following rapamycin addition (Fig 5.1A-B).

As expected, the dynamics of viral capsids in non-transfected and motor domain only transfected cells did not significantly change upon addition of rapamycin (Fig 5.1C). Co-expressing the Kif5C (kinesin-1 family) tail domain with the Kif5C motor domain resulted in a dramatic reduction in the percentage of viral capsid runs over 1.5 μm/min. Expression of Kif17 (kinesin-2 family) resulted in no observable change to dynamics. Kif1A, Kif1Ba, Kif1Bb, Kif13A and Kif13B (kinesin- 3 family) tail domain all showed an increase in the percentage of viral capsid runs over 1.5 μm/min. This suggests that that tail domain from these kinesins may be interacting with viral capsids. Kif13B was the only kinesin-3 family member to show a statistically significant increase in viral capsid dynamics. Kif21B (kinesin-4 family) also showed a slight increase in the number of capsids that travelled over 1.5 μm/min, although not statistically significant (Fig 5.1C). These findings suggest that Kif13B could be responsible for transporting viral capsids during egress.

To further confirm these findings, a short hairpin RNA (shRNA) mediated knockdown approach was employed. Plasmids that express two different shRNAs to target Kif13A and Kif13B were employed as well as shRNA against luciferase as a control. These plasmids also expressed mCherry tagged α-

tubulin to aid the identification of transfected cells. Transfected CEFs were maintained together with CEFs infected with RB1B UL35-GFP virus. Transfected cells that became infected were then imaged, and viral capsids dynamics were measured (Fig 5.2A).

Approximately 17% of viral capsids travelled more than 3 μm when transfected with shRNA against luciferase. This decreased to ~12 % when treated with shRNA (1) and ~14 % with shRNA (2) against Kif13B (Fig 5.2C). These changes were statistically significant. No significant change to capsid dynamics was observed with shRNAs against Kif13A (Fig 5.2C). shRNA Kif13B (1) was effective at reducing mRNA levels, whereas both shRNAs against Kif13A were not (Fig 5.2B). In line with this, only shRNA against Kif13B caused a significant reduction in viral capsid transport. These findings suggest that reducing the levels of Kif13B mRNA results in fewer viral capsids that are actively transported and therefore that Kif13B contributes transporting MDV viral capsids during egress. The drop from 17% to 12% must be considered biologically significant as high levels of redundancy between kinesin family members make it hard to completely knock-down 100% of transport as other kinesins are thought to take over transport. From the split-kinesin-assay all kinesin-3 family members showed a slight increase in capsid transport suggesting multiple members could transport viral capsids, therefore by only knocking out a single member of the kinesin-3 family a massive drop in capsid transport was not expected.

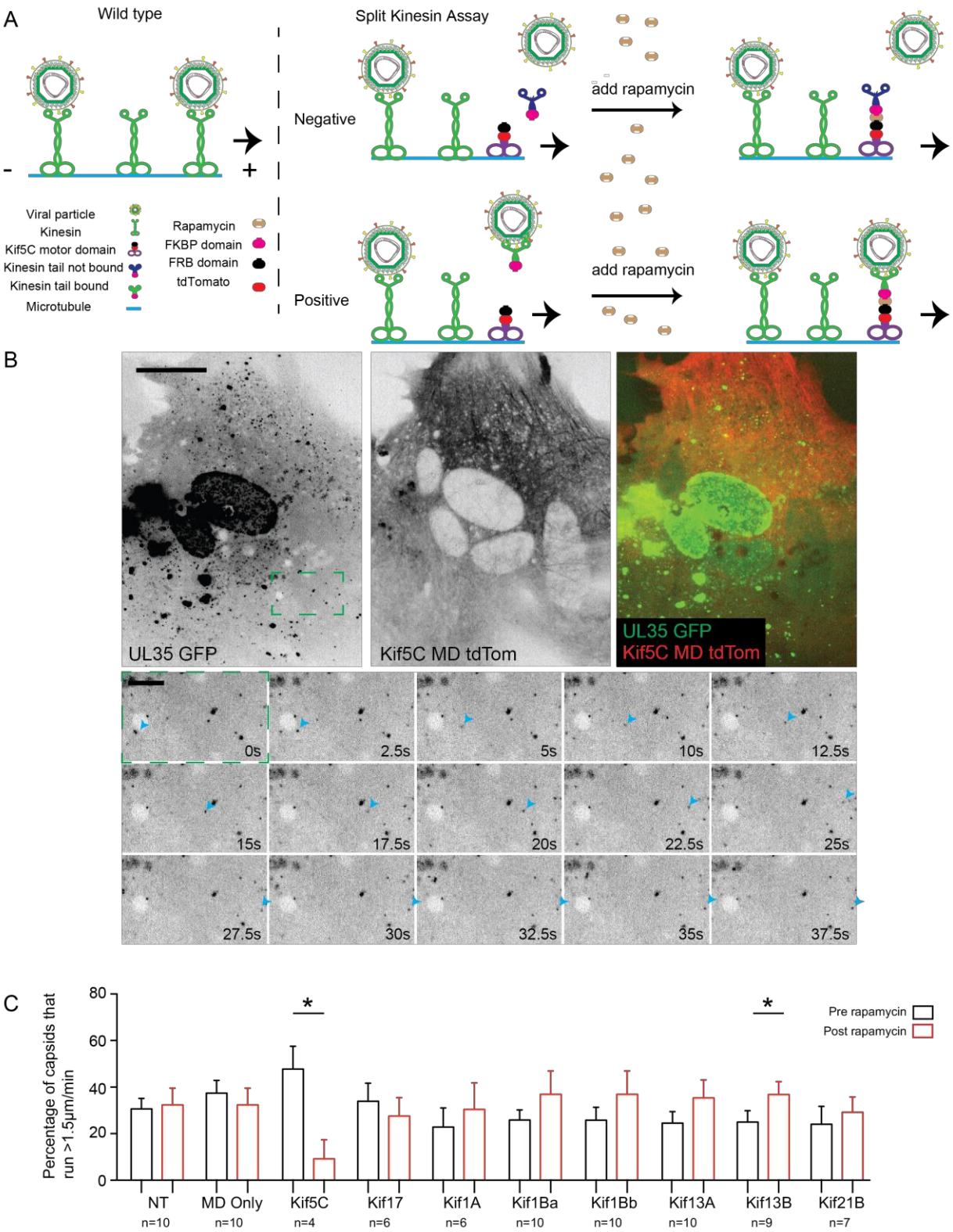


**Figure 5.1: Split Kinesin Assay: Kinesin 3's transport MDV capsids**

(A) Schematic describing the split kinesin assay. Briefly; In wild type a kinesin would interact with the viral particle to transport it along a microtubule. During the split kinesin assay CEFs are transfected with the Kif5C motor domain fused to FRB and a kinesin tail domain fused to FKBP. The tail domain either interacts with the viral capsid or does not.

Upon addition of rapamycin, the Kif5C motor domain, and the tail domain come together to form a chimeric kinesin. If the tail is bound to a viral capsid, then this results in directional transport of the viral capsid. (B) Representative images of CEFs infected with RB1B UL35 GFP (green) also expressing Kif5C motor domain with a tdTomato marker (red). Scale bar is 20 μm. Green box indicates area in montage showing viral capsids being transported during a split kinesin assay. Blue arrows are indicating and following a viral capsid. Scale bar is 5 μm (C) Graph showing quantification of the percentage (%) of viral capsids that travelled more than 1.5μm/min. Black bars represent quantification of viral capsids dynamics before rapamycin, and red bars represent after rapamycin addition. Red bars were normalised for the effects of photobleaching, black bars did not require normalization. The kinesin tail transfected is stated below each pair of bars. N numbers are indicated blow each condition. Statistical significance is $p < 0.05$ = * (Paired t-test). Error bars are the standard deviation.

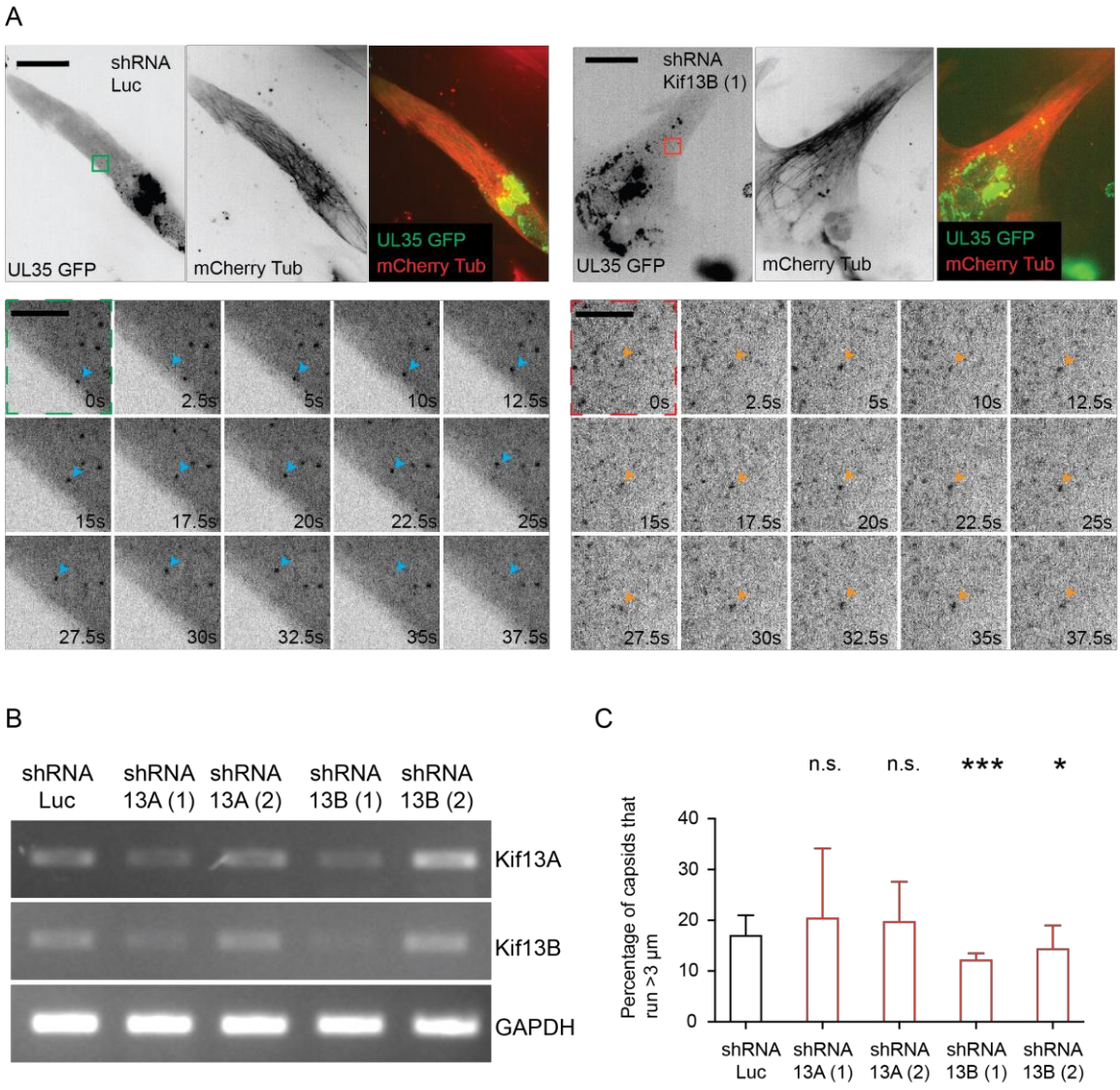


**Figure 5.2: Knock-down of Kif13B reduces the number of running capsids**

(A) Representative image of CEF transfected with plasmids expressing shRNA Luc and shRNA Kif13B(1) also expressing mCherry tubulin (red) as a marker for successful transfection and infected with RB1B UL35 GFP (green). Scale bar is 20 µm. Green box indicates montage of viral capsid transport from shRNA Luc treated cells. Red box indicates montage of viral capsid transport from shRNA Kif13B(1) treated cells. Blue arrow indicates and follows viral capsid being transported. Orange arrow indicates stationary capsid. Scale bar is 5 µm. (B) PCR using cDNA made from whole cell mRNA. Primers were against Kif13A, Kif13B and GAPDH. (C) Graph showing quantification of the percentage (%) of viral capsids that travelled over 3 µm during acquisition. The black bar is negative control shRNA against luciferase, and red bars are shRNA against Kif13A and Kif13B (two separate shRNAs used for each kinesin). n.s. is not significant, $p < 0.05$ = * $p < 0.005$ = ** $p < 0.0005$ = *** (two-sample t-test). Error bars show standard deviation.

## 5.2: Dynein also transports MDV capsids

MDV viral capsids display bi-directional behaviour during egress (Table 9), and this suggests that minus end-directed motors may also be involved in transporting viral capsids. Cytoplasmic dynein is the major minus end-directed cargo transporter. To determine whether dynein is involved in transporting viral capsids Ciliobrevin D was used to inhibit the ATPase activity of dynein preventing it from stepping and therefore halting cargo transport (Cao et al., 2003, Chou et al., 2011, Firestone et al., 2012, Janiesch et al., 2007, Sainath and Gallo, 2015, Ye et al., 2001). CEFs infected with RB1B UL35 GFP virus were treated with 100 μM Ciliobrevin D for an hour prior to imaging. The distance viral capsids travel was then quantified.

There is a drastic reduction in viral capsid transport upon treatment with Ciliobrevin D: only 5.4 % of viral capsids travel over 3 μm in 3 minutes compared to the DMSO control of around 29.3 % (Fig 5.3A-B). This suggests that the ATPase activity of dynein is crucial to viral capsid dynamics. The loss of dynein's cargo transporting abilities suggests that dynein is also required for the transport of viral capsids during egress.

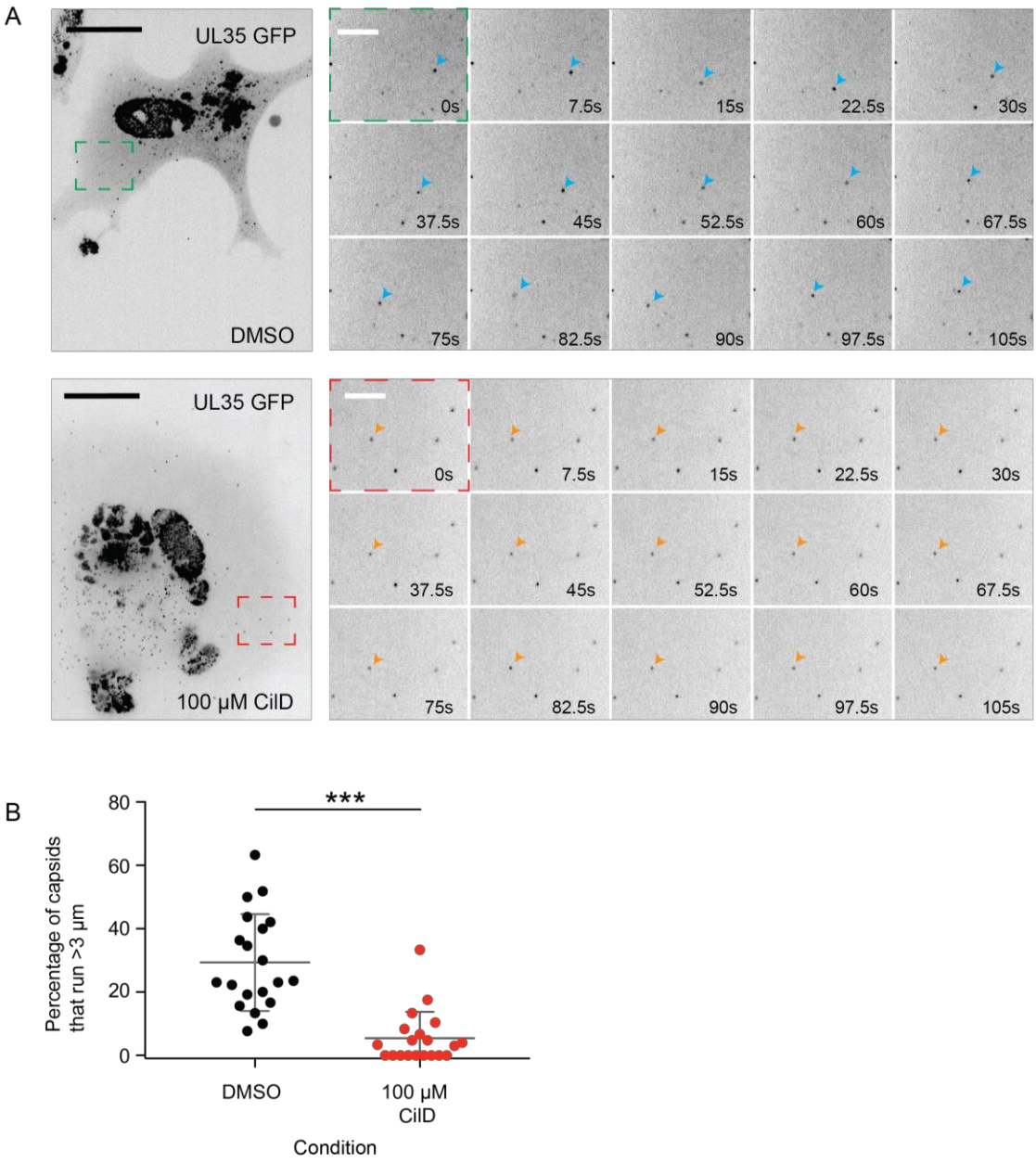


**Figure 5.3: Ciliobrevin D treatment reduces the distance viral capsids travel.**

(A) Representative images of control RB1B UL35 GFP infected CEFs, and 100 µM CilD treated RB1B UL35 GFP infected CEFs. GFP highlights individual viral capsids. The green box indicates the area shown in the montage of DMSO treated cells. The red box indicates the area shown in the montage of 100 µM Ciliobrevin D treated cells. Blue arrow indicates a viral capsid that travels over 3 µm. Orange arrow indicates stationary capsid. Scale bar is 20 µm. (B) Quantification of the percentage of capsids that ran over 3 µm. n=20 cells for each condition. Error bars are the standard deviation. Statistical significance *** p= 0.0005 (two sample t-test).

## 5.3: Discussion

This study has shown that Kif13B contributes to the transport of MDV viral capsids towards the cell periphery. Dynein is also required for transport (Fig 6.1). Knockdown of Kif13B results in about a 30% reduction of directional transport events. This significant but not dramatic reduction points towards the possibility that there may be redundancy amongst the motors that transport MDV capsids and Kif13B may not be the only plus end-directed motor contribute MDV capsid transport. The split kinesin assay hinted at the possibility of various kinesin-3 family members being able to transport MDV capsids as all the tail domains of kinesin-3 family members showed a slight increase in the number of capsids being transported but Kif13B was the only statistically significant tail domain to suggest transport. Lack of statistical significance does not necessarily rule out the biological significance of other kinesin-3 members transporting MDV, especially as the number of repeats were low due to the difficulty of the experiment. There is significant redundancy in cargo transport between kinesins (Goldstein, 1991). Therefore, it could be speculated that several kinesins-3s (Kif1A, Kif1Ba, Kif1Bb, Kif13A and Kif13B) would contribute to MDV viral capsid transport but Kif13B could be the dominant transporter.

Another motor that may be involved in transporting MDV viral capsids is the minus end directed cytoplasmic dynein. By inhibiting the ATPase activity of dynein, it was possible to reduce the percentage of viral capsid transport by 73%. This suggests that dynein is a major transporter of MDV viral capsids. It is interesting that such a dramatic reduction in capsid transport occurs when dynein is inhibited. This could be due to the fact that kinesin-3 motor proteins usually do not transport cargo without an adaptor protein and the dynein complex being present (Ally et al., 2009, Bielska et al., 2014, Theisen et al., 2012, Tien et al., 2011). It can be hypothesised that inactive dynein also fails to initiate viral capsid transport mediated by kinesin-3 motor proteins, resulting in a significant reduction in viral capsid transport.

Several motor proteins were identified to transport other *Alphaherpesviruses* capsids. Dynein is required for *Alphaherpesvirus* viral particle transport (Dohner et al., 2002, Mabit et al., 2002, Zaichick et al., 2013). It has been suggested that tegument proteins UL36 from PRV couple the dynein/dynactin complex to the viral capsid by associating with dynactin and viral capsid protein UL25 (Dohner et al., 2002). This distinct method of recruiting dynein to PRV viral capsids raise questions regarding how MDV viral capsid could recruit dynein to the newly formed viral capsid or newly invading viral particles.

The Kinesin-3 family member Kif1A has been shown to directly interact with the viral protein US9 to promote plus end-directed transport during egress of PRV viral particles. The same protein (US9) from HSV-1 has been shown to recruit kinesin-1 to facilitate egress (Diefenbach et al., 2016, DuRaine et al., 2018) additionally, US11, a tegument protein has been shown to bind to kinesin-1 (Diefenbach et al., 2002). Based on these findings it is possible to hypothesise that MDV viral capsids could recruit Kif13B via the tegument protein US11 to promote transport of nucleocapsids or via US9 to promote transport of enveloped viral particles. This could be confirmed in the future by using a knockout MDV virus or by fluorescently tagging each component of transport machinery or by studying protein – to – protein interactions.

## 5.3: Summary

By using a split kinesin assay, kinesin-3s have been shown to be involved in the transport of MDV viral capsids during egress. Knocking-down Kif13B using shRNA has shown that fewer viral capsids are directionally transported. This suggests Kif13B contributes to the transport of viral capsids during egress. The requirement of dynein during egress was also confirmed by using a dynein inhibitor. The number of viral capsids that showed directional transport reduced significantly when treated with Ciliobrevin D. This suggests that dynein is crucial to viral capsid transport during egress.

# Chapter 6: General discussion

Egress, the transport of viral particles from site of origin to cell periphery is a necessary process for efficient intra and intercellular viral spread. Here, the requirement of the host cytoskeletal elements, microtubules and actin during MDV infection was described. It was shown that cells undergo cell shape changes during MDV infection, which requires dynamic microtubules. Individual viral capsids are associated with microtubules and most viral particles in the cytoplasm lack an envelope. Furthermore, it has been shown that Kif13B and dynein are responsible for viral capsid dynamics during egress. All these findings together suggest that microtubules are essential for efficient MDV viral spread.

Findings from this study are important for two separate fields of study; herpesvirology and microtubule motors. Firstly, it provides evidence for microtubule-based transport of MDV, which was previously thought not be directly involved in the MDV life cycle. This finding is in line with other *Alphaherpesviruses* like HSV-1 suggesting that microtubules are essential for their life cycles (Akhtar and Shukla, 2009, Diefenbach et al., 2002, Kotsakis et al., 2001, Mettenleiter, 2002). By first showing that microtubules are important for efficient viral spread by using plaque assays it has been established that microtubules play an important role during the MDV life cycle. This is an important establishment as it opens a brand-new avenue of study for the MDV virology field. Research that was previously carried out suggesting that microtubules are dispensable for MDV infection (Schumacher et al., 2005) would need to be re-evaluated and the importance of microtubules would need to be considered for future experiments. By using super-resolution microscopy it has been shown that MDV viral particles are directly transported on microtubules, and this finding is in line with other studies carried out with HSV-1 and PRV, where live cell imaging, in vitro reconstitution and, correlative live and electron microscopy showed HSV-1 and PRV viral particles being transported on microtubules (Ibiricu et al., 2011, E Lee et al., 2006, Hogue et al., 2014a).

To the best of our knowledge it is the first time for a study to use SRRF microscopy to study herpes virus transport in infected cells. This is an important milestone to show that these new techniques can be employed to understand and illuminate previously unknown aspects of MDV viral infections. Using super-resolution microscopy can further aid in understanding certain aspects of the *Alphaherpesvirus* life cycle, for example, dSTORM has been used to illuminate and identify where certain tegument proteins are located in a mature HSV-1 viral particle and it has been able to clearly distinguish between the inner and outer tegument which was previously hard to achieve (Laine et al., 2015). One of the main aspects of the herpes life cycle that is under debate is the site of secondary envelopment (Owen et al., 2015) and using a combination of high temporal microscopy and super-resolution microscopy to visualise secondary envelopment and its location can provide strong evidence, therefore it is important continue perusing and dissecting the viral life cycle using super-resolution microscopy techniques.

The findings from this thesis is also important for the microtubule motors field as it identifies a new cargo for kinesin-3 family member Kif13B. Historically, it was not straight forward to identify specific cargoes for individual kinesins due to the 'cargo problem' (Terada and Hirokawa, 2000). Yeast two hybrid assays and immunoprecipitation assays have been used to identify biochemical interactions between kinesins, cargo proteins and adaptor molecules. Although this approach allows the identification of the binding partners it is not possible to gain insight into these interactions *in vivo* where these may be regulated (Hirokawa and Noda, 2008). Another strategy is to use RNAi or induce dominant negative mutations to disrupt specific kinesin motors and then examine the phenotypic changes that have occurred to presumed cargo, this can lead to unintended nonspecific secondary effects (Hirokawa et al., 2010). These approaches also don't take in to account for the possibility that more than one kinesin could be responsible for transporting a particular cargo. The split kinesin assay is a great tool for both identifying possible transporters of cargo and helps address the 'cargo problem' (Jenkins et al., 2012) Therefore, by employing the split kinesin assay along with RNAi depletion we

show that it is possible to identify which molecular motors are responsible for transporting cargo, including viral particles.

Establishing that microtubules and Kif13B are important and required for efficient MDV spread has a lot of potential as a target for therapeutic drug treatment. With further research the importance of Kif13B during the development of poultry can be illuminated and potentially be targeted therapeutically. As there is currently no treatment for MDV infected poultry (Boodhoo et al., 2016) this could be the first therapeutic target to inhibit MDV viral spread in flocks. The current vaccines used do not stop the spread of MDV in flock and only stop the emergence of server symptoms like immunosuppression, oncogenic disease and neuropathy before slaughter (Nair, 2005). Potentially targeting Kif13B could inhibit or slow down the spread of wild type MDV in flocks. Targeting Kif13B has the potential to have side effects as targeting kinesin spindle proteins with chemotherapy drugs is associated with neurotoxicity in humans (Huszar et al., 2009) and a similar severe side effect could exist if Kif13B is targeted in poultry. The combined use of current vaccination strategies with possible Kif13B targeting could lead to the possible eradication of MDV in poultry farms.

Based on our findings that dynein and kinesin-3 transport MDV viral particles and on literature that suggests certain viral proteins facilitate these interactions, two modes of MDV viral particle transport can be suggested during egress (Fig 6.1). The first is that nucleocapsids are transported by dynein and kinesin-3 via UL36 and US11 in a bi-directional manner, possibly to reach the secondary envelopment site. The second is that fully enveloped MDV particles are transported to the cell cortex via kinesin-3 and US9 interactions. This possible model still must be experimentally confirmed.

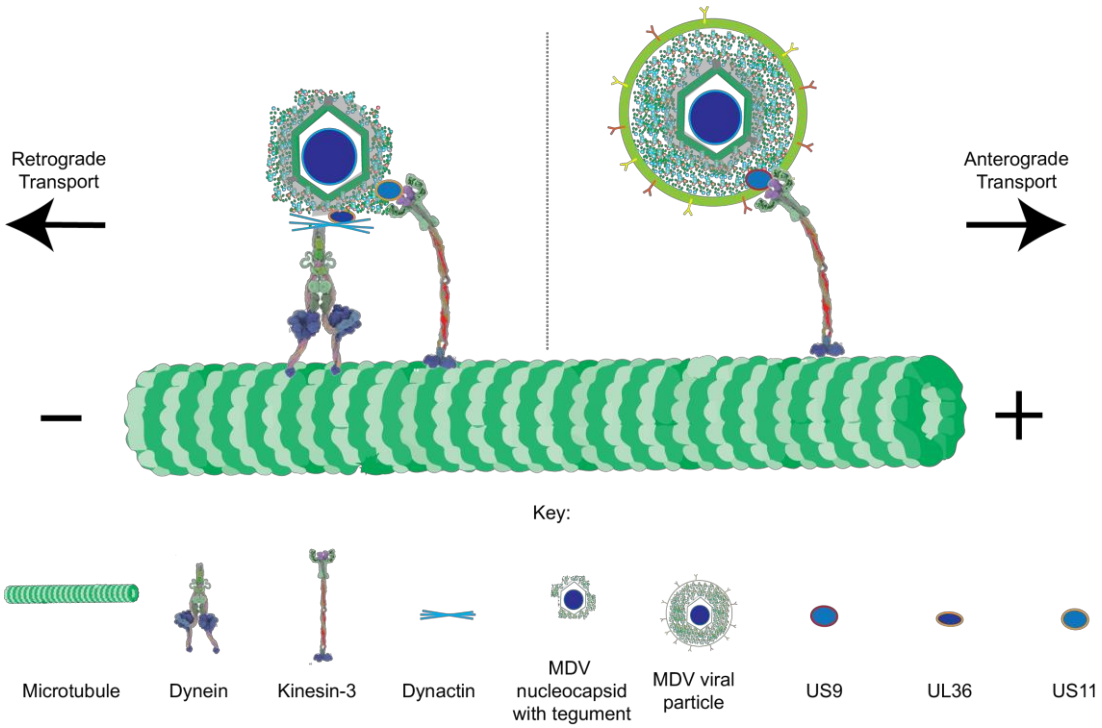


**Figure 6.1: Possible models on how MDV viral particles are transported**

Dynein could be recruited to nucleocapsids via dynactin and MDV encoded tegument protein UL36. Kinesin-3 could be recruited to nucleocapsids in the cytoplasm via US11 tegument protein. The two motor proteins would then transport nucleocapsid to secondary envelopment site using bi-directional transport. Viral capsids that have under gone secondary envelopment could be transported to the cell cortex using kinesin-3s and US9 protein interactions.

Our findings that actin filaments are essential for viral spread are in line with data reported previously (Richerioux et al., 2012, Schumacher et al., 2005). The Rho-ROCK and Rac-PAK signalling pathways that are involved in modulating F-actin have also been suggested to be essential for MDV viral spread. Efficient MDV spread is thought to require ROCK signalling and myosin II activity (Richerioux et al., 2012). The exact mechanisms to how these are important are yet to be confirmed. This study suggests that MDV viral spread requires both actin and microtubules for efficient viral spread. At which stage of the life cycle these two cytoskeletal elements come together to facilitate viral spread remains unknown.

It has also been shown that HSV-1 viral glycoproteins are enriched at specific sites on the host membrane with the aid of the viral glycoprotein gE to direct

them (Mingo et al., 2012). At these sites, actin is slightly depleted, and this was determined to be required for trafficking viral components to the egress locations on the host membrane. It was previously hypothesised that viral particles are released near these egress sites and then trafficked to the egress site using actin surfing. Actin is also crucial for maintaining the egress site structurally and disrupting actin results in dispersing the glycoprotein concentrations (Mingo et al., 2012). Actin is required for egress site maintenance and viral particle actin surfing at the cell cortex (Roberts and Baines, 2011). Microtubules grow towards the cell cortex and viral particles are transported along them. Microtubules could be important for delivering viral particles to the cell cortex.

## 6.1: Future Work

The findings that microtubules are indispensable for MDV viral spread raises further questions. In this study we only looked at microtubules as a form of transport for MDV viral particles, it is possible that microtubules could also be important for other aspects of the MDV live cycle. Next steps would be to see if MDV infection results in any changes to microtubule dynamics in infected cells and if so, how microtubule dynamics is regulated.

The identification and confirmation that MDV infection in CEF cells results in cellular shape changes is an important one and requires further study. Using 3D culture systems, it would be interesting to study MDV spread. During a plaque assay the spread of MDV can be followed using fluorescence and the same approach can be taken in a 3D environment. This could be achieved by using CEF derived organoids and then infecting with fluorescent virus to follow its spread. LLSM would need to be employed in order to resolve individually infected cells in the organoid and follow them to visualise how infection is spreading.

To further confirm that MDV viral capsids are transported by molecular motors co-localisation assays can be performed in infected cells, using a small fluorescent tag to visualise a molecular motor and viral particles could provide the final confirmation of direct interaction and transport of viral capsids by molecular motors *ex vivo*. As we have hypothesised the adaptor proteins (possibly viral US9, US11 and, UL36 proteins) that can possibly link the viral particle with the molecular can also be labelled fluorescently and using a multi camera system all elements can be imaged in high spatial and temporal resolution. Even further these complexes can also be reconstituted *in vitro* and visualised using TIRF microscopy. Finally, the molecular structure of the whole complex together with the viral particle, molecular motor and adaptor protein can be resolved.

Finally, the potential of targeting Kif13B was a therapeutic target needs to be explored, this can be achieved by first identifying a compound that will reduce or completely inhibit Kif13B activity. This can be achieved by a large-scale inhibitory compound screen. Once compounds that inhibit Kif13B activity are identified then small-scale trials can be carried out in MDV permissive poultry. The rate of spread between small flocks of chicken can be determined and possibly a combination effect with modern vaccination strategies and Kif13B inhibitory compound can be tested.

## 6.2: Conclusions

This study provides the first evidence that MDV infection is associated with microtubules, both for intracellular transport and cell-to-cell spread. The dynamic microtubules are important for cell shape changes induced during MDV infection. The importance of actin has also been reemphasized, although the processes actin is involved in during the viral life cycle have not been investigated here. Using state-of-the-art approaches like SRRF, MDV viral particles were shown to be bound and directionally transported along microtubules, placing microtubules in the centre of intracellular MDV viral particle transport. This study has also identified two microtubule-associated molecular motors that are involved in the directional transport of MDV viral particles on microtubules, cytoplasmic dynein and Kif13B. The findings from this study identify new components of the host machinery required for MDV biology and opened new avenues of research for the MDV field.

# Chapter 7: References


ADDINGER, H. K. & CALNEK, B. W. 1973. Pathogenesis of Marek's disease: early distribution of virus and viral antigens in infected chickens. *J Natl Cancer Inst,* 50**,** 1287-98.

ADIO, S., RETH, J., BATHE, F. & WOEHLKE, G. 2006. Review: regulation mechanisms of Kinesin-1. *J Muscle Res Cell Motil,* 27**,** 153-60.

AHMED, M. & SCHIDLOVSKY, G. 1968. Electron microscopic localization of herpesvirus-type particles in Marek's disease. *J Virol,* 2**,** 1443-57.

AKHMANOVA, A. & HAMMER, J. A., 3RD 2010. Linking molecular motors to membrane cargo. *Curr Opin Cell Biol,* 22**,** 479-87.

AKHTAR, J. & SHUKLA, D. 2009. Viral entry mechanisms: cellular and viral mediators of herpes simplex virus entry. *FEBS J,* 276**,** 7228-36.

AL-BASSAM, J., KIM, H., BROUHARD, G., VAN OIJEN, A., HARRISON, S. C. & CHANG, F. 2010. CLASP promotes microtubule rescue by recruiting tubulin dimers to the microtubule. *Dev Cell,* 19**,** 245-58.

AL-BASSAM, J., KIM, H., FLOR-PARRA, I., LAL, N., VELJI, H. & CHANG, F. 2012. Fission yeast Alp14 is a dose-dependent plus end-tracking microtubule polymerase. *Mol Biol Cell,* 23**,** 2878-90.

AL-DUJAILI, L. J., CLERKIN, P. P., CLEMENT, C., MCFERRIN, H. E., BHATTACHARJEE, P. S., VARNELL, E. D., KAUFMAN, H. E. & HILL, J. M. 2011. Ocular herpes simplex virus: how are latency, reactivation, recurrent disease and therapy interrelated? *Future Microbiol,* 6**,** 877-907.

ALBECKA, A., LAINE, R. F., JANSSEN, A. F. J., KAMINSKI, C. F. & CRUMP, C. M. 2016. HSV-1 Glycoproteins Are Delivered to Virus Assembly Sites Through Dynamin-Dependent Endocytosis. 17**,** 21-39.

ALLAN, V. J. 2011. Cytoplasmic dynein. *Biochem Soc Trans,* 39**,** 1169-78.

ALLY, S., LARSON, A. G., BARLAN, K., RICE, S. E. & GELFAND, V. I. 2009. Opposite-polarity motors activate one another to trigger cargo transport in live cells. *J Cell Biol,* 187**,** 1071-82.

AMRUTE-NAYAK, M. & BULLOCK, S. L. 2012. Single-molecule assays reveal that RNA localization signals regulate dynein-dynactin copy number on individual transcript cargoes. *Nat Cell Biol,* 14**,** 416-23.

ANDRIEUX, A., SALIN, P. A., VERNET, M., KUJALA, P., BARATIER, J., GORY-FAURE, S., BOSC, C., POINTU, H., PROIETTO, D., SCHWEITZER, A., DENARIER, E., KLUMPERMAN, J. & JOB, D. 2002. The suppression of brain cold-stable microtubules in mice induces synaptic defects associated with neuroleptic-sensitive behavioral disorders. *Genes Dev,* 16**,** 2350-64.

ANTINONE, S. E., SHUBEITA, G. T., COLLER, K. E., LEE, J. I., HAVERLOCK-MOYNS, S., GROSS, S. P. & SMITH, G. A. 2006. The Herpesvirus capsid surface protein, VP26, and the majority of the tegument proteins are dispensable for capsid transport toward the nucleus. *J Virol,* 80**,** 5494-8.

ANTINONE, S. E. & SMITH, G. A. 2006. Two modes of herpesvirus trafficking in neurons: membrane acquisition directs motion. *J Virol,* 80**,** 11235-40.

ANTINONE, S. E. & SMITH, G. A. 2010. Retrograde axon transport of herpes simplex virus and pseudorabies virus: a live-cell comparative analysis. *J Virol,* 84**,** 1504-12.

ANTINONE, S. E., ZAICHICK, S. V. & SMITH, G. A. 2010. Resolving the assembly state of herpes simplex virus during axon transport by live-cell imaging. *J Virol,* 84**,** 13019-30.

APLIN, A., JASIONOWSKI, T., TUTTLE, D. L., LENK, S. E. & DUNN, W. A., JR. 1992. Cytoskeletal elements are required for the formation and maturation of autophagic vacuoles. *J Cell Physiol,* 152**,** 458-66.

ARCE, C. A., RODRIGUEZ, J. A., BARRA, H. S. & CAPUTO, R. 1975. Incorporation of L-tyrosine, L-phenylalanine and L-3,4-dihydroxyphenylalanine as single units into rat brain tubulin. *Eur J Biochem,* 59**,** 145-9.

ARUMUGASWAMI, V., KUMAR, P. M., KONJUFCA, V., DIENGLEWICZ, R. L., REDDY, S. M. & PARCELLS, M. S. 2009. Latency of Marek's disease virus (MDV) in a reticuloendotheliosis virus-transformed T-cell line. II: expression of the latent MDV genome. *Avian Dis,* 53**,** 156-65.

ASENJO, A. B., CHATTERJEE, C., TAN, D., DEPAOLI, V., RICE, W. J., DIAZ-AVALOS, R., SILVESTRY, M. & SOSA, H. 2013. Structural model for tubulin recognition and deformation by kinesin-13 microtubule depolymerases. *Cell Rep,* 3**,** 759-68.

AULCHENKO, Y. S., HOPPENBROUWERS, I. A., RAMAGOPALAN, S. V., BROER, L., JAFARI, N., HILLERT, J., LINK, J., LUNDSTROM, W., GREINER, E., DESSA SADOVNICK, A., GOOSSENS, D., VAN BROECKHOVEN, C., DEL-FAVERO, J., EBERS, G. C., OOSTRA, B. A., VAN DUIJN, C. M. & HINTZEN, R. Q. 2008. Genetic variation in the KIF1B locus influences susceptibility to multiple sclerosis. *Nat Genet,* 40**,** 1402-3.

AVITABILE, E., DI GAETA, S., TORRISI, M. R., WARD, P. L., ROIZMAN, B. & CAMPADELLI-FIUME, G. 1995. Redistribution of microtubules and Golgi apparatus in herpes simplex virus-infected cells and their role in viral exocytosis. *J Virol,* 69**,** 7472-82.

AYSCOUGH, K. R. & DRUBIN, D. G. 1996. ACTIN: general principles from studies in yeast. *Annu Rev Cell Dev Biol,* 12**,** 129-60.

BAATEN, B. J., STAINES, K. A., SMITH, L. P., SKINNER, H., DAVISON, T. F. & BUTTER, C. 2009. Early replication in pulmonary B cells after infection with Marek's disease herpesvirus by the respiratory route. *Viral Immunol,* 22**,** 431-44.

BACHVAROFF, R. J., MILLER, F. & RAPAPORT, F. T. 1980. Appearance of cytoskeletal components on the surface of leukemia cells and of lymphocytes transformed by mitogens and Epstein-Barr virus. *Proc Natl Acad Sci U S A,* 77**,** 4979-83.

BAER, A. & KEHN-HALL, K. 2014. Viral concentration determination through plaque assays: using traditional and novel overlay systems. *J Vis Exp***,** e52065.

BARKALOW, K. & HARTWIG, J. H. 1995. Actin cytoskeleton. Setting the pace of cell movement. *Curr Biol,* 5**,** 1000-2.

BARROW, A. D., BURGESS, S. C., BAIGENT, S. J., HOWES, K. & NAIR, V. K. 2003. Infection of macrophages by a lymphotropic herpesvirus: a new tropism for Marek's disease virus. *J Gen Virol,* 84**,** 2635-45.

BEITIA ORTIZ DE ZARATE, I., KAELIN, K. & ROZENBERG, F. 2004. Effects of Mutations in the Cytoplasmic Domain of Herpes Simplex Virus Type 1 Glycoprotein B on Intracellular Transport and Infectivity. *Journal of Virology,* 78**,** 1540.

BELLETT, A. J., JACKSON, P., DAVID, E. T., BENNETT, E. J. & CRONIN, B. 1989. Functions of the two adenovirus early E1A proteins and their conserved domains in cell cycle alteration, actin reorganization, and gene activation in rat cells. *J Virol,* 63**,** 303-10.

BERTHIER, E., YOUNG, E. W. & BEEBE, D. 2012. Engineers are from PDMS-land, Biologists are from Polystyrenia. *Lab Chip,* 12**,** 1224-37.

BHABHA, G., JOHNSON, G. T., SCHROEDER, C. M. & VALE, R. D. 2016. How Dynein Moves Along Microtubules. *Trends Biochem Sci,* 41**,** 94-105.

BIELING, P., TELLEY, I. A., PIEHLER, J. & SURREY, T. 2008. Processive kinesins require loose mechanical coupling for efficient collective motility. *EMBO Rep,* 9**,** 1121-7.

BIELING, P., TELLEY, I. A. & SURREY, T. 2010. A minimal midzone protein module controls formation and length of antiparallel microtubule overlaps. *Cell,* 142**,** 420-32.

BIELSKA, E., SCHUSTER, M., ROGER, Y., BEREPIKI, A., SOANES, D. M., TALBOT, N. J. & STEINBERG, G. 2014. Hook is an adapter that coordinates kinesin-3 and dynein cargo attachment on early endosomes. *J Cell Biol,* 204**,** 989-1007.

BIGGS, P. M. & PAYNE, L. N. 1967. Studies on Marek's disease. I. Experimental transmission. *J Natl Cancer Inst,* 39**,** 267-80.

BOBINNEC, Y., MOUDJOU, M., FOUQUET, J. P., DESBRUYERES, E., EDDE, B. & BORNENS, M. 1998. Glutamylation of centriole and cytoplasmic tubulin in proliferating non-neuronal cells. *Cell Motil Cytoskeleton,* 39**,** 223-32.

BOLZANI, R., RUGGERI, F. & OLIVO, O. M. 1979. [Average normal temperature of the chicken in the morning and after 1-2 days of fasting]. *Boll Soc Ital Biol Sper,* 55**,** 1618-22.

BOODHOO, N., GURUNG, A., SHARIF, S. & BEHBOUDI, S. 2016. Marek's disease in chickens: a review with focus on immunology. *Veterinary research,* 47**,** 119-119.

BRE, M. H., DE NECHAUD, B., WOLFF, A. & FLEURY, A. 1994. Glutamylated tubulin probed in ciliates with the monoclonal antibody GT335. *Cell Motil Cytoskeleton,* 27**,** 337-49.

BROUHARD, G. J., STEAR, J. H., NOETZEL, T. L., AL-BASSAM, J., KINOSHITA, K., HARRISON, S. C., HOWARD, J. & HYMAN, A. A. 2008. XMAP215 is a processive microtubule polymerase. *Cell,* 132**,** 79-88.

BROWNE, H., BELL, S., MINSON, T. & WILSON, D. W. 1996. An endoplasmic reticulum-retained herpes simplex virus glycoprotein H is absent from secreted virions: evidence for reenvelopment during egress. *Journal of Virology,* 70**,** 4311.

BRZOZOWSKA, A., RYCHLOWSKI, M., LIPINSKA, A. D. & BIENKOWSKA-SZEWCZYK, K. 2010. Point mutations in BHV-1 Us3 gene abolish its ability to induce cytoskeletal changes in various cell types. *Vet Microbiol,* 143**,** 8-13.

BUCKMASTER, A. E., SCOTT, S. D., SANDERSON, M. J., BOURSNELL, M. E., ROSS, N. L. & BINNS, M. M. 1988. Gene sequence and mapping data from Marek's disease virus and herpesvirus of turkeys: implications for herpesvirus classification. *J Gen Virol,* 69 ( Pt 8)**,** 2033-42.

BURGESS, S. C. & DAVISON, T. F. 2002. Identification of the neoplastically transformed cells in Marek's disease herpesvirus-induced lymphomas: recognition by the monoclonal antibody AV37. *J Virol,* 76**,** 7276-92.

BURNS, K. M., WAGENBACH, M., WORDEMAN, L. & SCHRIEMER, D. C. 2014. Nucleotide exchange in dimeric MCAK induces longitudinal and lateral stress at microtubule ends to support depolymerization. *Structure,* 22**,** 1173-1183.

CABALLERO OTEYZA, A., BATTALOGLU, E., OCEK, L., LINDIG, T., REICHBAUER, J., REBELO, A. P., GONZALEZ, M. A., ZORLU, Y., OZES, B., TIMMANN, D., BENDER, B., WOEHLKE, G., ZUCHNER, S., SCHOLS, L. & SCHULE, R. 2014. Motor protein mutations cause a new form of hereditary spastic paraplegia. *Neurology,* 82**,** 2007-16.

CALISTRI, A., MUNEGATO, D., TOFFOLETTO, M., CELESTINO, M., FRANCHIN, E., COMIN, A., SARTORI, E., SALATA, C., PAROLIN, C. & PALÙ, G. 2015. Functional Interaction Between the ESCRT-I Component TSG101 and the HSV-1 Tegument Ubiquitin Specific Protease. *Journal of Cellular Physiology,* 230**,** 1794-1806.

CALISTRI, A., SETTE, P., SALATA, C., CANCELLOTTI, E., FORGHIERI, C., COMIN, A., GOTTLINGER, H., CAMPADELLI-FIUME, G., PALU, G. & PAROLIN, C. 2007. Intracellular trafficking and maturation of herpes simplex virus type 1 gB and virus egress require functional biogenesis of multivesicular bodies. *J Virol,* 81**,** 11468-78.

CALNEK, B. W. 2001. Pathogenesis of Marek's disease virus infection. *Curr Top Microbiol Immunol,* 255**,** 25-55.

CAMPADELLI-FIUME, G., AMASIO, M., AVITABILE, E., CERRETANI, A., FORGHIERI, C., GIANNI, T. & MENOTTI, L. 2007. The multipartite system that mediates entry of herpes simplex virus into the cell. *Rev Med Virol,* 17**,** 313-26.

CAMPADELLI, G., BRANDIMARTI, R., DI LAZZARO, C., WARD, P. L., ROIZMAN, B. & TORRISI, M. R. 1993. Fragmentation and dispersal of Golgi proteins and redistribution of glycoproteins and glycolipids processed through the Golgi apparatus after infection with herpes simplex virus 1. *Proc Natl Acad Sci U S A,* 90**,** 2798-802.

CAO, K., NAKAJIMA, R., MEYER, H. H. & ZHENG, Y. 2003. The AAA-ATPase Cdc48/p97 regulates spindle disassembly at the end of mitosis. *Cell,* 115**,** 355-67.

CHANG, J. T., SCHMID, M. F., RIXON, F. J. & CHIU, W. 2007. Electron cryotomography reveals the portal in the herpesvirus capsid. *J Virol,* 81**,** 2065-8.

CHANG, Y. E. & ROIZMAN, B. 1993. The product of the UL31 gene of herpes simplex virus 1 is a nuclear phosphoprotein which partitions with the nuclear matrix. *J Virol,* 67**,** 6348-56.

CHEISHVILI, D., MAAYAN, C., COHEN-KUPIEC, R., LEFLER, S., WEIL, M., AST, G. & RAZIN, A. 2011. IKAP/Elp1 involvement in cytoskeleton regulation and implication for familial dysautonomia. *Hum Mol Genet,* 20**,** 1585-94.

CHENG, H., NIIKURA, M., KIM, T., MAO, W., MACLEA, K. S., HUNT, H., DODGSON, J., BURNSIDE, J., MORGAN, R., OUYANG, M., LAMONT, S., DEKKERS, J., FULTON, J., SOLLER, M. & MUIR, W. 2008. Using integrative genomics to elucidate genetic resistance to Marek's disease in chickens. *Dev Biol (Basel),* 132**,** 365-72.

CHEUNG, P., BANFIELD, B. W. & TUFARO, F. 1991. Brefeldin A arrests the maturation and egress of herpes simplex virus particles during infection. *Journal of Virology,* 65**,** 1893.

CHOI, J., CHEN, J., SCHREIBER, S. L. & CLARDY, J. 1996. Structure of the FKBP12-rapamycin complex interacting with the binding domain of human FRAP. *Science,* 273**,** 239-42.

CHOU, T. F., BROWN, S. J., MINOND, D., NORDIN, B. E., LI, K., JONES, A. C., CHASE, P., PORUBSKY, P. R., STOLTZ, B. M., SCHOENEN, F. J., PATRICELLI, M. P., HODDER, P., ROSEN, H. & DESHAIES, R. J. 2011. Reversible inhibitor of p97, DBeQ, impairs both ubiquitin-dependent and autophagic protein clearance pathways. *Proc Natl Acad Sci U S A,* 108**,** 4834-9.

CHURCHILL, A. E. 1968. Herpes-type virus isolated in cell culture from tumors of chickens with Marek's disease. I. Studies in cell culture. *J Natl Cancer Inst,* 41**,** 939-50.

CHURCHILL, A. E. & BIGGS, P. M. 1967. Agent of Marek's disease in tissue culture. *Nature,* 215**,** 528-30.

COLE, N. L. 1992. Temperature sensitivity of herpes simplex virus type 1 is a tissue-dependent phenomenon. *Arch Virol,* 127**,** 49-63.

COWIN, P. & BURKE, B. 1996. Cytoskeleton-membrane interactions. *Curr Opin Cell Biol,* 8**,** 56-65.

COY, D. L., WAGENBACH, M. & HOWARD, J. 1999. Kinesin takes one 8-nm step for each ATP that it hydrolyzes. *J Biol Chem,* 274**,** 3667-71.

CREVENNA, A. H., MADATHIL, S., COHEN, D. N., WAGENBACH, M., FAHMY, K. & HOWARD, J. 2008. Secondary structure and compliance of a predicted flexible domain in kinesin-1 necessary for cooperation of motors. *Biophys J,* 95**,** 5216-27.

CRUMP, C. 2018. Virus Assembly and Egress of HSV. *In:* KAWAGUCHI, Y., MORI, Y. & KIMURA, H. (eds.) *Human Herpesviruses.* Singapore: Springer Singapore.

CRUMP, C. M., BRUUN, B., BELL, S., POMERANZ, L. E., MINSON, T. & BROWNE, H. M. 2004. Alphaherpesvirus glycoprotein M causes the relocalization of plasma membrane proteins. 85**,** 3517-3527.

CRUMP, C. M., YATES, C. & MINSON, T. 2007. Herpes simplex virus type 1 cytoplasmic envelopment requires functional Vps4. *J Virol,* 81**,** 7380-7.

DANIEL, G. R., SOLLARS, P. J., PICKARD, G. E. & SMITH, G. A. 2015. Pseudorabies Virus Fast Axonal Transport Occurs by a pUS9-Independent Mechanism. *J Virol,* 89**,** 8088-91.

DANIEL, G. R., SOLLARS, P. J., PICKARD, G. E. & SMITH, G. A. 2016. The pseudorabies virus protein, pUL56, enhances virus dissemination and virulence but is dispensable for axonal transport. *Virology,* 488**,** 179-86.

DAVISON, A. J., EBERLE, R., EHLERS, B., HAYWARD, G. S., MCGEOCH, D. J., MINSON, A. C., PELLETT, P. E., ROIZMAN, B., STUDDERT, M. J. & THIRY, E. 2009. The order Herpesvirales. *Arch Virol,* 154**,** 171-7.

DE FORGES, H., BOUISSOU, A. & PEREZ, F. 2012. Interplay between microtubule dynamics and intracellular organization. *Int J Biochem Cell Biol,* 44**,** 266-74.

DELUCA, J. G., GALL, W. E., CIFERRI, C., CIMINI, D., MUSACCHIO, A. & SALMON, E. D. 2006. Kinetochore microtubule dynamics and attachment stability are regulated by Hec1. *Cell,* 127**,** 969-82.

DENG, B., O'CONNOR, C. M., KEDES, D. H. & ZHOU, Z. H. 2007. Direct visualization of the putative portal in the Kaposi's sarcoma-associated herpesvirus capsid by cryoelectron tomography. *J Virol,* 81**,** 3640-4.

DERR, N. D., GOODMAN, B. S., JUNGMANN, R., LESCHZINER, A. E., SHIH, W. M. & RECK-PETERSON, S. L. 2012. Tug-of-war in motor protein ensembles revealed with a programmable DNA origami scaffold. *Science,* 338**,** 662-5.

DESAI, A., VERMA, S., MITCHISON, T. J. & WALCZAK, C. E. 1999. Kin I kinesins are microtubule-destabilizing enzymes. *Cell,* 96**,** 69-78.

DESAI, P., DELUCA, N. A. & PERSON, S. 1998. Herpes simplex virus type 1 VP26 is not essential for replication in cell culture but influences production of infectious virus in the nervous system of infected mice. *Virology,* 247**,** 115-24.

DIEFENBACH, R. J. 2015. Conserved tegument protein complexes: Essential components in the assembly of herpesviruses. *Virus Res,* 210**,** 308-17.

DIEFENBACH, R. J., DAVIS, A., MIRANDA-SAKSENA, M., FERNANDEZ, M. A., KELLY, B. J., JONES, C. A., LAVAIL, J. H., XUE, J., LAI, J. & CUNNINGHAM, A. L. 2016. The Basic Domain of Herpes Simplex Virus 1 pUS9 Recruits Kinesin-1 To Facilitate Egress from Neurons. *J Virol,* 90**,** 2102-11.

DIEFENBACH, R. J., MIRANDA-SAKSENA, M., DIEFENBACH, E., HOLLAND, D. J., BOADLE, R. A., ARMATI, P. J. & CUNNINGHAM, A. L. 2002. Herpes simplex virus tegument protein US11 interacts with conventional kinesin heavy chain. *J Virol,* 76**,** 3282-91.

DIENES, H. P., HILLER, G., MULLER, S. & FALKE, D. 1987. Microtubules and intermediate filaments of herpes simplex virus infected cells. *Arch Virol,* 94**,** 15-28.

DIGARD, P., BEBRIN, W. R., WEISSHART, K. & COEN, D. M. 1993. The extreme C terminus of herpes simplex virus DNA polymerase is crucial for functional interaction with processivity factor UL42 and for viral replication. *J Virol,* 67**,** 398-406.

DINGWELL, K. S., BRUNETTI, C. R., HENDRICKS, R. L., TANG, Q., TANG, M., RAINBOW, A. J. & JOHNSON, D. C. 1994. Herpes simplex virus glycoproteins E and I facilitate cell-to-cell spread in vivo and across junctions of cultured cells. *Journal of Virology,* 68**,** 834.

DINGWELL, K. S. & JOHNSON, D. C. 1998. The Herpes Simplex Virus gE-gI Complex Facilitates Cell-to-Cell Spread and Binds to Components of Cell Junctions. *Journal of Virology,* 72**,** 8933.

DIXIT, R., TIWARI, V. & SHUKLA, D. 2008. Herpes simplex virus type 1 induces filopodia in differentiated P19 neural cells to facilitate viral spread. *Neurosci Lett,* 440**,** 113-8.

DOCEUL, V., HOLLINSHEAD, M., VAN DER LINDEN, L. & SMITH, G. L. 2010. Repulsion of Superinfecting Virions: A Mechanism for Rapid Virus Spread. *Science,* 327**,** 873.

DODDING, M. P. & WAY, M. 2011. Coupling viruses to dynein and kinesin-1. *EMBO J,* 30**,** 3527-39.

DOHNER, K., NAGEL, C. H. & SODEIK, B. 2005. Viral stop-and-go along microtubules: taking a ride with dynein and kinesins. *Trends Microbiol,* 13**,** 320-7.

DOHNER, K., RADTKE, K., SCHMIDT, S. & SODEIK, B. 2006. Eclipse phase of herpes simplex virus type 1 infection: Efficient dynein-mediated capsid transport without the small capsid protein VP26. *J Virol,* 80**,** 8211-24.

DOHNER, K., WOLFSTEIN, A., PRANK, U., ECHEVERRI, C., DUJARDIN, D., VALLEE, R. & SODEIK, B. 2002. Function of dynein and dynactin in herpes simplex virus capsid transport. *Mol Biol Cell,* 13**,** 2795-809.

DOR, T., CINNAMON, Y., RAYMOND, L., SHAAG, A., BOUSLAM, N., BOUHOUCHE, A., GAUSSEN, M., MEYER, V., DURR, A., BRICE, A., BENOMAR, A., STEVANIN, G., SCHUELKE, M. & EDVARDSON, S. 2014. KIF1C mutations in two families with hereditary spastic paraparesis and cerebellar dysfunction. *J Med Genet,* 51**,** 137-42.

DOUGLAS, M. W., DIEFENBACH, R. J., HOMA, F. L., MIRANDA-SAKSENA, M., RIXON, F. J., VITTONE, V., BYTH, K. & CUNNINGHAM, A. L. 2004. Herpes simplex virus type 1 capsid protein VP26 interacts with dynein light chains RP3 and Tctex1 and plays a role in retrograde cellular transport. *J Biol Chem,* 279**,** 28522-30.

DRERUP, C. M., LUSK, S. & NECHIPORUK, A. 2016. Kif1B Interacts with KBP to Promote Axon Elongation by Localizing a Microtubule Regulator to Growth Cones. *J Neurosci,* 36**,** 7014-26.

DUNN, S., MORRISON, E. E., LIVERPOOL, T. B., MOLINA-PARIS, C., CROSS, R. A., ALONSO, M. C. & PECKHAM, M. 2008. Differential trafficking of Kif5c on tyrosinated and detyrosinated microtubules in live cells. *J Cell Sci,* 121**,** 1085-95.

DURAINE, G., WISNER, T. W., HOWARD, P. & JOHNSON, D. C. 2018. Kinesin-1 proteins KIF5A, 5B and 5C promote anterograde transport of herpes simplex virus enveloped virions in axons. *J Virol*.

DUVAL, K., GROVER, H., HAN, L. H., MOU, Y., PEGORARO, A. F., FREDBERG, J. & CHEN, Z. 2017. Modeling Physiological Events in 2D vs. 3D Cell Culture. *Physiology (Bethesda),* 32**,** 266-277.

E LEE, G., MURRAY, J., W WOLKOFF, A. & WILSON, D. 2006. *Reconstitution of Herpes Simplex Virus Microtubule-Dependent Trafficking In Vitro*.

EDDE, B., ROSSIER, J., LE CAER, J. P., DESBRUYERES, E., GROS, F. & DENOULET, P. 1990. Posttranslational glutamylation of alpha-tubulin. *Science,* 247**,** 83-5.

ELLIOTT, G. & O'HARE, P. 1998. Herpes simplex virus type 1 tegument protein VP22 induces the stabilization and hyperacetylation of microtubules. *J Virol,* 72**,** 6448-55.

ENCALADA, S. E., SZPANKOWSKI, L., XIA, C. H. & GOLDSTEIN, L. S. 2011. Stable kinesin and dynein assemblies drive the axonal transport of mammalian prion protein vesicles. *Cell,* 144**,** 551-65.

ENGELKE, M. F., BURCKHARDT, C. J., MORF, M. K. & GREBER, U. F. 2011. The dynactin complex enhances the speed of microtubule-dependent motions of adenovirus both towards and away from the nucleus. *Viruses,* 3**,** 233-253.

FARNSWORTH, A., GOLDSMITH, K. & JOHNSON, D. C. 2003. Herpes Simplex Virus Glycoproteins gD and gE/gI Serve Essential but Redundant Functions during Acquisition of the Virion Envelope in the Cytoplasm. *Journal of Virology,* 77**,** 8481.

FARNSWORTH, A. & JOHNSON, D. C. 2006a. Herpes Simplex Virus gE/gI Must Accumulate in the <em>trans</em>-Golgi Network at Early Times and Then Redistribute to Cell Junctions To Promote Cell-Cell Spread. *Journal of Virology,* 80**,** 3167.

FARNSWORTH, A. & JOHNSON, D. C. 2006b. Herpes simplex virus gE/gI must accumulate in the trans-Golgi network at early times and then redistribute to cell junctions to promote cell-cell spread. *J Virol,* 80**,** 3167-79.

FARNSWORTH, A., WISNER, T. W. & JOHNSON, D. C. 2007. Cytoplasmic Residues of Herpes Simplex Virus Glycoprotein gE Required for Secondary Envelopment and Binding of Tegument Proteins VP22 and UL11 to gE and gD. *Journal of Virology,* 81**,** 319.

FAVOREEL, H. W., VAN MINNEBRUGGEN, G., ADRIAENSEN, D. & NAUWYNCK, H. J. 2005. Cytoskeletal rearrangements and cell extensions induced by the US3 kinase of an alphaherpesvirus are associated with enhanced spread. *Proc Natl Acad Sci U S A,* 102**,** 8990-5.

FEIERBACH, B., BISHER, M., GOODHOUSE, J. & ENQUIST, L. W. 2007. In vitro analysis of transneuronal spread of an alphaherpesvirus infection in peripheral nervous system neurons. *J Virol,* 81**,** 6846-57.

FEIERBACH, B., PICCINOTTI, S., BISHER, M., DENK, W. & ENQUIST, L. W. 2006. Alpha-herpesvirus infection induces the formation of nuclear actin filaments. *PLoS Pathog,* 2**,** e85.

FIRESTONE, A. J., WEINGER, J. S., MALDONADO, M., BARLAN, K., LANGSTON, L. D., O'DONNELL, M., GELFAND, V. I., KAPOOR, T. M. & CHEN, J. K. 2012. Small-molecule inhibitors of the AAA+ ATPase motor cytoplasmic dynein. *Nature,* 484**,** 125-9.

FLORES-RODRIGUEZ, N., ROGERS, S. S., KENWRIGHT, D. A., WAIGH, T. A., WOODMAN, P. G. & ALLAN, V. J. 2011. Roles of dynein and dynactin in early endosome dynamics revealed using automated tracking and global analysis. *PLoS One,* 6**,** e24479.

FOREST, T., BARNARD, S. & BAINES, J. D. 2005. Active intranuclear movement of herpesvirus capsids. *Nat Cell Biol,* 7**,** 429-31.

FOSTER, T. P., MELANCON, J. M., BAINES, J. D. & KOUSOULAS, K. G. 2004a. The Herpes Simplex Virus Type 1 UL20 Protein Modulates Membrane Fusion Events during Cytoplasmic Virion Morphogenesis and Virus-Induced Cell Fusion. *Journal of Virology,* 78**,** 5347.

FOSTER, T. P., MELANCON, J. M., OLIVIER, T. L. & KOUSOULAS, K. G. 2004b. Herpes Simplex Virus Type 1 Glycoprotein K and the UL20 Protein Are Interdependent for Intracellular Trafficking and <em>trans</em>-Golgi Network Localization. *Journal of Virology,* 78**,** 13262.

FOSTER, T. P., MELANCON, J. M., OLIVIER, T. L. & KOUSOULAS, K. G. 2004c. Herpes Simplex Virus Type 1 Glycoprotein K and the UL20 Protein Are Interdependent for Intracellular Trafficking and trans-Golgi Network Localization. 78**,** 13262-13277.

FOUREST-LIEUVIN, A., PERIS, L., GACHE, V., GARCIA-SAEZ, I., JUILLAN-BINARD, C., LANTEZ, V. & JOB, D. 2006. Microtubule regulation in mitosis: tubulin phosphorylation by the cyclin-dependent kinase Cdk1. *Mol Biol Cell,* 17**,** 1041-50.

FRIEDMAN, D. S. & VALE, R. D. 1999. Single-molecule analysis of kinesin motility reveals regulation by the cargo-binding tail domain. *Nat Cell Biol,* 1**,** 293-7.

FU, M. M. & HOLZBAUR, E. L. 2014. Integrated regulation of motor-driven organelle transport by scaffolding proteins. *Trends Cell Biol,* 24**,** 564-74.

FUCHS, W., KLUPP, B. G., GRANZOW, H., OSTERRIEDER, N. & METTENLEITER, T. C. 2002. The interacting UL31 and UL34 gene products of pseudorabies virus are involved in egress from the host-cell nucleus and represent components of primary enveloped but not mature virions. *J Virol,* 76**,** 364-78.

FUNK, C., OTT, M., RASCHBICHLER, V., NAGEL, C. H., BINZ, A., SODEIK, B., BAUERFEIND, R. & BAILER, S. M. 2015. The Herpes Simplex Virus Protein pUL31 Escorts Nucleocapsids to Sites of Nuclear Egress, a Process Coordinated by Its N-Terminal Domain. *PLoS Pathog,* 11**,** e1004957.

GARDNER, M. K., ZANIC, M., GELL, C., BORMUTH, V. & HOWARD, J. 2011. Depolymerizing kinesins Kip3 and MCAK shape cellular microtubule architecture by differential control of catastrophe. *Cell,* 147**,** 1092-103.

GENNERICH, A. & VALE, R. D. 2009. Walking the walk: how kinesin and dynein coordinate their steps. *Curr Opin Cell Biol,* 21**,** 59-67.

GHOSH-ROY, A., GONCHAROV, A., JIN, Y. & CHISHOLM, A. D. 2012. Kinesin-13 and tubulin posttranslational modifications regulate microtubule growth in axon regeneration. *Dev Cell,* 23**,** 716-28.

GIBSON, W. 2008. Structure and formation of the cytomegalovirus virion. *Curr Top Microbiol Immunol,* 325**,** 187-204.

GIMENO, I. M. 2008. Marek's disease vaccines: a solution for today but a worry for tomorrow? *Vaccine,* 26 Suppl 3**,** C31-41.

GODDETTE, D. W. & FRIEDEN, C. 1986. Actin polymerization. The mechanism of action of cytochalasin D. *J Biol Chem,* 261**,** 15974-80.

GOLDSTEIN, L. S. 1991. The kinesin superfamily: tails of functional redundancy. *Trends Cell Biol,* 1**,** 93-8.

GOODSON, H. V., VALETTI, C. & KREIS, T. E. 1997. Motors and membrane traffic. *Curr Opin Cell Biol,* 9**,** 18-28.

GRAESSMANN, A., GRAESSMANN, M., TJIAN, R. & TOPP, W. C. 1980. Simian virus 40 small-t protein is required for loss of actin cable networks in rat cells. *J Virol,* 33**,** 1182-91.

GRANZOW, H., KLUPP, B. G., FUCHS, W., VEITS, J., OSTERRIEDER, N. & METTENLEITER, T. C. 2001. Egress of alphaherpesviruses: comparative ultrastructural study. *J Virol,* 75**,** 3675-84.

GRANZOW, H., KLUPP, B. G. & METTENLEITER, T. C. 2005. Entry of pseudorabies virus: an immunogold-labeling study. *J Virol,* 79**,** 3200-5.

GROSS, S. T., HARLEY, C. A. & WILSON, D. W. 2003. The cytoplasmic tail of Herpes simplex virus glycoprotein H binds to the tegument protein VP16 in vitro and in vivo. *Virology,* 317**,** 1-12.

GUSTAFSSON, N., CULLEY, S., ASHDOWN, G., OWEN, D. M., PEREIRA, P. M. & HENRIQUES, R. 2016. Fast live-cell conventional fluorophore nanoscopy with ImageJ through super-resolution radial fluctuations. *Nat Commun,* 7**,** 12471.

HALLAK, M. E., RODRIGUEZ, J. A., BARRA, H. S. & CAPUTTO, R. 1977. Release of tyrosine from tyrosinated tubulin. Some common factors that affect this process and the assembly of tubulin. *FEBS Lett,* 73**,** 147-50.

HAMBLETON, S., GERSHON, M. D. & GERSHON, A. A. 2004. The role of the trans-Golgi network in varicella zoster virus biology. *Cell Mol Life Sci,* 61**,** 3047-56.

HAMMOND, J. W., CAI, D., BLASIUS, T. L., LI, Z., JIANG, Y., JIH, G. T., MEYHOFER, E. & VERHEY, K. J. 2009. Mammalian Kinesin-3 motors are dimeric in vivo and move by processive motility upon release of autoinhibition. *PLoS Biol,* 7**,** e72.

HAN, J., CHADHA, P., MECKES, D. G., BAIRD, N. L. & WILLS, J. W. 2011. Interaction and Interdependent Packaging of Tegument Protein UL11 and Glycoprotein E of Herpes Simplex Virus. *Journal of Virology,* 85**,** 9437.

HANCOCK, W. O. 2014. Bidirectional cargo transport: moving beyond tug of war. *Nat Rev Mol Cell Biol,* 15**,** 615-28.

HARTMAN, M. A. & SPUDICH, J. A. 2012. The myosin superfamily at a glance. *J Cell Sci,* 125**,** 1627-32.

HAY, J. & RUYECHAN, W. T. 2007. Alphaherpesvirus DNA replication. *In:* ARVIN, A., CAMPADELLI-FIUME, G., MOCARSKI, E., MOORE, P. S., ROIZMAN, B., WHITLEY, R. & YAMANISHI, K. (eds.) *Human Herpesviruses: Biology, Therapy, and Immunoprophylaxis.* Cambridge.

HENAFF, D., RADTKE, K. & LIPPE, R. 2012. Herpesviruses exploit several host compartments for envelopment. *Traffic,* 13**,** 1443-9.

HENDRICKS, A. G., PERLSON, E., ROSS, J. L., SCHROEDER, H. W., 3RD, TOKITO, M. & HOLZBAUR, E. L. 2010. Motor coordination via a tug-of-war mechanism drives bidirectional vesicle transport. *Curr Biol,* 20**,** 697-702.

HEPPERLA, A. J., WILLEY, P. T., COOMBES, C. E., SCHUSTER, B. M., GERAMI-NEJAD, M., MCCLELLAN, M., MUKHERJEE, S., FOX, J., WINEY, M., ODDE, D. J., O'TOOLE, E. & GARDNER, M. K. 2014. Minus-end-directed Kinesin-14 motors align antiparallel microtubules to control metaphase spindle length. *Dev Cell,* 31**,** 61-72.

HERRERA, F. J. & TRIEZENBERG, S. J. 2004. VP16-dependent association of chromatin-modifying coactivators and underrepresentation of histones at immediate-early gene promoters during herpes simplex virus infection. *J Virol,* 78**,** 9689-96.

HIROKAWA, N., NIWA, S. & TANAKA, Y. 2010. Molecular Motors in Neurons: Transport Mechanisms and Roles in Brain Function, Development, and Disease. *Neuron,* 68**,** 610-638.

HIROKAWA, N. & NODA, Y. 2008. Intracellular transport and kinesin superfamily proteins, KIFs: structure, function, and dynamics. *Physiol Rev,* 88**,** 1089-118.

HIROKAWA, N., NODA, Y., TANAKA, Y. & NIWA, S. 2009. Kinesin superfamily motor proteins and intracellular transport. *Nat Rev Mol Cell Biol,* 10**,** 682-96.

HIROKAWA, N. & TANAKA, Y. 2015. Kinesin superfamily proteins (KIFs): Various functions and their relevance for important phenomena in life and diseases. *Exp Cell Res,* 334**,** 16-25.

HOGUE, I. B., BOSSE, J. B., HU, J.-R., THIBERGE, S. Y. & ENQUIST, L. W. 2014a. Cellular Mechanisms of Alpha Herpesvirus Egress: Live Cell Fluorescence Microscopy of Pseudorabies Virus Exocytosis. *PLOS Pathogens,* 10**,** e1004535.

HOGUE, I. B., BOSSE, J. B., HU, J. R., THIBERGE, S. Y. & ENQUIST, L. W. 2014b. Cellular mechanisms of alpha herpesvirus egress: live cell fluorescence microscopy of pseudorabies virus exocytosis. *PLoS Pathog,* 10**,** e1004535.

HOLLINSHEAD, M., JOHNS, H. L., SAYERS, C. L., GONZALEZ-LOPEZ, C., SMITH, G. L. & ELLIOTT, G. 2012. Endocytic tubules regulated by Rab GTPases 5 and 11 are used for envelopment of herpes simplex virus. *EMBO J,* 31**,** 4204-20.

HOOK, P. & VALLEE, R. B. 2006. The dynein family at a glance. *J Cell Sci,* 119**,** 4369-71.
HORIGUCHI, K., HANADA, T., FUKUI, Y. & CHISHTI, A. H. 2006. Transport of PIP3 by GAKIN, a kinesin-3 family protein, regulates neuronal cell polarity. *J Cell Biol,* 174**,** 425-36.
HOWARD, J. & HYMAN, A. A. 2009. Growth, fluctuation and switching at microtubule plus ends. *Nat Rev Mol Cell Biol,* 10**,** 569-74.
HUANG, C. R., LIN, S. S., CHOU, M. Y., HO, C. C., WANG, L., LEE, Y. L., CHEN, C. S. & YANG, C. C. 2005. Demonstration of different modes of cell death upon herpes simplex virus 1 infection in different types of oral cells. *Acta Virol,* 49**,** 7-15.
HUANG, J., LAZEAR, H. M. & FRIEDMAN, H. M. 2011. Completely assembled virus particles detected by transmission electron microscopy in proximal and mid-axons of neurons infected with herpes simplex virus type 1, herpes simplex virus type 2 and pseudorabies virus. *Virology,* 409**,** 12-6.
HUNTER, A. W., CAPLOW, M., COY, D. L., HANCOCK, W. O., DIEZ, S., WORDEMAN, L. & HOWARD, J. 2003. The kinesin-related protein MCAK is a microtubule depolymerase that forms an ATP-hydrolyzing complex at microtubule ends. *Mol Cell,* 11**,** 445-57.
HUSZAR, D., THEOCLITOU, M.-E., SKOLNIK, J. & HERBST, R. 2009. Kinesin motor proteins as targets for cancer therapy. *Cancer and Metastasis Reviews,* 28**,** 197-208.
IBIRICU, I., HUISKONEN, J., DÖHNER, K., BRADKE, F., SODEIK, B. & GRÜNEWALD, K. 2011. *Cryo Electron Tomography of Herpes Simplex Virus during Axonal Transport and Secondary Envelopment in Primary Neurons*.
INGBER, D. E. 2003. Tensegrity II. How structural networks influence cellular information processing networks. *J Cell Sci,* 116**,** 1397-408.
INGBER, D. E. 2006. Mechanical control of tissue morphogenesis during embryological development. *Int J Dev Biol,* 50**,** 255-66.
IVANOVA, L., BUCH, A., DOHNER, K., POHLMANN, A., BINZ, A., PRANK, U., SANDBAUMHUTER, M., BAUERFEIND, R. & SODEIK, B. 2016. Conserved Tryptophan Motifs in the Large Tegument Protein pUL36 Are Required for Efficient Secondary Envelopment of Herpes Simplex Virus Capsids. *J Virol,* 90**,** 5368-5383.
JAMBUNATHAN, N., CHOULJENKO, D., DESAI, P., CHARLES, A.-S., SUBRAMANIAN, R., CHOULJENKO, V. N. & KOUSOULAS, K. G. 2014. Herpes Simplex Virus 1 Protein UL37 Interacts with Viral Glycoprotein gK and Membrane Protein UL20 and Functions in Cytoplasmic Virion Envelopment. *Journal of Virology,* 88**,** 5927.
JANIESCH, P. C., KIM, J., MOUYSSET, J., BARIKBIN, R., LOCHMULLER, H., CASSATA, G., KRAUSE, S. & HOPPE, T. 2007. The ubiquitin-selective chaperone CDC-48/p97 links myosin assembly to human myopathy. *Nat Cell Biol,* 9**,** 379-90.
JANKE, C. & BULINSKI, J. C. 2011. Post-translational regulation of the microtubule cytoskeleton: mechanisms and functions. *Nat Rev Mol Cell Biol,* 12**,** 773-86.
JAUD, J., BATHE, F., SCHLIWA, M., RIEF, M. & WOEHLKE, G. 2006. Flexibility of the neck domain enhances Kinesin-1 motility under load. *Biophys J,* 91**,** 1407-12.
JAYACHANDRA, S., BAGHIAN, A. & KOUSOULAS, K. G. 1997. Herpes simplex virus type 1 glycoprotein K is not essential for infectious virus production in actively replicating cells but is required for efficient envelopment and translocation of

infectious virions from the cytoplasm to the extracellular space. *Journal of Virology,* 71**,** 5012.

JENKINS, B., DECKER, H., BENTLEY, M., LUISI, J. & BANKER, G. 2012. A novel split kinesin assay identifies motor proteins that interact with distinct vesicle populations. *J Cell Biol,* 198**,** 749-61.

JOHNS, H. L., GONZALEZ-LOPEZ, C., SAYERS, C. L., HOLLINSHEAD, M. & ELLIOTT, G. 2014. Rab6 dependent post-Golgi trafficking of HSV1 envelope proteins to sites of virus envelopment. *Traffic (Copenhagen, Denmark),* 15**,** 157-178.

JOHNSON, D. C., WEBB, M., WISNER, T. W. & BRUNETTI, C. 2001. Herpes Simplex Virus gE/gI Sorts Nascent Virions to Epithelial Cell Junctions, Promoting Virus Spread. *Journal of Virology,* 75**,** 821.

JOHNSON, D. C., WISNER, T. W. & WRIGHT, C. C. 2011. Herpes Simplex Virus Glycoproteins gB and gD Function in a Redundant Fashion To Promote Secondary Envelopment. *Journal of Virology,* 85**,** 4910.

JOHNSON, E. A., BURKE, C. N., FREDRICKSON, T. N. & DICAPUA, R. A. 1975. Morphogenesis of marek's disease virus in feather follicle epithelium. *J Natl Cancer Inst,* 55**,** 89-99.

JOHNSON, J. E. & CHIU, W. 2007. DNA packaging and delivery machines in tailed bacteriophages. *Curr Opin Struct Biol,* 17**,** 237-43.

JOVASEVIC, V., NAGHAVI, M. H. & WALSH, D. 2015. Microtubule plus end-associated CLIP-170 initiates HSV-1 retrograde transport in primary human cells. *J Cell Biol,* 211**,** 323-37.

KADAVATH, H., HOFELE, R. V., BIERNAT, J., KUMAR, S., TEPPER, K., URLAUB, H., MANDELKOW, E. & ZWECKSTETTER, M. 2015. Tau stabilizes microtubules by binding at the interface between tubulin heterodimers. *Proc Natl Acad Sci U S A,* 112**,** 7501-6.

KELLY, B. J., DIEFENBACH, E., FRAEFEL, C. & DIEFENBACH, R. J. 2012. Identification of host cell proteins which interact with herpes simplex virus type 1 tegument protein pUL37. *Biochem Biophys Res Commun,* 417**,** 961-5.

KEVENAAR, J. T., BIANCHI, S., VAN SPRONSEN, M., OLIERIC, N., LIPKA, J., FRIAS, C. P., MIKHAYLOVA, M., HARTERINK, M., KEIJZER, N., WULF, P. S., HILBERT, M., KAPITEIN, L. C., DE GRAAFF, E., AHKMANOVA, A., STEINMETZ, M. O. & HOOGENRAAD, C. C. 2016. Kinesin-Binding Protein Controls Microtubule Dynamics and Cargo Trafficking by Regulating Kinesin Motor Activity. *Curr Biol,* 26**,** 849-61.

KHAITLINA, S. Y. 2014. Intracellular transport based on actin polymerization. *Biochemistry (Mosc),* 79**,** 917-27.

KHAN, A. O., SIMMS, V. A., PIKE, J. A., THOMAS, S. G. & MORGAN, N. V. 2017. CRISPR-Cas9 Mediated Labelling Allows for Single Molecule Imaging and Resolution. *Sci Rep,* 7**,** 8450.

KHARKWAL, H., SMITH, C. G. & WILSON, D. W. 2014. Blocking ESCRT-mediated envelopment inhibits microtubule-dependent trafficking of alphaherpesviruses in vitro. *J Virol,* 88**,** 14467-78.

KLOPFENSTEIN, D. R., TOMISHIGE, M., STUURMAN, N. & VALE, R. D. 2002. Role of phosphatidylinositol(4,5)bisphosphate organization in membrane transport by the Unc104 kinesin motor. *Cell,* 109**,** 347-58.

KOLLMAN, J. M., POLKA, J. K., ZELTER, A., DAVIS, T. N. & AGARD, D. A. 2010. Microtubule nucleating gamma-TuSC assembles structures with 13-fold microtubule-like symmetry. *Nature,* 466**,** 879-82.

KOMAROVA, Y., DE GROOT, C. O., GRIGORIEV, I., GOUVEIA, S. M., MUNTEANU, E. L., SCHOBER, J. M., HONNAPPA, S., BUEY, R. M., HOOGENRAAD, C. C., DOGTEROM, M., BORISY, G. G., STEINMETZ, M. O. & AKHMANOVA, A. 2009. Mammalian end binding proteins control persistent microtubule growth. *J Cell Biol,* 184**,** 691-706.

KORNFEIND, E. M. & VISALLI, R. J. 2018. Human herpesvirus portal proteins: Structure, function, and antiviral prospects. *Rev Med Virol,* 28**,** e1972.

KOSHIZUKA, T., KAWAGUCHI, Y. & NISHIYAMA, Y. 2005. Herpes simplex virus type 2 membrane protein UL56 associates with the kinesin motor protein KIF1A. *J Gen Virol,* 86**,** 527-33.

KOTSAKIS, A., POMERANZ, L. E., BLOUIN, A. & BLAHO, J. A. 2001. Microtubule reorganization during herpes simplex virus type 1 infection facilitates the nuclear localization of VP22, a major virion tegument protein. *J Virol,* 75**,** 8697-711.

KOYAMA, A. H. & UCHIDA, T. J. A. O. V. 1994. Inhibition by Brefeldin A of the envelopment of nucleocapsids in herpes simplex virus type 1-infected Vero cells. 135**,** 305-317.

KRAMER, T., GRECO, T. M., TAYLOR, M. P., AMBROSINI, A. E., CRISTEA, I. M. & ENQUIST, L. W. 2012. Kinesin-3 mediates axonal sorting and directional transport of alphaherpesvirus particles in neurons. *Cell Host Microbe,* 12**,** 806-14.

KRAUTWALD, M., MARESCH, C., KLUPP, B. G., FUCHS, W. & METTENLEITER, T. C. 2008. Deletion or green fluorescent protein tagging of the pUL35 capsid component of pseudorabies virus impairs virus replication in cell culture and neuroinvasion in mice. *J Gen Virol,* 89**,** 1346-51.

KREITZER, G., LIAO, G. & GUNDERSEN, G. G. 1999. Detyrosination of tubulin regulates the interaction of intermediate filaments with microtubules in vivo via a kinesin-dependent mechanism. *Mol Biol Cell,* 10**,** 1105-18.

KUHN, M., DESLOGES, N., RAHAUS, M. & WOLFF, M. H. 2005. Varicella-zoster virus infection influences expression and organization of actin and alpha-tubulin but does not affect lamin A and vimentin. *Intervirology,* 48**,** 312-20.

KUMAR, N. & FLAVIN, M. 1981. Preferential action of a brain detyrosinolating carboxypeptidase on polymerized tubulin. *J Biol Chem,* 256**,** 7678-86.

KURIYAMA, R. & NISLOW, C. 1992. Molecular components of the mitotic spindle. *Bioessays,* 14**,** 81-8.

KUT, E. & RASSCHAERT, D. 2004. Assembly of Marek's disease virus (MDV) capsids using recombinant baculoviruses expressing MDV capsid proteins. *J Gen Virol,* 85**,** 769-74.

L'HERNAULT, S. W. & ROSENBAUM, J. L. 1985. Chlamydomonas alpha-tubulin is posttranslationally modified by acetylation on the epsilon-amino group of a lysine. *Biochemistry,* 24**,** 473-8.

LAINE, R. F., ALBECKA, A., VAN DE LINDE, S., REES, E. J., CRUMP, C. M. & KAMINSKI, C. F. 2015. Structural analysis of herpes simplex virus by optical super-resolution imaging. *Nature Communications,* 6**,** 5980.

LAM, K. M. 1995. Apoptosis in chicken embryo fibroblasts caused by Newcastle disease virus. *Vet Microbiol,* 47**,** 357-63.

LAU, K. S.-Y. & CRUMP, M. C. 2015. HSV-1 gM and the gK/pUL20 Complex Are Important for the Localization of gD and gH/L to Viral Assembly Sites. *Viruses,* 7.

LAWRENCE, C. J., DAWE, R. K., CHRISTIE, K. R., CLEVELAND, D. W., DAWSON, S. C., ENDOW, S. A., GOLDSTEIN, L. S., GOODSON, H. V., HIROKAWA, N., HOWARD, J., MALMBERG, R. L., MCINTOSH, J. R., MIKI, H., MITCHISON, T. J., OKADA, Y., REDDY, A. S., SAXTON, W. M., SCHLIWA, M., SCHOLEY, J. M., VALE, R. D., WALCZAK, C. E. & WORDEMAN, L. 2004. A standardized kinesin nomenclature. *J Cell Biol,* 167**,** 19-22.

LEDIZET, M. & PIPERNO, G. 1987. Identification of an acetylation site of Chlamydomonas alpha-tubulin. *Proc Natl Acad Sci U S A,* 84**,** 5720-4.

LEE, J. C., FIELD, D. J. & LEE, L. L. 1980. Effects of nocodazole on structures of calf brain tubulin. *Biochemistry,* 19**,** 6209-15.

LEEGE, T., FUCHS, W., GRANZOW, H., KOPP, M., KLUPP, B. G. & METTENLEITER, T. C. 2009. Effects of Simultaneous Deletion of pUL11 and Glycoprotein M on Virion Maturation of Herpes Simplex Virus Type 1. *Journal of Virology,* 83**,** 896.

LEOPOLD, P. L., KREITZER, G., MIYAZAWA, N., REMPEL, S., PFISTER, K. K., RODRIGUEZ-BOULAN, E. & CRYSTAL, R. G. 2000. Dynein- and Microtubule-Mediated Translocation of Adenovirus Serotype 5 Occurs after Endosomal Lysis. 11**,** 151-165.

LIAO, G. & GUNDERSEN, G. G. 1998. Kinesin is a candidate for cross-bridging microtubules and intermediate filaments. Selective binding of kinesin to detyrosinated tubulin and vimentin. *J Biol Chem,* 273**,** 9797-803.

LINDQVIST, R. F. T. 1931. The viscosity of the blood in narrow capillary tubes *american journal of physiology,* 96**,** 562.

LORET, S., GUAY, G. & LIPPE, R. 2008. Comprehensive characterization of extracellular herpes simplex virus type 1 virions. *J Virol,* 82**,** 8605-18.

LUKINAVICIUS, G., UMEZAWA, K., OLIVIER, N., HONIGMANN, A., YANG, G., PLASS, T., MUELLER, V., REYMOND, L., CORREA, I. R., JR., LUO, Z. G., SCHULTZ, C., LEMKE, E. A., HEPPENSTALL, P., EGGELING, C., MANLEY, S. & JOHNSSON, K. 2013. A near-infrared fluorophore for live-cell super-resolution microscopy of cellular proteins. *Nat Chem,* 5**,** 132-9.

MABIT, H., NAKANO, M. Y., PRANK, U., SAAM, B., DOHNER, K., SODEIK, B. & GREBER, U. F. 2002. Intact microtubules support adenovirus and herpes simplex virus infections. *J Virol,* 76**,** 9962-71.

MACHESKY, L. M., ATKINSON, S. J., AMPE, C., VANDEKERCKHOVE, J. & POLLARD, T. D. 1994. Purification of a cortical complex containing two unconventional actins from Acanthamoeba by affinity chromatography on profilin-agarose. *J Cell Biol,* 127**,** 107-15.

MACKEM, S. & ROIZMAN, B. 1982. Structural features of the herpes simplex virus alpha gene 4, 0, and 27 promoter-regulatory sequences which confer alpha regulation on chimeric thymidine kinase genes. *J Virol,* 44**,** 939-49.

MANDELKOW, E. & MANDELKOW, E. M. 1989. Microtubular structure and tubulin polymerization. *Curr Opin Cell Biol,* 1**,** 5-9.

MARCHISIO, P. C., CAPASSO, O., NITSCH, L., CANCEDDA, R. & GIONTI, E. 1984. Cytoskeleton and adhesion patterns of cultured chick embryo chondrocytes during cell spreading and Rous sarcoma virus transformation. *Exp Cell Res,* 151**,** 332-43.

MARESCH, C., GRANZOW, H., NEGATSCH, A., KLUPP, B. G., FUCHS, W., TEIFKE, J. P. & METTENLEITER, T. C. 2010. Ultrastructural analysis of virion formation and anterograde intraaxonal transport of the alphaherpesvirus pseudorabies virus in primary neurons. *J Virol,* 84**,** 5528-39.

MARINGER, K., STYLIANOU, J. & ELLIOTT, G. 2012. A Network of Protein Interactions around the Herpes Simplex Virus Tegument Protein VP22. *Journal of Virology,* 86**,** 12971.

MAROZIN, S., PRANK, U. & SODEIK, B. 2004. Herpes simplex virus type 1 infection of polarized epithelial cells requires microtubules and access to receptors present at cell-cell contact sites. *J Gen Virol,* 85**,** 775-86.

MARTINEZ, N. W., XUE, X., BERRO, R. G., KREITZER, G. & RESH, M. D. 2008. Kinesin KIF4 regulates intracellular trafficking and stability of the human immunodeficiency virus type 1 Gag polyprotein. *J Virol,* 82**,** 9937-50.

MASTERS, T. A., KENDRICK-JONES, J. & BUSS, F. 2017. Myosins: Domain Organisation, Motor Properties, Physiological Roles and Cellular Functions. *Handb Exp Pharmacol,* 235**,** 77-122.

MATSUSHITA, M., YAMAMOTO, R., MITSUI, K. & KANAZAWA, H. 2009. Altered motor activity of alternative splice variants of the mammalian kinesin-3 protein KIF1B. *Traffic,* 10**,** 1647-54.

MCDONALD, D., VODICKA, M. A., LUCERO, G., SVITKINA, T. M., BORISY, G. G., EMERMAN, M. & HOPE, T. J. 2002. Visualization of the intracellular behavior of HIV in living cells. *J Cell Biol,* 159**,** 441-52.

MCELWEE, M., BEILSTEIN, F., LABETOULLE, M., RIXON, F. J. & PASDELOUP, D. 2013. Dystonin/BPAG1 promotes plus-end-directed transport of herpes simplex virus 1 capsids on microtubules during entry. *J Virol,* 87**,** 11008-18.

MCKENNEY, R. J., HUYNH, W., TANENBAUM, M. E., BHABHA, G. & VALE, R. D. 2014. Activation of cytoplasmic dynein motility by dynactin-cargo adapter complexes. *Science,* 345**,** 337-41.

MCKENNEY, R. J., WEIL, S. J., SCHERER, J. & VALLEE, R. B. 2011. Mutually exclusive cytoplasmic dynein regulation by NudE-Lis1 and dynactin. *J Biol Chem,* 286**,** 39615-22.

MCLEAN, W. H. & LANE, E. B. 1995. Intermediate filaments in disease. *Curr Opin Cell Biol,* 7**,** 118-25.

MCMILLAN, T. N. & JOHNSON, D. C. 2001. Cytoplasmic Domain of Herpes Simplex Virus gE Causes Accumulation in the <em>trans</em>-Golgi Network, a Site of Virus Envelopment and Sorting of Virions to Cell Junctions. *Journal of Virology,* 75**,** 1928.

MCPHERSON, M. C. & DELANY, M. E. 2016. Virus and host genomic, molecular, and cellular interactions during Marek's disease pathogenesis and oncogenesis. *Poult Sci,* 95**,** 412-29.

MCWHORTER, F. Y., WANG, T., NGUYEN, P., CHUNG, T. & LIU, W. F. 2013. Modulation of macrophage phenotype by cell shape. *Proc Natl Acad Sci U S A,* 110**,** 17253-8.

MELANCON, J. M., FOSTER, T. P. & KOUSOULAS, K. G. 2004. Genetic Analysis of the Herpes Simplex Virus Type 1 UL20 Protein Domains Involved in Cytoplasmic Virion Envelopment and Virus-Induced Cell Fusion. *Journal of Virology,* 78**,** 7329.

METTENLEITER, T. C. 2002. Herpesvirus assembly and egress. *J Virol,* 76**,** 1537-47.

METTENLEITER, T. C. 2004. Budding events in herpesvirus morphogenesis. *Virus Res,* 106**,** 167-80.

METTENLEITER, T. C., KLUPP, B. G. & GRANZOW, H. 2006. Herpesvirus assembly: a tale of two membranes. *Curr Opin Microbiol,* 9**,** 423-9.

METTENLEITER, T. C., KLUPP, B. G. & GRANZOW, H. 2009. Herpesvirus assembly: an update. *Virus Res,* 143**,** 222-34.

MIKI, H., OKADA, Y. & HIROKAWA, N. 2005. Analysis of the kinesin superfamily: insights into structure and function. *Trends Cell Biol,* 15**,** 467-76.

MINGO, R. M., HAN, J., NEWCOMB, W. W. & BROWN, J. C. 2012. Replication of herpes simplex virus: egress of progeny virus at specialized cell membrane sites. *J Virol,* 86**,** 7084-97.

MIRANDA-SAKSENA, M., BOADLE, R. A., AGGARWAL, A., TIJONO, B., RIXON, F. J., DIEFENBACH, R. J. & CUNNINGHAM, A. L. 2009. Herpes Simplex Virus Utilizes the Large Secretory Vesicle Pathway for Anterograde Transport of Tegument and Envelope Proteins and for Viral Exocytosis from Growth Cones of Human Fetal Axons. *Journal of Virology,* 83**,** 3187.

MIRANDA-SAKSENA, M., DENES, C. E., DIEFENBACH, R. J. & CUNNINGHAM, A. L. 2018. Infection and Transport of Herpes Simplex Virus Type 1 in Neurons: Role of the Cytoskeleton. *Viruses,* 10.

MITCHISON, T. & KIRSCHNER, M. 1984. Dynamic instability of microtubule growth. *Nature,* 312**,** 237-42.

MOORES, C. A., YU, M., GUO, J., BERAUD, C., SAKOWICZ, R. & MILLIGAN, R. A. 2002. A mechanism for microtubule depolymerization by KinI kinesins. *Mol Cell,* 9**,** 903-9.

MOU, F., WILLS, E. & BAINES, J. D. 2009. Phosphorylation of the U(L)31 protein of herpes simplex virus 1 by the U(S)3-encoded kinase regulates localization of the nuclear envelopment complex and egress of nucleocapsids. *J Virol,* 83**,** 5181-91.

MULLER, M. J., KLUMPP, S. & LIPOWSKY, R. 2008. Tug-of-war as a cooperative mechanism for bidirectional cargo transport by molecular motors. *Proc Natl Acad Sci U S A,* 105**,** 4609-14.

MULLER, T., HAHN, E. C., TOTTEWITZ, F., KRAMER, M., KLUPP, B. G., METTENLEITER, T. C. & FREULING, C. 2011. Pseudorabies virus in wild swine: a global perspective. *Arch Virol,* 156**,** 1691-705.

MULLINS, R. D., HEUSER, J. A. & POLLARD, T. D. 1998. The interaction of Arp2/3 complex with actin: nucleation, high affinity pointed end capping, and formation of branching networks of filaments. *Proc Natl Acad Sci U S A,* 95**,** 6181-6.

NAGHAVI, M. H., GUNDERSEN, G. G. & WALSH, D. 2013. Plus-end tracking proteins, CLASPs, and a viral Akt mimic regulate herpesvirus-induced stable microtubule formation and virus spread. *Proc Natl Acad Sci U S A,* 110**,** 18268-73.

NAGHAVI, M. H. & WALSH, D. 2017. Microtubule Regulation and Function during Virus Infection. *J Virol,* 91.

NAHIDIAZAR, L., AGRONSKAIA, A. V., BROERTJES, J., VAN DEN BROEK, B. & JALINK, K. 2016. Optimizing Imaging Conditions for Demanding Multi-Color Super Resolution Localization Microscopy. *PLoS One,* 11**,** e0158884.

NAIR, V. 2005. Evolution of Marek's disease -- a paradigm for incessant race between the pathogen and the host. *Vet J,* 170**,** 175-83.

NAZERIAN, K., SOLOMON, J. J., WITTER, R. L. & BURMESTER, B. R. 1968. Studies on the etiology of Marek's disease. II. Finding of a herpesvirus in cell culture. *Proc Soc Exp Biol Med,* 127**,** 177-82.

NEERUKONDA, S. N., KATNENI, U. K., GOLOVAN, S. & PARCELLS, M. S. 2016. Evaluation and validation of reference gene stability during Marek's disease virus (MDV) infection. *J Virol Methods,* 236**,** 111-116.

NEGATSCH, A., GRANZOW, H., MARESCH, C., KLUPP, B. G., FUCHS, W., TEIFKE, J. P. & METTENLEITER, T. C. 2010. Ultrastructural analysis of virion formation and intraaxonal transport of herpes simplex virus type 1 in primary rat neurons. *J Virol,* 84**,** 13031-5.

NELLISSERY, J. K., SZCZEPANIAK, R., LAMBERTI, C. & WELLER, S. K. 2007. A putative leucine zipper within the herpes simplex virus type 1 UL6 protein is required for portal ring formation. *J Virol,* 81**,** 8868-77.

NEWCOMB, W. W., HOMA, F. L., THOMSEN, D. R., BOOY, F. P., TRUS, B. L., STEVEN, A. C., SPENCER, J. V. & BROWN, J. C. 1996. Assembly of the herpes simplex virus capsid: characterization of intermediates observed during cell-free capsid formation. *J Mol Biol,* 263**,** 432-46.

NEWCOMB, W. W., JONES, L. M., DEE, A., CHAUDHRY, F. & BROWN, J. C. 2012. Role of a reducing environment in disassembly of the herpesvirus tegument. *Virology,* 431**,** 71-9.

NIKOLIC, D. S., LEHMANN, M., FELTS, R., GARCIA, E., BLANCHET, F. P., SUBRAMANIAM, S. & PIGUET, V. 2011. HIV-1 activates Cdc42 and induces membrane extensions in immature dendritic cells to facilitate cell-to-cell virus propagation. *Blood,* 118**,** 4841-52.

NIWA, S., TANAKA, Y. & HIROKAWA, N. 2008. KIF1Bbeta- and KIF1A-mediated axonal transport of presynaptic regulator Rab3 occurs in a GTP-dependent manner through DENN/MADD. *Nat Cell Biol,* 10**,** 1269-79.

NOGALES, E., WOLF, S. G. & DOWNING, K. H. 1998. Structure of the alpha beta tubulin dimer by electron crystallography. *Nature,* 391**,** 199-203.

O'DONNELL, L. A., CLEMMER, J. A., CZYMMEK, K. & SCHMIDT, C. J. 2002. Marek's disease virus VP22: subcellular localization and characterization of carboxyl terminal deletion Mutations. *Virology,* 292**,** 235-40.

OH, M. J., AKHTAR, J., DESAI, P. & SHUKLA, D. 2010. A role for heparan sulfate in viral surfing. *Biochem Biophys Res Commun,* 391**,** 176-81.

OKADA, Y. & HIROKAWA, N. 1999. A processive single-headed motor: kinesin superfamily protein KIF1A. *Science,* 283**,** 1152-7.

OSTERRIEDER, N., KAMIL, J. P., SCHUMACHER, D., TISCHER, B. K. & TRAPP, S. 2006. Marek's disease virus: from miasma to model. *Nat Rev Microbiol,* 4**,** 283-94.

OVESNY, M., KRIZEK, P., BORKOVEC, J., SVINDRYCH, Z. & HAGEN, G. M. 2014. ThunderSTORM: a comprehensive ImageJ plug-in for PALM and STORM data analysis and super-resolution imaging. *Bioinformatics,* 30**,** 2389-90.

OWEN, D. J., CRUMP, C. M. & GRAHAM, S. C. 2015. Tegument Assembly and Secondary Envelopment of Alphaherpesviruses. *Viruses,* 7**,** 5084-5114.

PALAZZO, A. F., ENG, C. H., SCHLAEPFER, D. D., MARCANTONIO, E. E. & GUNDERSEN, G. G. 2004. Localized stabilization of microtubules by integrin- and FAK-facilitated Rho signaling. *Science,* 303**,** 836-9.

PASDELOUP, D., LABETOULLE, M. & RIXON, F. J. 2013a. Differing effects of herpes simplex virus 1 and pseudorabies virus infections on centrosomal function. *J Virol,* 87**,** 7102-12.

PASDELOUP, D., MCELWEE, M., BEILSTEIN, F., LABETOULLE, M. & RIXON, F. J. 2013b. Herpesvirus tegument protein pUL37 interacts with dystonin/BPAG1 to promote capsid transport on microtubules during egress. *J Virol,* 87**,** 2857-67.

PAUL-GILLOTEAUX, P., HEILIGENSTEIN, X., BELLE, M., DOMART, M. C., LARIJANI, B., COLLINSON, L., RAPOSO, G. & SALAMERO, J. 2017. eC-CLEM: flexible multidimensional registration software for correlative microscopies. *Nat Methods,* 14**,** 102-103.

PAWLICZEK, T. & CRUMP, C. M. 2009a. Herpes simplex virus type 1 production requires a functional ESCRT-III complex but is independent of TSG101 and ALIX expression. *J Virol,* 83**,** 11254-64.

PAWLICZEK, T. & CRUMP, C. M. 2009b. Herpes Simplex Virus Type 1 Production Requires a Functional ESCRT-III Complex but Is Independent of TSG101 and ALIX Expression. *Journal of Virology,* 83**,** 11254.

PERDIZ, D., MACKEH, R., POUS, C. & BAILLET, A. 2011. The ins and outs of tubulin acetylation: more than just a post-translational modification? *Cell Signal,* 23**,** 763-71.

PERGAM, S. A., LIMAYE, A. P. & PRACTICE, A. S. T. I. D. C. O. 2009. Varicella zoster virus (VZV) in solid organ transplant recipients. *Am J Transplant,* 9 Suppl 4**,** S108-15.

PERIS, L., WAGENBACH, M., LAFANECHERE, L., BROCARD, J., MOORE, A. T., KOZIELSKI, F., JOB, D., WORDEMAN, L. & ANDRIEUX, A. 2009. Motor-dependent microtubule disassembly driven by tubulin tyrosination. *J Cell Biol,* 185**,** 1159-66.

PIXLEY, F. J. 2012. Macrophage Migration and Its Regulation by CSF-1. *Int J Cell Biol,* 2012**,** 501962.

POLLARD, T. D. & BELTZNER, C. C. 2002. Structure and function of the Arp2/3 complex. *Curr Opin Struct Biol,* 12**,** 768-74.

POLLARD, T. D. & BORISY, G. G. 2003. Cellular motility driven by assembly and disassembly of actin filaments. *Cell,* 112**,** 453-65.

POLLARD, T. D. & COOPER, J. A. 2009. Actin, a central player in cell shape and movement. *Science,* 326**,** 1208-12.

QUINONES, G. B., DANOWSKI, B. A., DEVARAJ, A., SINGH, V. & LIGON, L. A. 2011. The posttranslational modification of tubulin undergoes a switch from detyrosination to acetylation as epithelial cells become polarized. *Mol Biol Cell,* 22**,** 1045-57.

RADTKE, K., KIENEKE, D., WOLFSTEIN, A., MICHAEL, K., STEFFEN, W., SCHOLZ, T., KARGER, A. & SODEIK, B. 2010. Plus- and minus-end directed microtubule motors bind simultaneously to herpes simplex virus capsids using different inner tegument structures. *PLoS Pathog,* 6**,** e1000991.

REDEKER, V., LEVILLIERS, N., SCHMITTER, J. M., LE CAER, J. P., ROSSIER, J., ADOUTTE, A. & BRE, M. H. 1994. Polyglycylation of tubulin: a posttranslational modification in axonemal microtubules. *Science,* 266**,** 1688-91.

REED, N. A., CAI, D., BLASIUS, T. L., JIH, G. T., MEYHOFER, E., GAERTIG, J. & VERHEY, K. J. 2006. Microtubule acetylation promotes kinesin-1 binding and transport. *Curr Biol,* 16**,** 2166-72.

REMY, S., BLONDEAU, C., LE VERN, Y., LEMESLE, M., VAUTHEROT, J. F. & DENESVRE, C. 2013. Fluorescent tagging of VP22 in N-terminus reveals that VP22 favors Marek's disease virus (MDV) virulence in chickens and allows morphogenesis study in MD tumor cells. *Vet Res,* 44**,** 125.

RETZER, K., LACEK, J., SKOKAN, R., DEL GENIO, C. I., VOSOLSOBE, S., LANKOVA, M., MALINSKA, K., KONSTANTINOVA, N., ZAZIMALOVA, E., NAPIER, R. M., PETRASEK, J. & LUSCHNIG, C. 2017. Evolutionary Conserved Cysteines Function as cis-Acting Regulators of Arabidopsis PIN-FORMED 2 Distribution. *Int J Mol Sci,* 18.

REYNOLDS, A. E., WILLS, E. G., ROLLER, R. J., RYCKMAN, B. J. & BAINES, J. D. 2002. Ultrastructural localization of the herpes simplex virus type 1 UL31, UL34, and US3 proteins suggests specific roles in primary envelopment and egress of nucleocapsids. *J Virol,* 76**,** 8939-52.

RICHERIOUX, N., BLONDEAU, C., WIEDEMANN, A., REMY, S., VAUTHEROT, J. F. & DENESVRE, C. 2012. Rho-ROCK and Rac-PAK signaling pathways have opposing effects on the cell-to-cell spread of Marek's Disease Virus. *PLoS One,* 7**,** e44072.

RIXON, F. J., ADDISON, C. & MCLAUCHLAN, J. 1992. Assembly of enveloped tegument structures (L particles) can occur independently of virion maturation in herpes simplex virus type 1-infected cells. 73**,** 277-284.

ROBERTS, A. J., KON, T., KNIGHT, P. J., SUTOH, K. & BURGESS, S. A. 2013. Functions and mechanics of dynein motor proteins. *Nat Rev Mol Cell Biol,* 14**,** 713-26.

ROBERTS, K. L. & BAINES, J. D. 2010. Myosin Va Enhances Secretion of Herpes Simplex Virus 1 Virions and Cell Surface Expression of Viral Glycoproteins. *Journal of Virology,* 84**,** 9889.

ROBERTS, K. L. & BAINES, J. D. 2011. Actin in herpesvirus infection. *Viruses,* 3**,** 336-346.

ROBERTS, K. L. & SMITH, G. L. 2008. Vaccinia virus morphogenesis and dissemination. *Trends in Microbiology,* 16**,** 472-479.

ROGERS, K. R., WEISS, S., CREVEL, I., BROPHY, P. J., GEEVES, M. & CROSS, R. 2001. KIF1D is a fast non-processive kinesin that demonstrates novel K-loop-dependent mechanochemistry. *EMBO J,* 20**,** 5101-13.

ROGERS, S. S., FLORES-RODRIGUEZ, N., ALLAN, V. J., WOODMAN, P. G. & WAIGH, T. A. 2010. The first passage probability of intracellular particle trafficking. *Phys Chem Chem Phys,* 12**,** 3753-61.

ROLLER, R. J., ZHOU, Y., SCHNETZER, R., FERGUSON, J. & DESALVO, D. 2000. Herpes simplex virus type 1 U(L)34 gene product is required for viral envelopment. *J Virol,* 74**,** 117-29.

RUST, M. J., BATES, M. & ZHUANG, X. 2006. Sub-diffraction-limit imaging by stochastic optical reconstruction microscopy (STORM). *Nat Methods,* 3**,** 793-5.

SAINATH, R. & GALLO, G. 2015. The dynein inhibitor Ciliobrevin D inhibits the bidirectional transport of organelles along sensory axons and impairs NGF-mediated regulation of growth cones and axon branches. *Dev Neurobiol,* 75**,** 757-77.

SAKSENA, M. M., WAKISAKA, H., TIJONO, B., BOADLE, R. A., RIXON, F., TAKAHASHI, H. & CUNNINGHAM, A. L. 2006. Herpes simplex virus type 1 accumulation, envelopment, and exit in growth cones and varicosities in mid-distal regions of axons. *J Virol,* 80**,** 3592-606.

SALINAS, S., BILSLAND, L. G., HENAFF, D., WESTON, A. E., KERIEL, A., SCHIAVO, G. & KREMER, E. J. 2009. CAR-associated vesicular transport of an adenovirus in motor neuron axons. *PLoS pathogens,* 5**,** e1000442-e1000442.

SANDBAUMHUTER, M., DOHNER, K., SCHIPKE, J., BINZ, A., POHLMANN, A., SODEIK, B. & BAUERFEIND, R. 2013. Cytosolic herpes simplex virus capsids not only require binding inner tegument protein pUL36 but also pUL37 for active transport prior to secondary envelopment. *Cell Microbiol,* 15**,** 248-69.

SATAKE, T., OTSUKI, K., BANBA, Y., SUENAGA, J., HIRANO, H., YAMANAKA, Y., OHNO, S. & HIRAI, S. 2013. The interaction of Kinesin-1 with its adaptor protein JIP1 can be regulated via proteins binding to the JIP1-PTB domain. *BMC Cell Biol,* 14**,** 12.

SCHAT, K. A., SCHINAZI, R. F. & CALNEK, B. W. 1984. Cell-specific antiviral activity of 1-(2-fluoro-2-deoxy-beta-D-arabinofuranosyl)-5-iodocytosine (FIAC) against Marek's disease herpesvirus and turkey herpesvirus. *Antiviral Res,* 4**,** 259-70.

SCHEPIS, A., STAUBER, T. & KRIJNSE LOCKER, J. 2007. Kinesin-1 plays multiple roles during the vaccinia virus life cycle. *Cell Microbiol,* 9**,** 1960-73.

SCHLAGER, M. A., HOANG, H. T., URNAVICIUS, L., BULLOCK, S. L. & CARTER, A. P. 2014. In vitro reconstitution of a highly processive recombinant human dynein complex. *EMBO J,* 33**,** 1855-68.

SCHLAGER, M. A., KAPITEIN, L. C., GRIGORIEV, I., BURZYNSKI, G. M., WULF, P. S., KEIJZER, N., DE GRAAFF, E., FUKUDA, M., SHEPHERD, I. T., AKHMANOVA, A. & HOOGENRAAD, C. C. 2010. Pericentrosomal targeting of Rab6 secretory vesicles by Bicaudal-D-related protein 1 (BICDR-1) regulates neuritogenesis. *EMBO J,* 29**,** 1637-51.

SCHOLEY, J. M. 2008. Intraflagellar transport motors in cilia: moving along the cell's antenna. *J Cell Biol,* 180**,** 23-9.

SCHUMACHER, D., MCKINNEY, C., KAUFER, B. B. & OSTERRIEDER, N. 2008. Enzymatically inactive U(S)3 protein kinase of Marek's disease virus (MDV) is capable of depolymerizing F-actin but results in accumulation of virions in perinuclear invaginations and reduced virus growth. *Virology,* 375**,** 37-47.

SCHUMACHER, D., TISCHER, B. K., TRAPP, S. & OSTERRIEDER, N. 2005. The protein encoded by the US3 orthologue of Marek's disease virus is required for

efficient de-envelopment of perinuclear virions and involved in actin stress fiber breakdown. *J Virol,* 79**,** 3987-97.

SHEK, W. R., CALNEK, B. W., SCHAT, K. A. & CHEN, C. H. 1983. Characterization of Marek's disease virus-infected lymphocytes: discrimination between cytolytically and latently infected cells. *J Natl Cancer Inst,* 70**,** 485-91.

SHIBA, C., DAIKOKU, T., GOSHIMA, F., TAKAKUWA, H., YAMAUCHI, Y., KOIWAI, O. & NISHIYAMA, Y. 2000. The UL34 gene product of herpes simplex virus type 2 is a tail-anchored type II membrane protein that is significant for virus envelopment. *J Gen Virol,* 81**,** 2397-405.

SHIMOJIMA, Y., JANG, H. K., ONO, M., KAI, C. & MIKAMI, T. 1997. Identification and DNA sequence analysis of the Marek's disease virus serotype 2 gene homologous to the herpes simplex virus type 1 glycoprotein H. *J Vet Med Sci,* 59**,** 629-34.

SHUBEITA, G. T., TRAN, S. L., XU, J., VERSHININ, M., CERMELLI, S., COTTON, S. L., WELTE, M. A. & GROSS, S. P. 2008. Consequences of motor copy number on the intracellular transport of kinesin-1-driven lipid droplets. *Cell,* 135**,** 1098-107.

SIDDIQUI, N. & STRAUBE, A. 2017. Intracellular Cargo Transport by Kinesin-3 Motors. *Biochemistry (Mosc),* 82**,** 803-815.

SIRAJUDDIN, M., RICE, L. M. & VALE, R. D. 2014. Regulation of microtubule motors by tubulin isotypes and post-translational modifications. *Nat Cell Biol,* 16**,** 335-44.

SKALITER, R. & LEHMAN, I. R. 1994. Rolling circle DNA replication in vitro by a complex of herpes simplex virus type 1-encoded enzymes. *Proc Natl Acad Sci U S A,* 91**,** 10665-9.

SMITH, G. A., GROSS, S. P. & ENQUIST, L. W. 2001. Herpesviruses use bidirectional fast-axonal transport to spread in sensory neurons. *Proc Natl Acad Sci U S A,* 98**,** 3466-70.

SMITH, G. A., POMERANZ, L., GROSS, S. P. & ENQUIST, L. W. 2004. Local modulation of plus-end transport targets herpesvirus entry and egress in sensory axons. *Proc Natl Acad Sci U S A,* 101**,** 16034-9.

SMITH, G. L., VANDERPLASSCHEN, A. & LAW, M. 2002. The formation and function of extracellular enveloped vaccinia virus. 83**,** 2915-2931.

SNYDER, A., WISNER, T. W. & JOHNSON, D. C. 2006. Herpes simplex virus capsids are transported in neuronal axons without an envelope containing the viral glycoproteins. *J Virol,* 80**,** 11165-77.

SODEIK, B. 2000. Mechanisms of viral transport in the cytoplasm. *Trends Microbiol,* 8**,** 465-72.

SODEIK, B., EBERSOLD, M. W. & HELENIUS, A. 1997. Microtubule-mediated transport of incoming herpes simplex virus 1 capsids to the nucleus. *J Cell Biol,* 136**,** 1007-21.

SOLOMON, J. J., WITTER, R. L., NAZERIAN, K. & BURMESTER, B. R. 1968. Studies on the etiology of Marek's disease. I. Propagation of the agent in cell culture. *Proc Soc Exp Biol Med,* 127**,** 173-7.

SOPPINA, V., NORRIS, S. R., DIZAJI, A. S., KORTUS, M., VEATCH, S., PECKHAM, M. & VERHEY, K. J. 2014. Dimerization of mammalian kinesin-3 motors results in superprocessive motion. *Proc Natl Acad Sci U S A,* 111**,** 5562-7.

SOPPINA, V., RAI, A. K., RAMAIYA, A. J., BARAK, P. & MALLIK, R. 2009. Tug-of-war between dissimilar teams of microtubule motors regulates transport and fission of endosomes. *Proc Natl Acad Sci U S A,* 106**,** 19381-6.

SOPPINA, V. & VERHEY, K. J. 2014. The family-specific K-loop influences the microtubule on-rate but not the superprocessivity of kinesin-3 motors. *Mol Biol Cell,* 25**,** 2161-70.

SPEAR, P. G. 2004. Herpes simplex virus: receptors and ligands for cell entry. *Cell Microbiol,* 6**,** 401-10.

SPLINTER, D., TANENBAUM, M. E., LINDQVIST, A., JAARSMA, D., FLOTHO, A., YU, K. L., GRIGORIEV, I., ENGELSMA, D., HAASDIJK, E. D., KEIJZER, N., DEMMERS, J., FORNEROD, M., MELCHIOR, F., HOOGENRAAD, C. C., MEDEMA, R. H. & AKHMANOVA, A. 2010. Bicaudal D2, dynein, and kinesin-1 associate with nuclear pore complexes and regulate centrosome and nuclear positioning during mitotic entry. *PLoS Biol,* 8**,** e1000350.

STACKPOLE, C. W. 1969. Herpes-type virus of the frog renal adenocarcinoma. I. Virus development in tumor transplants maintained at low temperature. *J Virol,* 4**,** 75-93.

STEINMETZ, M. O. & AKHMANOVA, A. 2008. Capturing protein tails by CAP-Gly domains. *Trends Biochem Sci,* 33**,** 535-45.

STOW, N. D. 1993. Sequences at the C-terminus of the herpes simplex virus type 1 UL30 protein are dispensable for DNA polymerase activity but not for viral origin-dependent DNA replication. *Nucleic Acids Res,* 21**,** 87-92.

STRAUBE, A. & MERDES, A. 2007. EB3 regulates microtubule dynamics at the cell cortex and is required for myoblast elongation and fusion. *Curr Biol,* 17**,** 1318-25.

SUOMALAINEN, M., NAKANO, M. Y., KELLER, S., BOUCKE, K., STIDWILL, R. P. & GREBER, U. F. 1999. Microtubule-dependent plus- and minus end-directed motilities are competing processes for nuclear targeting of adenovirus. *J Cell Biol,* 144**,** 657-72.

SVITKINA, T. M., VERKHOVSKY, A. B. & BORISY, G. G. 1996. Plectin sidearms mediate interaction of intermediate filaments with microtubules and other components of the cytoskeleton. *J Cell Biol,* 135**,** 991-1007.

SZILÁGYI, J. F. & CUNNINGHAM, C. 1991. Identification and characterization of a novel non-infectious herpes simplex virus-related particle. 72**,** 661-668.

TAKEMURA, R., OKABE, S., UMEYAMA, T., KANAI, Y., COWAN, N. J. & HIROKAWA, N. 1992. Increased microtubule stability and alpha tubulin acetylation in cells transfected with microtubule-associated proteins MAP1B, MAP2 or tau. *J Cell Sci,* 103 ( Pt 4)**,** 953-64.

TAM, J., CORDIER, G. A., BALINT, S., SANDOVAL ALVAREZ, A., BORBELY, J. S. & LAKADAMYALI, M. 2014. A microfluidic platform for correlative live-cell and super-resolution microscopy. *PLoS One,* 9**,** e115512.

TANENBAUM, M. E. & MEDEMA, R. H. 2010. Mechanisms of centrosome separation and bipolar spindle assembly. *Dev Cell,* 19**,** 797-806.

TAYLOR, M. P. & ENQUIST, L. W. 2015. Axonal spread of neuroinvasive viral infections. *Trends Microbiol,* 23**,** 283-8.

TERADA, S. & HIROKAWA, N. 2000. Moving on to the cargo problem of microtubule-dependent motors in neurons. *Current Opinion in Neurobiology,* 10**,** 566-573.

THEISEN, U., STRAUBE, E. & STRAUBE, A. 2012. Directional persistence of migrating cells requires Kif1C-mediated stabilization of trailing adhesions. *Dev Cell,* 23**,** 1153-66.

THERY, M. 2010. Micropatterning as a tool to decipher cell morphogenesis and functions. *J Cell Sci,* 123**,** 4201-13.

THOMPSON, R. F. & LANGFORD, G. M. 2002. Myosin superfamily evolutionary history. *Anat Rec,* 268**,** 276-89.

TIEN, N. W., WU, G. H., HSU, C. C., CHANG, C. Y. & WAGNER, O. I. 2011. Tau/PTL-1 associates with kinesin-3 KIF1A/UNC-104 and affects the motor's motility characteristics in C. elegans neurons. *Neurobiol Dis,* 43**,** 495-506.

TOEPKE, M. W. & BEEBE, D. J. 2006. PDMS absorption of small molecules and consequences in microfluidic applications. *Lab Chip,* 6**,** 1484-6.

TOMISHIGE, M., KLOPFENSTEIN, D. R. & VALE, R. D. 2002. Conversion of Unc104/KIF1A kinesin into a processive motor after dimerization. *Science,* 297**,** 2263-7.

TONG, Y., TEMPEL, W., WANG, H., YAMADA, K., SHEN, L., SENISTERRA, G. A., MACKENZIE, F., CHISHTI, A. H. & PARK, H. W. 2010. Phosphorylation-independent dual-site binding of the FHA domain of KIF13 mediates phosphoinositide transport via centaurin alpha1. *Proc Natl Acad Sci U S A,* 107**,** 20346-51.

TOPP, K. S., MEADE, L. B. & LAVAIL, J. H. 1994. Microtubule polarity in the peripheral processes of trigeminal ganglion cells: relevance for the retrograde transport of herpes simplex virus. *J Neurosci,* 14**,** 318-25.

TRAPP, S., PARCELLS, M. S., KAMIL, J. P., SCHUMACHER, D., TISCHER, B. K., KUMAR, P. M., NAIR, V. K. & OSTERRIEDER, N. 2006. A virus-encoded telomerase RNA promotes malignant T cell lymphomagenesis. *J Exp Med,* 203**,** 1307-17.

UETAKE, Y. & SLUDER, G. 2007. Cell-cycle progression without an intact microtuble cytoskeleton. *Curr Biol,* 17**,** 2081-6.

VALENTINE, M. T. & GILBERT, S. P. 2007. To step or not to step? How biochemistry and mechanics influence processivity in Kinesin and Eg5. *Curr Opin Cell Biol,* 19**,** 75-81.

VAN DER VAART, B., VAN RIEL, W. E., DOODHI, H., KEVENAAR, J. T., KATRUKHA, E. A., GUMY, L., BOUCHET, B. P., GRIGORIEV, I., SPANGLER, S. A., YU, K. L., WULF, P. S., WU, J., LANSBERGEN, G., VAN BATTUM, E. Y., PASTERKAMP, R. J., MIMORI-KIYOSUE, Y., DEMMERS, J., OLIERIC, N., MALY, I. V., HOOGENRAAD, C. C. & AKHMANOVA, A. 2013. CFEOM1-associated kinesin KIF21A is a cortical microtubule growth inhibitor. *Dev Cell,* 27**,** 145-160.

VERHEY, K. J., KAUL, N. & SOPPINA, V. 2011. Kinesin assembly and movement in cells. *Annu Rev Biophys,* 40**,** 267-88.

WANI, M. C., TAYLOR, H. L., WALL, M. E., COGGON, P. & MCPHAIL, A. T. 1971. Plant antitumor agents. VI. The isolation and structure of taxol, a novel antileukemic and antitumor agent from Taxus brevifolia. *J Am Chem Soc,* 93**,** 2325-7.

WARD, B. M. 2011. The taking of the cytoskeleton one two three: how viruses utilize the cytoskeleton during egress. *Virology,* 411**,** 244-50.

WARD, B. M. & MOSS, B. 2001. Vaccinia Virus Intracellular Movement Is Associated with Microtubules and Independent of Actin Tails. *Journal of Virology,* 75**,** 11651.

WEAVER, B. A. 2014. How Taxol/paclitaxel kills cancer cells. *Mol Biol Cell,* 25**,** 2677-81.

WEGEL, E., GOHLER, A., LAGERHOLM, B. C., WAINMAN, A., UPHOFF, S., KAUFMANN, R. & DOBBIE, I. M. 2016. Imaging cellular structures in super-resolution with SIM, STED and Localisation Microscopy: A practical comparison. *Sci Rep,* 6**,** 27290.

WEIHS, F., WACNIK, K., TURNER, R. D., CULLEY, S., HENRIQUES, R. & FOSTER, S. J. 2018. Heterogeneous localisation of membrane proteins in Staphylococcus aureus. *Sci Rep,* 8**,** 3657.

WEISENBERG, R. C. 1972. Microtubule formation in vitro in solutions containing low calcium concentrations. *Science,* 177**,** 1104-5.

WEISENBERG, R. C., DEERY, W. J. & DICKINSON, P. J. 1976. Tubulin-nucleotide interactions during the polymerization and depolymerization of microtubules. *Biochemistry,* 15**,** 4248-54.

WELTE, M. A. 2004. Bidirectional transport along microtubules. *Curr Biol,* 14**,** R525-37.

WESTERHOLM-PARVINEN, A., VERNOS, I. & SERRANO, L. 2000. Kinesin subfamily UNC104 contains a FHA domain: boundaries and physicochemical characterization. *FEBS Lett,* 486**,** 285-90.

WHITELEY, A., BRUUN, B., MINSON, T. & BROWNE, H. 1999. Effects of Targeting Herpes Simplex Virus Type 1 gD to the Endoplasmic Reticulum and <em>trans</em>-Golgi Network. *Journal of Virology,* 73**,** 9515.

WILD, P., KAECH, A., SCHRANER, E. M., WALSER, L. & ACKERMANN, M. 2017. Endoplasmic reticulum-to-Golgi transitions upon herpes virus infection. *F1000Res,* 6**,** 1804.

WILD, P., LEISINGER, S., DE OLIVEIRA, A. P., SCHRANER, E. M., KAECH, A., ACKERMANN, M. & TOBLER, K. 2015. Herpes simplex virus 1 Us3 deletion mutant is infective despite impaired capsid translocation to the cytoplasm. *Viruses,* 7**,** 52-71.

WISNER, T. W., SUGIMOTO, K., HOWARD, P. W., KAWAGUCHI, Y. & JOHNSON, D. C. 2011. Anterograde transport of herpes simplex virus capsids in neurons by both separate and married mechanisms. *J Virol,* 85**,** 5919-28.

WITTER, R. L. 1997. Increased virulence of Marek's disease virus field isolates. *Avian Dis,* 41**,** 149-63.

WOLFF, A., DE NECHAUD, B., CHILLET, D., MAZARGUIL, H., DESBRUYERES, E., AUDEBERT, S., EDDE, B., GROS, F. & DENOULET, P. 1992. Distribution of glutamylated alpha and beta-tubulin in mouse tissues using a specific monoclonal antibody, GT335. *Eur J Cell Biol,* 59**,** 425-32.

WOODRUM, D. T., RICH, S. A. & POLLARD, T. D. 1975. Evidence for biased bidirectional polymerization of actin filaments using heavy meromyosin prepared by an improved method. *J Cell Biol,* 67**,** 231-7.

XIANG, W., ROBERTI, M. J., HERICHE, J. K., HUET, S., ALEXANDER, S. & ELLENBERG, J. 2018. Correlative live and super-resolution imaging reveals the dynamic structure of replication domains. *J Cell Biol,* 217**,** 1973-1984.

XIANG, X., QIU, R., YAO, X., ARST, H. N., JR., PENALVA, M. A. & ZHANG, J. 2015. Cytoplasmic dynein and early endosome transport. *Cell Mol Life Sci,* 72**,** 3267-80.

XING, B. M., YANG, Y. R., DU, J. X., CHEN, H. J., QI, C., HUANG, Z. H., ZHANG, Y. & WANG, Y. 2012. Cyclin-dependent kinase 5 controls TRPV1 membrane trafficking and the heat sensitivity of nociceptors through KIF13B. *J Neurosci,* 32**,** 14709-21.

XUE, X., JAULIN, F., ESPENEL, C. & KREITZER, G. 2010. PH-domain-dependent selective transport of p75 by kinesin-3 family motors in non-polarized MDCK cells. *J Cell Sci,* 123**,** 1732-41.

YAMADA, K. H., HANADA, T. & CHISHTI, A. H. 2007. The effector domain of human Dlg tumor suppressor acts as a switch that relieves autoinhibition of kinesin-3 motor GAKIN/KIF13B. *Biochemistry,* 46**,** 10039-45.

YAMADA, K. H., NAKAJIMA, Y., GEYER, M., WARY, K. K., USHIO-FUKAI, M., KOMAROVA, Y. & MALIK, A. B. 2014. KIF13B regulates angiogenesis through Golgi to plasma membrane trafficking of VEGFR2. *J Cell Sci,* 127**,** 4518-30.

YANG, C. & SVITKINA, T. 2011. Filopodia initiation: focus on the Arp2/3 complex and formins. *Cell Adh Migr,* 5**,** 402-8.

YE, G. J., VAUGHAN, K. T., VALLEE, R. B. & ROIZMAN, B. 2000. The herpes simplex virus 1 U(L)34 protein interacts with a cytoplasmic dynein intermediate chain and targets nuclear membrane. *J Virol,* 74**,** 1355-63.

YE, Y., MEYER, H. H. & RAPOPORT, T. A. 2001. The AAA ATPase Cdc48/p97 and its partners transport proteins from the ER into the cytosol. *Nature,* 414**,** 652-6.

YONEKAWA, Y., HARADA, A., OKADA, Y., FUNAKOSHI, T., KANAI, Y., TAKEI, Y., TERADA, S., NODA, T. & HIROKAWA, N. 1998. Defect in synaptic vesicle precursor transport and neuronal cell death in KIF1A motor protein-deficient mice. *J Cell Biol,* 141**,** 431-41.

YUE, Y., SHENG, Y., ZHANG, H. N., YU, Y., HUO, L., FENG, W. & XU, T. 2013. The CC1-FHA dimer is essential for KIF1A-mediated axonal transport of synaptic vesicles in C. elegans. *Biochem Biophys Res Commun,* 435**,** 441-6.

ZAICHICK, S. V., BOHANNON, K. P., HUGHES, A., SOLLARS, P. J., PICKARD, G. E. & SMITH, G. A. 2013. The herpesvirus VP1/2 protein is an effector of dynein-mediated capsid transport and neuroinvasion. *Cell Host Microbe,* 13**,** 193-203.

ZANIC, M., WIDLUND, P. O., HYMAN, A. A. & HOWARD, J. 2013. Synergy between XMAP215 and EB1 increases microtubule growth rates to physiological levels. *Nat Cell Biol,* 15**,** 688-93.

ZELNIK, V. 2003. Marek's disease virus research in the post-sequencing era: new tools for the study of gene functions and virus-host interactions. *Avian Pathol,* 32**,** 323-33.

ZENNER, H. L., YOSHIMURA, S.-I., BARR, F. A. & CRUMP, C. M. 2011. Analysis of Rab GTPase-Activating Proteins Indicates that Rab1a/b and Rab43 Are Important for Herpes Simplex Virus 1 Secondary Envelopment. *Journal of Virology,* 85**,** 8012.

ZHANG, Z., NISHIMURA, Y. & KANCHANAWONG, P. 2017. Extracting microtubule networks from superresolution single-molecule localization microscopy data. *Mol Biol Cell,* 28**,** 333-345.

ZINK, S., GROSSE, L., FREIKAMP, A., BANFER, S., MUKSCH, F. & JACOB, R. 2012. Tubulin detyrosination promotes monolayer formation and apical trafficking in epithelial cells. *J Cell Sci,* 125**,** 5998-6008.

ZUCCOLA, H. J., FILMAN, D. J., COEN, D. M. & HOGLE, J. M. 2000. The crystal structure of an unusual processivity factor, herpes simplex virus UL42, bound to the C terminus of its cognate polymerase. *Mol Cell,* 5**,** 267-78.